

19

Nondestructive Test Methods*

by

Nicholas J. Carino

Research structural engineer in the Structures Division at the National Institute of Standards and Technology, Gaithersburg MD. Expert in nondestructive test methods for concrete.

19.1	Introduction	19-1
19.2	Methods to Estimate In-Place Strength	19-2
	Historical Background • Rebound Hammer • Ultrasonic Pulse Velocity • Probe Penetration • Pullout Test • Break-Off Test • Maturity Method • Statistical Methods	
19.3	Methods for Flaw Detection and Condition Assessment	19-28
	Introduction • Visual Inspection • Stress-Wave Propagation Methods • Infrared Thermography • Ground-Penetrating Radar (GPR) • Electrical and Magnetic Methods for Reinforcement • Nuclear (Radioactive) Methods	
19.4	Concluding Remarks	19-58

19.1 Introduction

Concrete differs from other construction materials in that it can be made from an infinite combination of suitable materials and its final properties are dependent on the treatment it undergoes after it arrives at the job site. The efficiency of the consolidation and the effectiveness of curing procedures are critical for attaining the full potential of a concrete mixture. While concrete is known for its durability, it is susceptible to a range of environmental degradation factors, which can limit its service life. There has always been a need for test methods to measure the in-place properties of concrete for quality assurance and for evaluation of existing conditions. Ideally, these methods should be nondestructive so that they do not impair the function of the structure and permit retesting at the same locations to evaluate changes in properties with time.

Compared with the development of nondestructive test (NDT) methods for steel structures, the development of NDT methods for concrete has progressed at a slower pace, because concrete is inherently more difficult to test than steel. Concrete is highly heterogenous on a macroscopic scale, it is electrically nonconductive but usually contains significant amounts of steel reinforcement, and it is often used in thick members. Thus it has not been easy to transfer the NDT technology developed for steel to the inspection of concrete. In addition, there has been little interest in the

*Contribution of National Institute of Standards and Technology and is not subject to copyright in the United States.

traditional NDT community (physicists, electrical engineers, mechanical engineers) to develop test methods for concrete.

There is no standard definition for **nondestructive tests** as applied to concrete. For some people, they are tests that do not alter the concrete. For others, they are simply tests that do not impair the function of a structure, in which case the drilling of cores is considered to be a NDT test. For still others, they are tests that do less damage to the structure than does drilling of cores. This chapter deals with methods that either do not alter the concrete or that result only in superficial local damage. The author prefers to divide the various methods into two groups: (1) those whose main purpose is to estimate strength; and (2) those whose main purpose is evaluate conditions other than strength, that is, to evaluate integrity. It will be shown that the most reliable tests for strength are those that result in superficial local damage, and the author prefers the term **in-place tests** for this group. The integrity tests, on the other hand, are nondestructive.

The purpose of this chapter is to provide an introduction to commonly used NDT methods for concrete. Table 19.1 lists the various test methods that will be considered. Emphasis is placed on the principles underlying the various methods so that the reader may understand their advantages and inherent limitations. Additional information on the application of these methods is available in ACI 228.1R (1995), Malhotra and Carino (1991), and Bungey (1989), and the reader is urged to consult these additional references for more in-depth information when necessary. Portions of this chapter are based on previously published works of the author [Carino, 1992a, 1994].

TABLE 19.1 Nondestructive and In-Place Tests

In-Place Tests to Estimate Strength	Nondestructive Tests for Integrity
Rebound hammer	Visual inspection
Ultrasonic pulse velocity	Stress wave propagation methods
Probe penetration	Ground penetrating radar
Pullout	Electrical/magnetic methods
Break-off	Nuclear methods
Maturity method	Infrared thermography

19.2 Methods to Estimate In-Place Strength

19.2.1 Historical Background

Some of the first methods to evaluate the in-place strength of concrete were adaptations of the Brinell hardness¹ test for metals, which involves pushing a high-strength steel ball into the test piece under a given force and measuring the area of the indentation. In the metals test, the load is applied by an hydraulic loading system. Modifications were required to enable this type of test to be made on a concrete structure. In 1934, Professor K. Gaede (Hanover, Germany) reported on the use of a spring-driven impactor to supply the force to drive a steel ball into the concrete [Malhotra, 1976]. A nonlinear, empirical relationship was obtained between cube strength and indentation diameter. In 1936, J.P. Williams (England) reported on a spring-loaded, pistol-shaped device, in which a 4-mm ball was attached to a plunger [Malhotra, 1976]. The spring was compressed by turning a screw, a trigger released the compressed spring, and the plunger was propelled toward the concrete. The diameter of the indentation produced by the ball was measured with a magnifying scale.

In 1938 there appeared a landmark paper by D.G. Skramtajev, of the Central Institute for Industrial Building Research, Moscow [Skramtajev, 1938]. It summarized 14 different techniques, 10 of which were developed in the Soviet Union, for measuring the in-place strength of concrete. This paper should be read by every student of nondestructive testing for its historical content. Skramtajev

¹The term **hardness** is used routinely in the description of a series of tests of metals and concrete, yet this is not a readily quantified mechanical property. If one considers the nature of the hardness test methods that have been developed for metals, it can be concluded that these tests measure the amount of penetration caused by a specific indenter under a specific load. Therefore a more descriptive term for these methods might be **indentation tests**.

divided the test methods into two groups: (1) those that required installation of test hardware prior to placement of concrete, and (2) those that did not require preinstallation of hardware. The methods described by Skramtajev included the following: molds placed in the structure to form in-place test specimens; pullout tests of embedded bars; an in-place punching shear test; an in-place fracture test using a pincer device; penetration with a chisel driven by hammer blows; guns that fired indentors into the concrete; and penetration with a ball powered by a spring-driven apparatus. Readers who are familiar with modern in-place test methods (to be discussed later) will recognize that many of them are variations of methods suggested over one-half century ago.

Skramtajev also commented on the need for in-place testing. For example, he noted that [Skramtajev, 1938]:

- The curing conditions of standard test specimens are not representative of the concrete in the structure.
- The number of standard test specimens is insufficient to assure the adequacy of all members in a structure.
- Standard test specimens that are tested at an age of one month provide no information on the later-age strength of concrete in the structure.
- Surface tests may not provide an indication of the actual concrete strength owing to the effects of carbonation, laitance, and moisture condition.
- Methods requiring preplacement of hardware tend to provide more precise estimates of strength than those that do not require preplacement of hardware, but they lack flexibility for use at any desired location in an existing structure.

It is interesting that 50 years later, the same arguments and limitations are quoted in relation to in-place testing [ACI 228.1R, 1995].

19.2.2 Rebound Hammer

In 1948, Ernst Schmidt, a Swiss engineer, developed a device for testing concrete based upon the rebound principle [Malhotra, 1976, 1991]. As was the case with earlier indentation tests, the motivation for this new device came from tests developed to measure the hardness of metals. In this case, the new device was an outgrowth of the Scleroscope² test, which involves measuring the rebound height of a diamond-tipped hammer, or mass, that is dropped from a fixed height above the test surface.

As noted by Kolek (1958), when concrete is struck by a hammer, the degree of rebound is an indicator of the hardness of the concrete. Schmidt standardized the hammer blow by developing a spring-loaded hammer and devised a method to measure the rebound of the hammer. Several different models of the device were built [Greene, 1954], and Figure 19.1 is a schematic of the model that was eventually adopted for field use. The essential parts of the Schmidt rebound hammer are the outer body, the hammer, the plunger, the spring, and the slide indicator. To perform the test, the plunger is extended from the body of the instrument, which causes a latch mechanism to grab hold of the hammer (Figure 19.1a). The body of the instrument is then pushed toward the concrete surface, which stretches the spring attached to the hammer and the body (Figure 19.1b). When the body is pushed to the limit, the latch is released and the hammer is propelled toward the concrete by a combination of gravity and spring forces (Figure 19.1c). The hammer strikes the shoulder of the plunger and it rebounds (Figure 19.1d). The rebound distance is measured on a scale by a slide indicator. The rebound distance is expressed as a rebound number, which is the percentage of the initial extension of the spring [Kolek, 1958]. Currently, different models of the instrument are available, which differ in the mass of the hammer and the stiffness of the spring. Thus different impact energies can be used for different materials.

²In Greek, the word "sklero" means "hard."

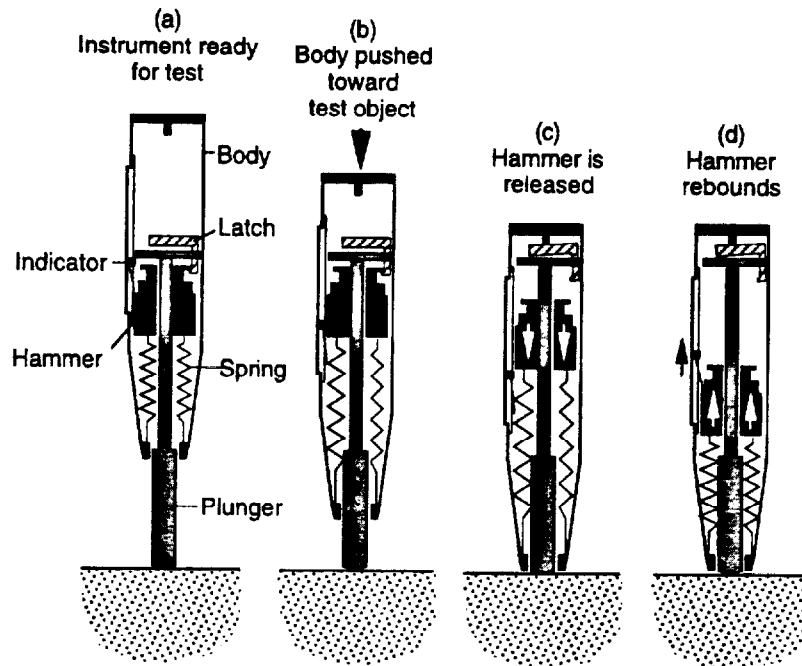


FIGURE 19.1 Schematic cross section of rebound hammer showing principle of operation.

Owing to its simplicity and low cost, the Schmidt rebound hammer is, by far, the most widely used nondestructive test device for concrete. While the test appears simple, there is no simple relationship between the rebound number and the strength of concrete. In principle, the rebound is affected by the movement of the end of the plunger in contact with the concrete. The more the end of the plunger moves, the lower is the rebound. Thus the rebound number is likely to be influenced by the elastic stiffness and the strength of the concrete.

Since the rebound number is indicative of the near-surface properties of the concrete, it may not be indicative of the bulk concrete in a structural member. The report of ACI Committee 228 [ACI 228.1R, 1995] outlines some of the factors that may result in rebound numbers that are not representative of the bulk concrete.

- The moisture condition of the surface concrete affects the rebound number; a dry surface results in a higher rebound number.
- The presence of a surface layer of carbonation increases the rebound number.
- The surface texture affects the rebound number, with smooth hard-troweled surfaces giving higher values than a rough-textured surface.
- The rebound number is affected by the orientation of the instrument in relation to the direction of gravity (approximate correction factors are available).

Because the rebound number is affected by the near-surface conditions, erratic results may occur if the plunger is located directly over a coarse aggregate particle or a subsurface air void. To account for these possibilities, ASTM C 805 requires that 10 rebound numbers be taken for a test. If a reading differs by more than seven units from the average, that reading should be discarded and a new average should be computed based on the remaining readings. If more than two readings differ from the average by seven units, the entire set of readings is discarded.

The rebound hammer was constructed and tested extensively at the Swiss Federal Materials Testing and Experimental Institute in Zurich. A correlation was developed between the compressive strength of standard cubes and the rebound number, and this correlation was provided with the instrument. However, as other investigators began to develop correlations between strength and rebound number, it became evident that there was not a unique relationship between strength and rebound number [Kolek, 1958]. The current recommended practice [ASTM C 805, ACI 228.1R, 1995] is to develop the strength relationship using the same concrete and forming materials as will be used in construction. Without such a correlation, the rebound hammer is useful only for detecting gross changes in concrete quality throughout a structure.

In summary, the rebound number method is recognized as a useful tool for performing quick surveys to assess the uniformity of concrete. However, because of the many factors besides concrete strength than can affect rebound number, it is not generally recommended where accurate strength estimates are needed.

19.2.3 Ultrasonic Pulse Velocity

The ultrasonic pulse velocity method is a stress wave propagation method that involves measuring the travel time, over a known path length, of a pulse of ultrasonic compressional waves (these are waves associated with normal stress). The pulses are introduced into the concrete by a piezoelectric transducer, and a similar transducer acts as receiver to monitor the surface vibration caused by the arrival of the pulse. A timing circuit is used to measure the time it takes for the pulse to travel from the transmitting to the receiving transducers. Figure 19.2 is a schematic of the ultrasonic pulse velocity technique. The speed of compressional waves in a solid is related to the elastic constants (modulus of elasticity and Poisson's ratio) and the density. By conducting tests at various points on a structure, lower quality concrete can be identified by its lower pulse velocity. Naik and Malhotra (1991) provide additional information on the development and application of this method for estimating concrete strength.

The development of a field instrument to measure the pulse velocity occurred nearly simultaneously in Canada and in England [Whitehurst, 1967]. These developments were outgrowths of

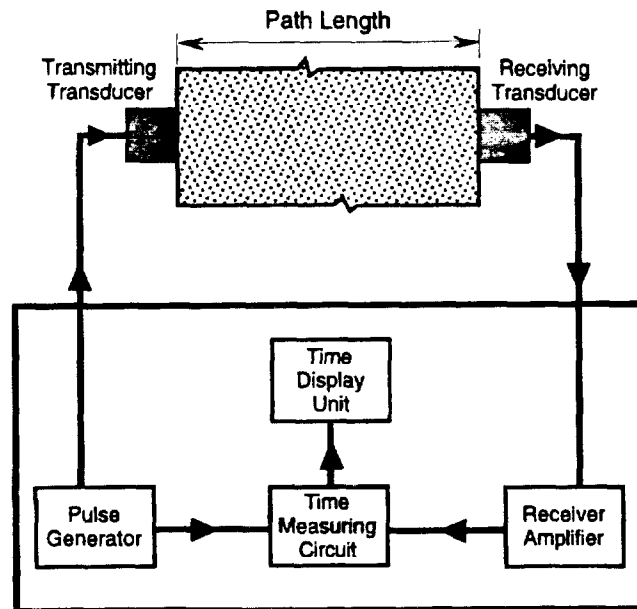


FIGURE 19.2 Schematic of ultrasonic pulse velocity method.

earlier successful work by the U.S. Army Corps of Engineers to measure the speed of a mechanical stress pulse moving through concrete [Long et al., 1945]. The Army Corps of Engineers approach involved two receivers attached to the concrete surface. A horizontal hammer blow was applied in line with the receivers, and a specially designed electronic interval timer was used to measure the time for the pulse to travel from the first to the second receiver. The major purpose of this technique was to calculate the in-place modulus of elasticity.

In 1946 and 1947, engineers at the Hydro-Electric Power Commission of Ontario (Ontario Hydro) worked on the development of a device to investigate the extent of cracking in dams [Leslie and Cheesman, 1949]. The device developed to do so was called the Soniscope. It had a 20-kHz transmitting transducer, was capable of penetrating up to 15 m of concrete, and could measure the travel time with an accuracy of 3%. The stated purposes of the Soniscope were to identify the presence of internal cracking, determine the depth of surface-opening cracks, and determine the dynamic modulus of concrete [Leslie and Cheesman, 1949]. It was further stated that the fundamental measurement was the travel time. The amplitude of the received signal was said to be of secondary importance because the transfer of energy between the transducers and the concrete could not be controlled. It was also emphasized that interpretation of results required knowledge of the history of the structure being investigated.

Early uses of the Soniscope on mass concrete emphasized measuring the pulse velocity rather than estimating strength or calculating the elastic stiffness [Parker, 1953]. Based on velocity readings on a gridwork, the presence of distressed concrete could be easily detected. Parker (1953) reported Ontario Hydro's early attempts to develop relationships between pulse velocity and compressive strength. Forty-six mixtures involving the same aggregate, different cement types, and different admixtures were investigated. The results indicated no significant differences in the velocity-strength relationships for the different mixtures. The results were therefore treated as one group, and the best-fit relationship was determined. Figure 19.3 shows the relationship between estimated strength and pulse velocity and the lower 95% confidence limit for estimated strength. Owing to large scatter, the lower confidence limit was about 45% of the mean strength. Thus the inherent uncertainty in

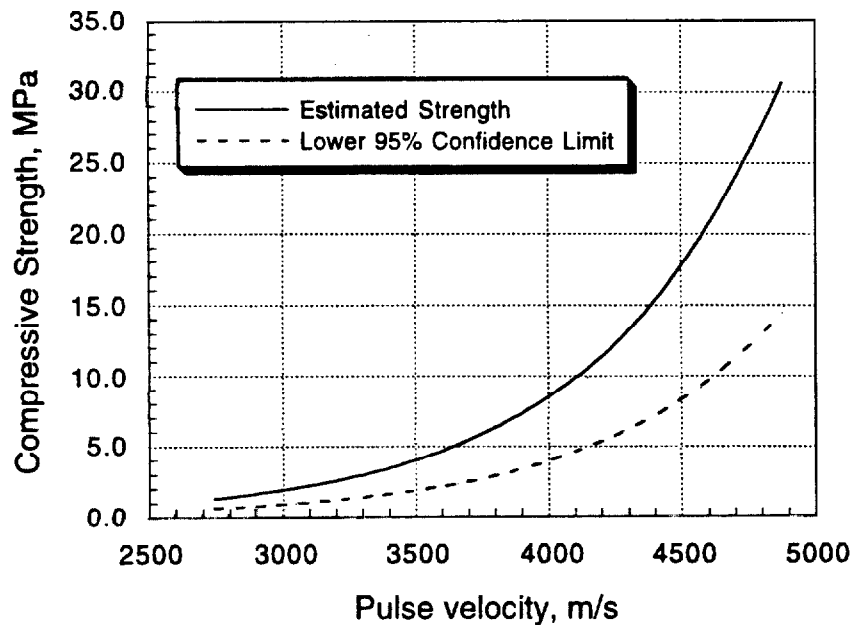


FIGURE 19.3 Compressive strength versus pulse velocity relationship based upon 46 mixtures made with the same aggregate [based on Parker, 1953].

using pulse velocity to estimate strength was established very early. Figure 19.3 also shows that the change in pulse velocity per unit change in strength decreases with increasing strength. This means that pulse velocity is relatively insensitive to strength for mature concrete.

While work on the Soniscope was in progress in Canada, R. Jones and co-workers at the Road Research Laboratory (RRL) in England were involved in independent research to develop an ultrasonic testing apparatus [Jones, 1949a]. The RRL researchers were interested in testing the quality of concrete pavements, which involved shorter path lengths compared with the work at Ontario Hydro. As a result, the apparatus that was developed operated at a higher frequency than the Soniscope, and it was called the ultrasonic concrete tester. Transducers with resonant frequencies from 60 to 200 kHz were used, depending on the desired penetration [Jones, 1953]. Besides using a different operating frequency, the RRL device used a different approach than the Soniscope to measure travel time. This was necessary because of the shorter path lengths in the RRL work. It was reported that the ultrasonic concrete tester could measure travel times to within $\pm 0.2 \mu\text{s}$.

Jones (1949b) reviewed the test program carried out with the newly developed ultrasonic concrete tester. Among these programs were the following:

- There was an investigation of the variation of pulse velocity with height in standard cube specimens and with depth in slabs. This is one of the first studies to document the top-to-bottom effect that is often mentioned as a problem when planning and interpreting in-place tests [ACI 228.1R, 1995].
- An investigation was performed on the influence of watercement ratio, aggregate type, and aggregate content on pulse velocity. These studies demonstrated the importance of aggregate type and aggregate content on pulse velocity.
- There was an investigation of the relationships between pulse velocity and compressive strength. These studies demonstrated that for a given mixture under uniform conditions there was good correlation between strength and pulse velocity.

Thus Jones established the problems inherent in using the pulse velocity to estimate concrete strength. Despite these early findings, numerous researchers sought to establish correlations between pulse velocity and strength, and many reached the same conclusions as Jones [Sturup et al., 1984].

In the United States, a Soniscope was developed in 1947 at the Portland Cement Association in cooperation with Ontario Hydro, and field applications were reported by Whitehurst (1951). In his summary of industry's experience in the U.S., Whitehurst published the following tentative classification for using pulse velocity as an indicator of quality:

Pulse Velocity, m/s	Condition
Above 4570	excellent
3660 to 4570	generally good
3050 to 3660	questionable
2130 to 3050	generally poor
Below 2130	very poor

This table was quoted in many subsequent publications. However, Whitehurst warned that these values were established on the basis of tests of normal concrete having a density of about 2400 kg/m^3 and that the boundaries between "conditions" could not be sharply drawn. He mentioned that, rather than using these limits, a better approach would be to compare velocities with the velocity in portions of the structure that are known to be of acceptable quality. Nevertheless, inexperienced investigators often used the above table as the sole basis for interpreting test results.

After the publication of these landmark papers in the late 1940s and early 1950s, a flurry of activity occurred worldwide, and efforts were begun to develop test standards. In the United States, a proposed ASTM test method was published by Leslie (1955), but it was not until 1967 that it finally

became a tentative test method [ASTM C 597]. In Europe, the International Union of Testing and Research Laboratories for Materials and Structures (RILEM) organized a working group to study nondestructive testing (R. Jones was appointed chairman), and in 1969, draft recommendations for testing concrete by the ultrasonic pulse method were published [Jones and Făcăoaru, 1969]. In Eastern Europe, the method was used extensively in precast concrete plants.

During the 1960s and 1970s, considerable attention was devoted to gaining more knowledge about the effects of different factors on pulse velocity. Researchers continued to explore the relationship between compressive strength and pulse velocity. However, they appear to have reached a consensus that there is no unique relationship. Numerous studies showed that the type and quantity of aggregate have major effects on pulse velocity but not on strength. Significant effort was also expended to examine whether attenuation measurements could provide additional information about concrete strength. These results were, in general, found to be impractical in field situations because of difficulties in achieving consistent coupling of the transducers, which is critical for measuring attenuation.

Perhaps the most significant advances during this period were in the development of improved field instrumentation. Owing to advances in microelectronic circuitry, the cumbersome instruments developed in the 1940s and 1950s gave way to compact portable devices. In the late 1960s, TNO (Netherlands Organization for Applied Scientific Research) in Delft, Netherlands, developed a portable, battery-operated pulse velocity device that incorporated a digital display of the travel time. In the earlier devices, travel time was measured by examination of oscilloscope displays, which was a time-consuming process. The portable instrument had a resolution of $1 \mu\text{s}$, which resulted in low accuracy for short path lengths, and it had limited penetrating ability [Făcăoaru, 1969]. At about the same time, R.H. Elvery of University College, London, developed a similar portable device that was called PUNDIT (Portable Ultrasonic Nondestructive Digital Indicating Tester). It weighed 3.2 kg, had a resolution of $0.5 \mu\text{s}$, and could be powered by rechargeable batteries [Malhotra, 1976]. These and other relatively low-cost, portable devices simplified testing and resulted in a worldwide increase in the number of consultants and researchers who could perform this type of testing. Later models of these devices had resolutions of $0.1 \mu\text{s}$, and some provided an optional output terminal to allow the received signal to be displayed on an oscilloscope.

In summary, the ultrasonic pulse velocity method is a relatively simple test to perform on site provided it is possible to gain access to both sides of the member. While tests can be performed with the transducers placed on the same surface, the results are not easy to interpret and this method of measurement is not recommended. Care must be exercised to assure that good and consistent coupling with the concrete surfaces is achieved. Other important factors, besides concrete strength, that can affect the measured ultrasonic pulse velocity and that should be considered are discussed in the report of ACI Committee 228 [ACI 228.1R, 1995]. These include:

- moisture content—an increase in moisture content increases the pulse velocity;
- presence of reinforcement oriented parallel to the pulse propagation direction—the pulse may propagate through the bars and result in an apparent pulse velocity that is higher than that propagating through concrete; and
- presence of cracks and voids—these can increase the length of the travel path and result in a longer travel time.

Because of these factors, the ultrasonic pulse velocity should be used for estimating concrete strength only by experienced individuals. Like the rebound number test, the pulse velocity method is very useful for assessing the uniformity of concrete in a structure. It is often used to locate portions of a structure where other tests should be performed or where cores should be drilled.

19.2.4 Probe Penetration

The probe-penetration method involves using a gun to drive a hardened steel rod, or probe, into the concrete and measuring the exposed length of the probe. In principle, as the strength of the concrete increases, the exposed probe length also increases; by means of a suitable correla-

tion, the exposed length can be used to estimate compressive strength. Skramtajev mentioned a similar concept in his 1938 summary paper, and Malhotra (1976) mentions that similar techniques were reported in 1954. Malhotra and Carette (1991) provide an in-depth summary of this technique.

Development of the probe penetration test system began in about 1964 as a joint undertaking by T.R. Cantor of the Port of New York Authority and R. Kopf of the Windsor Machinery Co. [Arni, 1972]. The test system that was eventually commercialized became known as the Windsor probe. The apparatus is supplied with a table that relates exposed probe length to compressive strength for different aggregate hardness as measured by Mohs hardness scale³ of minerals. The basis for the values in the tables and their uncertainty were not provided [Arni, 1972]. In the late 1960s, independent investigations of the reliability of the Windsor probe system were carried out by the National Ready-Mixed Concrete Association [Gaynor, 1969], the Federal Highway Administration (FHWA) [Arni, 1972], and the Department of Energy, Mines and Resources (Canada) [Malhotra, 1974]. In general, it was found that the probe system had an acceptable within-test variability. However, scatter in the correlation between compressive strength and probe penetration led to rather high uncertainties in the estimated strength. All investigators cautioned against reliance on the manufacturer's correlation tables.

Arni's (1972) study of the uncertainties of the probe penetration and rebound hammer tests is very interesting and worth summarizing. He calculated the number of tests required to detect a strength difference of 1.4 MPa (200 psi) using test cylinders, probe penetration, or rebound number. These estimates were based on the variability of test results and slopes of the correlation equations developed in the FHWA study. For 90% confidence levels, the results were as follows:

Cylinders	8
Rebound	120
Probe	85

Note that these numbers apply for specific data used by Arni. Nevertheless, they point out the inherent inability of in-place tests to detect small differences in concrete strength unless large numbers of tests are performed. This important concept has been largely ignored.

The Windsor probe test method was adopted as a tentative ASTM standard (C 803) in 1975. In 1990, the standard was modified to include the use of a pin penetration device, in which a small pin is forced into the concrete using a spring-loaded driver [ACI 228.1R, 1995; Malhotra and Carette, 1991; Nasser and Al-Manseer, 1987a,b].

The report of ACI Committee 228 [ACI 228.1R, 1995] provides an explanation of the factors affecting probe penetration into concrete. Figure 19.4 is a schematic of the failure zone produced during probe penetration. The probe penetrates until its initial kinetic energy is absorbed by friction and the fracture of the mortar and aggregate. Hence the strength properties of the aggregate affect the penetration depth. As a result, the strength relationship is dependent on the aggregate type. For equal concrete strength, probe penetration would be deeper in a concrete with a soft aggregate than in a concrete with a hard aggregate. See Malhotra (1976), Bungey (1989), and Malhotra and Carette (1991) for additional information of the effects of aggregate type. Probe penetration is not strongly affected by the near-surface conditions and is therefore not as sensitive to surface conditions as the rebound-number method. The direction of penetration is not important provided that the probe is fired perpendicular to the surface. Care must be exercised when testing reinforced concrete to assure that tests are not carried out in the vicinity of the reinforcing steel, especially if the concrete cover is low.

³A qualitative scale in which the hardness of a mineral is determined by its ability to scratch, or be scratched by, another mineral.

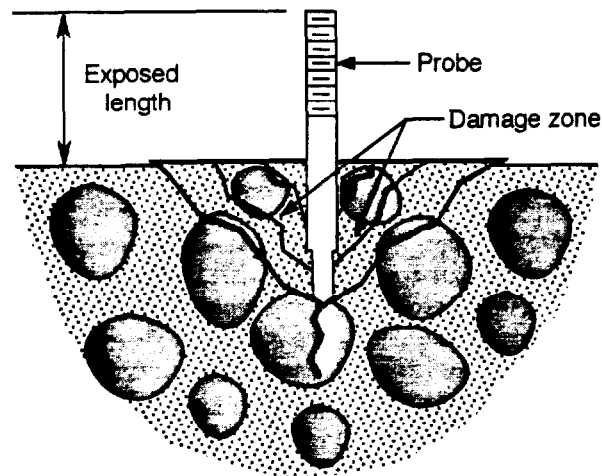


FIGURE 19.4 Schematic of conical failure zone during probe penetration test.

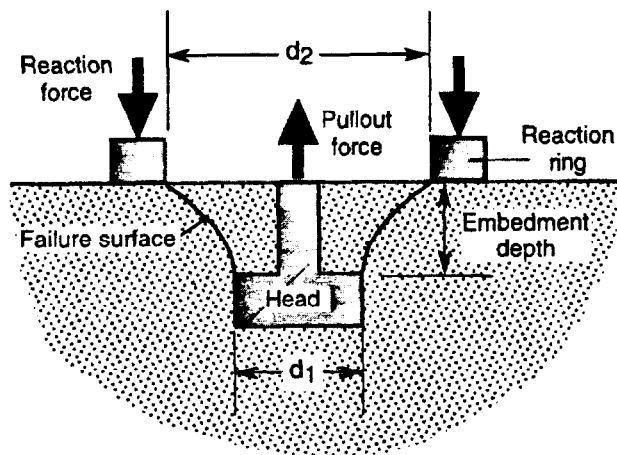


FIGURE 19.5 Schematic of cast-in-place pullout test.

19.2.5 Pullout Test

The cast-in-place pullout test is one of the most reliable techniques for estimating the in-place strength of concrete during construction. In this method, an insert with an enlarged head is cast in the concrete. The insert and the accompanying conical fragment of concrete are extracted by using a tension-loading device reacting against a bearing ring that is concentric with the insert (Figure 19.5). The force required to pull out the insert is an indicator of concrete strength. A comprehensive review of the history and theory of the pullout test is available [Carino, 1991b], and only a brief summary is provided here.

19.2.5.1 History

Ideas for pullout tests originated in the Soviet Union [Skramtajev, 1938]. Tremper (1944) was the first American to report on the correlation between pullout force and companion cylinder strength. An insert developed by Volf (of the Soviet Union) and the one used by Tremper are

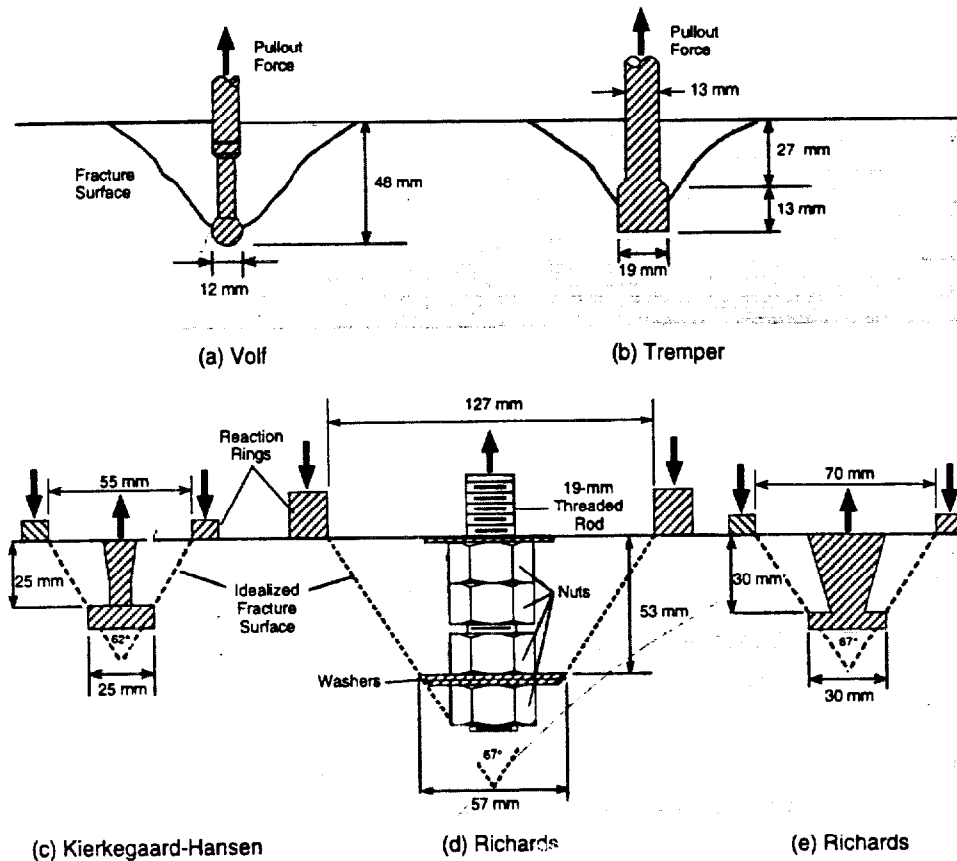


FIGURE 19.6 Various pullout test configurations.

shown in Figures 19.6a and 19.6b, respectively. In both cases, the reaction to the pullout force was applied sufficiently far from the insert that there was negligible interaction between the failure surface and the reaction system. As a result, failure was controlled primarily by the tensile strength of the concrete. This explains why Tremper found that the correlation between pullout force and compressive strength was nonlinear.

Despite Tremper's encouraging results, there was no additional documented work on the pullout test until 1962, when a comprehensive study began in Denmark [Kierkegaard-Hansen, 1975]. The objective was to find the optimum geometry for a field test system that would have a high correlation between pullout load and the compressive strength of concrete. Kierkegaard-Hansen found that the correlation could be improved by constraining the failure surface to follow a predefined path by using a relatively small-diameter reaction ring. The study resulted in the pullout test configuration shown in Figure 19.6c, which was eventually incorporated into the Lok-Test⁴ system, the most widely used commercial pullout test system.

Owen Richards, a materials consultant in the United States, carried out independent studies of a pullout test in the late 1960s and early 1970s. The early version of Richards' pullout test configuration was larger than that developed in Denmark. The inserts were manufactured from 19-mm threaded rods, and washers were used to provide the enlarged head. Nuts were used to add

⁴As explained by Kierkegaard-Hansen (1975), failure when a small reaction ring is used can be considered a punching type of failure. The Danish word for "punching" is *lokning*, so the term *lok-strength* was used to describe the strength measured by the test.

rigidity to the washers and to fix the embedment depth of the washers. The test geometry, which is shown in Figure 19.6d, resulted in an idealized failure surface with an area approximately equal to the area of a standard 152-mm diameter cylinder. Richards preferred to divide the pullout force by the nominal area of the idealized failure to obtain a pullout strength, which was a fictitious quantity because the pullout force was inclined to the surface area.

The first reported pullout tests using Richards' early system were performed at the Bureau of Reclamation [Rutenbeck, 1973]. Strong correlation was obtained between pullout tests performed on slabs and the compressive strength of companion cylinders. Good correlation between pullout strength and compressive strength was also obtained when the inserts were placed in shotcrete panels and compression specimens were cut from the panels. In 1975, Malhotra also reported on the applicability of Richards' pullout test [Malhotra, 1975]. It was found that the coefficient of variation for three replicate tests was less than 5%, which was very encouraging. In a later study [Malhotra and Carette, 1980], it was noted that similar correlations were obtained in different investigations of Richards' system.

Richards' pullout system produced encouraging results, but the large size of the insert required heavy testing equipment and produced significant surface damage. In 1977, a smaller version of the test system was introduced [Richards, 1977], as shown in Figure 19.6e. The apex angle of the conic frustum was maintained at 67° , but the insert was constructed from one piece of steel. The enlarged end of the shank accommodated a pull-rod that passed through a center-hole tension ram.

In the early 1960s, investigations of the pullout test were also conducted in Great Britain [Te'eni, 1970], but the work was apparently never carried to the stage of a practical field test system. A novel feature of the British work was the use of a power function for the correlation equation, rather than a straight line as had been used in Denmark, the United States, and Canada.

The usefulness of the pullout test for evaluating early-age strength was quickly recognized. In 1978, ASTM adopted a tentative test method for the pullout test (C 900-78T). In North America, J. Bickley became an early advocate of the pullout test method for achieving construction safety and economy [Bickley, 1982a].

19.2.5.2 Failure Mechanism

Ever since the test was first described by Skramtajev (1938), there has been an incomplete understanding of its failure mechanism. Skramtajev correctly noted that the tests subjects the concrete to a combination of tensile and shearing stresses. Kierkegaard-Hansen (1975), the inventor of the widely used Lok-Test system, tried to relate the shape of the extracted conical fragment to the intact cones often observed at the ends of cylinders tested in compression. Jensen and Braestrup (1976) used plasticity theory to relate the ultimate pullout force to the compressive strength of the concrete. Malhotra and Carette (1980) proposed that the pullout strength was related to the direct shear strength of concrete. Recent experimental and analytical studies have tried to gain a better understanding of the failure process during the pullout test [Ottosen, 1981; Stone and Carino, 1983; Yener, 1994; Ballarini et al., 1986; Krenchel and Shah, 1985; Hellier et al., 1987; Krenchel and Bickley, 1987].

From these independent analytical and experimental studies, it is now understood that the pullout test subjects the concrete to a nonuniform, three-dimensional state of stress. It also has been demonstrated that the failure process involves two circumferential crack systems: a stable system that starts at the insert head at about 1/3 of the ultimate load, propagates into the concrete at a large apex angle, and is arrested as it reaches a tension-free region; and a second system that propagates with increasing load and eventually defines the shape of the extracted cone. Figure 19.7 shows these cracking systems as predicted by Hellier et al. (1987) who used a discrete cracking, finite-element model based on nonlinear fracture mechanics.

Despite general agreement on the cracking process prior to the attainment of ultimate pullout load, there is no consensus on the failure mechanism at the ultimate load. Some believe that ultimate load occurs as a result of compressive failure along a strut running from the bottom of the bearing ring to the insert head [Ottosen, 1981; Krenchel and Shah, 1985; Krenchel and Bickley,

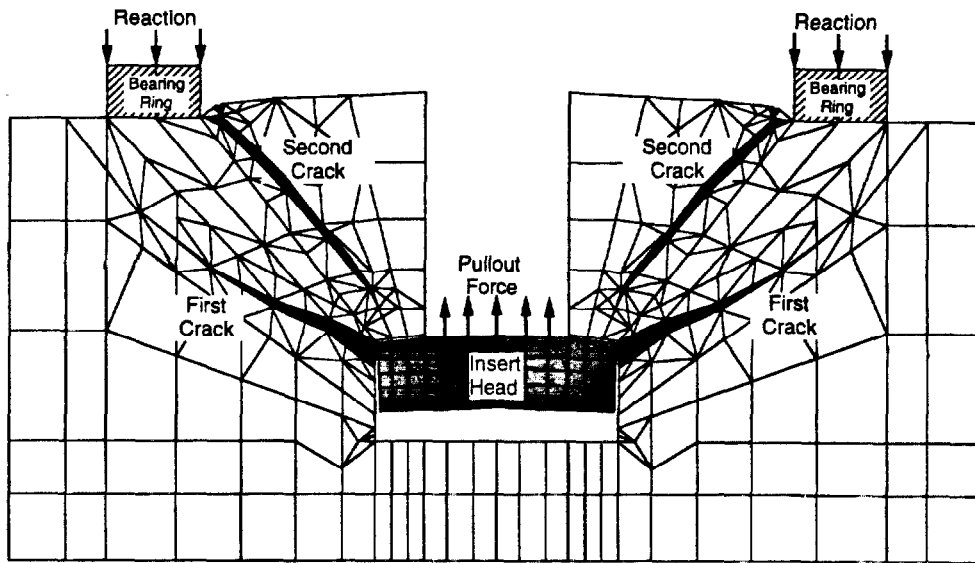


FIGURE 19.7 Crack systems formed during pullout test as predicted from finite-element fracture analysis [Hellier et al., 1987].

1987]. This mechanism has been used to explain the good correlation between pullout strength and compressive strength. Others believe that failure is governed by aggregate interlock across the secondary crack system, and the ultimate load is reached when sufficient aggregate particles have been pulled out of the mortar matrix [Stone and Carino, 1983; Hellier et al., 1987]. In this case, it is argued that there is correlation between pullout strength and compressive strength because both properties are controlled by the tensile strength of the mortar. In the compression test, the ultimate load is associated with the formation and growth of microcracks through the mortar.

While there is no agreement on the exact failure mechanism, it has been shown that the pullout strength has good correlation with the compressive strength of concrete and that the test has good repeatability. In a review of published data, ACI Committee 228 recommends a coefficient of variation (standard deviation divided by the mean) of 8% for the pullout test [ACI 228.1R, 1995]. Recent modifications of ASTM C 900 require a minimum of five individual pullout tests for each 115 m³ of concrete in a given placement.

19.2.5.3 Post-Installed Tests

A drawback of the standard pullout test is that the locations of the inserts have to be planned in advance of concrete placement and the inserts have to be fastened to the formwork. This limits the applicability of the standard method to new construction. In an effort to extend the application of pullout testing to existing structures, various techniques for performing post-installed pullout tests have been investigated. Some of the more promising approaches are shown in Figure 19.8. However, none of these methods have been standardized by ASTM.

During the 1970s, a need arose in the United Kingdom for in-place tests to evaluate distressed concrete structures built with high alumina cement. Researchers at the Building Research Establishment (BRE) developed a pullout technique using commercial anchor bolts, as shown in Figure 19.8a [Chabowski and Bryden-Smith, 1980]. A 6-mm diameter hole is drilled into the concrete and an anchor bolt is inserted so that the split-sleeve is at a depth of 20 mm. After applying an initial load to expand and engage the sleeve, the bolt is pulled out and the maximum load during the extraction is recorded. Because of the shallow embedment, failure occurs by concrete fracture. Reaction to the

pullout load is provided by three feet located along the perimeter of a 80-mm diameter ring. As the bolt is pulled, the sleeve imparts vertical and horizontal forces to the concrete. Hence the fracture surface differs from that in the cast-in-place (CIP) pullout test, and the test has been called an internal fracture test rather than a pullout test. The correlation between ultimate load and compressive strength was found to have a pronounced nonlinearity, indicating that the failure mechanism was probably related to the tensile strength of the concrete. Within-test variability was found to be greater than the CIP pullout test, and the 95% confidence limits of the correlation relationship were found to range between $\pm 30\%$ of the mean curve [Chabowski and Bryden-Smith, 1980]. The relatively low precision of the internal fracture test has been attributed to two principal causes [Bungey, 1981]: (1) the variability in the hole drilling and test preparation; and (2) the influence of aggregate particles on the load-transfer mechanism and the failure-initiation load.

Mailhot et al. (1979) also investigated the feasibility of several post-installed pullout tests. One of these used a split-sleeve and a tapered bolt assembly that was placed in a 19-mm diameter hole drilled into the concrete. As shown in Figure 19.8b, the details differ from the BRE method because the reaction to the pulling force acts through a specially designed high-strength, split-sleeve assembly. Thus the force transmitted to the concrete is predominantly a lateral load because the tapered bolt forces the sleeve to expand laterally. It is likely that failure occurs by indirect tensile splitting, similar to that in a standard splitting-tension test. As with the BRE test, the variability of this test was reported to be rather high. Another successful method involved epoxy-grouting a 16-mm diameter threaded rod into a 19-mm hole to a depth of 38 mm. After the epoxy had cured, the rod was pulled using a tension jack reacting against a bearing ring. This method was also reported to have high variability. The study concluded that these two methods had the potential for assessing the strength in existing construction. However, additional research was recommended to enhance their reliability.

Domone and Castro (1986) also developed a technique similar to the expanding sleeve method shown in Figure 19.8b. However, a torque meter was used to apply the load, and the embedment

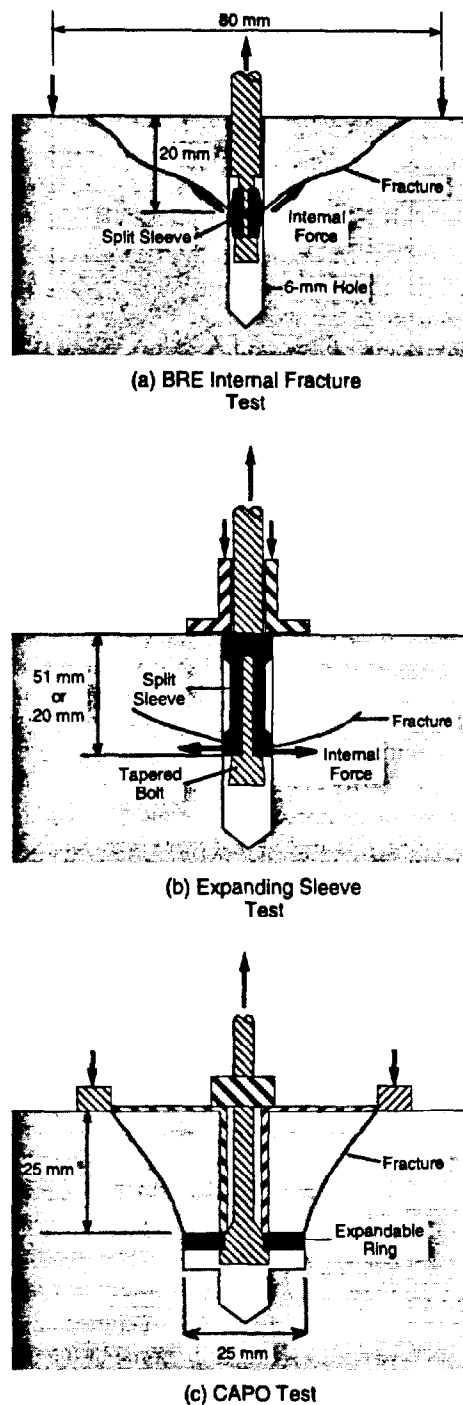


FIGURE 19.8 Examples of post-installed "pullout tests."

was 20 mm as in the BRE method. On the basis of a limited number of tests, it was concluded that this method gave better correlations than the BRE method.

Another method was developed by the manufacturer of the Lok-Test⁵ system and is referred to as the CAPO test (for cut and pullout) [Petersen, 1984]. The method involves drilling a 18-mm diameter hole into the concrete and using a special milling tool to undercut a 25-mm diameter slot at a depth of 25 mm. An expandable ring is placed in the hole, and the ring is expanded using special hardware. Figure 19.8c shows the ring after expansion. The entire assembly used to expand the ring is pulled out of the concrete using the same loading system as for a CIP pullout test. Unlike the methods discussed above, the CAPO test subjects the concrete to a similar state of stress as the CIP pullout test. The performance of the CAPO test in laboratory evaluations has been reported to be similar to the Lok-Test [Petersen, 1984]. Users of the CAPO test have indicated that the test is cumbersome to perform and care is needed to control the variability.⁶ The test surface must be flat and perpendicular to the drilled hole. If these conditions are not achieved, the bearing ring will not seat properly and test results will be erratic.

19.2.6 Break-Off Test

This test measures the force required to break off a cylindrical core from the concrete mass. The method was developed in the early 1970s by R. Johansen at the Cement and Concrete Research Institute in Norway. In cooperation with contractors, Johansen sought a simple, inexpensive, and robust method to measure in-place strength [Johansen, 1977, 1979]. The test method was standardized by ASTM in 1990 (ASTM C 1150). Naik (1991) provides a comprehensive review of research results.

Figure 19.9 is a schematic of the break-off test. For new construction, the core is formed by inserting a plastic sleeve into the fresh concrete. When the in-place strength is to be estimated, the sleeve is removed. Then a special, hand-operated, hydraulic loading jack is placed into the counterbore, and a force is applied to the top of the core until it ruptures from the concrete mass. The hydraulic fluid pressure is monitored with a pressure gage, and the maximum pressure gage reading in units of bars (1 bar = 0.1 MPa) is referred to as the break-off number of the concrete.

For new construction, the sleeves are inserted into the top surface of the member after the concrete has been leveled. Alternatively, the sleeves can be attached to the sides of the formwork and filled during concrete placement. For existing construction, a special drill bit can be used to cut the core and the counterbore.

For ease of sleeve insertion into the fresh concrete, the concrete must be workable. In addition, to minimize interference, the maximum aggregate size should be limited to a fraction of the sleeve diameter, which is 55 mm. According to ASTM C 1150, the break-off test is not recommended for concrete having a maximum nominal aggregate size greater than 25 mm. Sleeve insertion must be performed carefully to assure good compaction around the sleeve and a minimum of disturbance at the base of the formed core. Some problems have been reported with keeping the sleeves from floating out of very fluid concrete mixtures [Naik et al., 1987]

The break-off test subjects the concrete to a slowly applied force and measures a static strength property of the concrete. The core is loaded as a cantilever, and the concrete at the base of the core is subjected to a combination of bending and shearing stresses. In early work [Johansen, 1977, 1979], break-off strength was reported as a stress, arrived at by computing the flexural stress at the base of the core corresponding to the rupture force. In later applications (see review by Naik, 1991), the flexural strength was not computed, and the break-off number (pressure gage reading) was related

⁵Certain trade names and company products are mentioned to identify specific test equipment. In no case does such identification imply recommendation or endorsement by the National Institute of Standards and Technology, nor does it imply that the products are necessarily the best available for the purpose.

⁶Read, P.H., Bickley, J.A., and Omran, R. Simulated Field Trials. Draft Report for Strategic Highway Research Program (SHRP) Contract 88-C204. January, 1991.

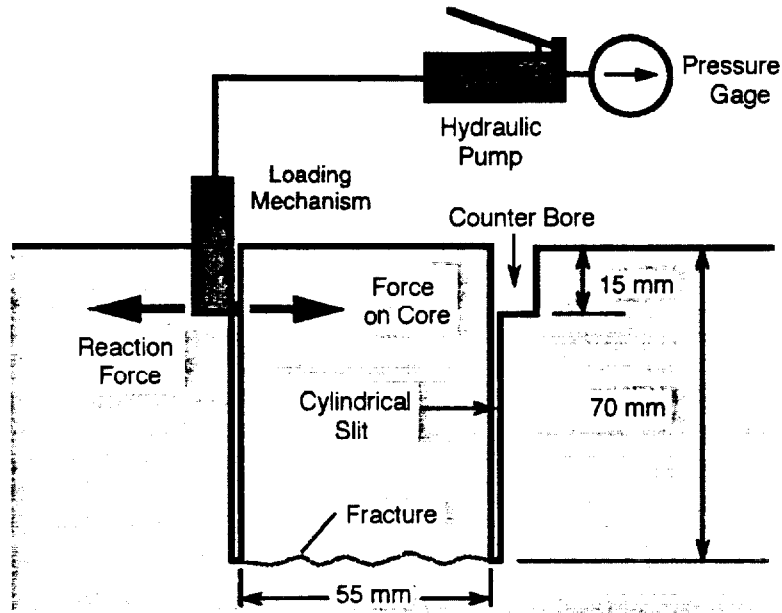


FIGURE 19.9 Schematic of break-off test.

directly to compressive strength. This approach simplifies data analysis, but calibration of the test instrument used in the field is mandatory to assure that the gage readings correspond to the actual forces applied to the test specimen.

The correlations between break-off strength and compressive strength have been found to be nonlinear [Johansen, 1977 and 1979; Barker and Ramirez, 1988], which is in accordance with the usual practice of relating the modulus of rupture of concrete to the square root of compressive strength. It has also been found that the correlation between break-off strength and modulus of rupture may be more uncertain than that between break-off strength and compressive strength [Barker and Ramirez, 1988].

Failure during the break-off test occurs by fracture at the base of the 55-mm diameter core. The crack initiates at the most highly stressed point. It then propagates through the mortar and, in most cases, around coarse aggregate particles located at the base of the core. The particular arrangement of aggregate particles within the failure region would be expected to affect the ultimate load in each test. Because of the relatively small size of the core and the heterogeneous nature of concrete, the distribution of aggregate particles will be different at each test location. Hence one would expect the within-test variability of the break-off test to be higher than that of other standard strength tests that involve larger test specimens. One would also expect that the variability might be affected by maximum aggregate size and aggregate shape. The developer of the break-off test reported a within-test coefficient of variation of about 9% [Johansen, 1979]. This value has, in general, been confirmed by other investigators [Carino, 1992a].

19.2.7 Maturity Method

The **maturity method** is a technique for estimating the strength development of concrete during its curing period by measuring the temperature history of the concrete. Carino (1991a) provides a comprehensive review of the history of the method and some of its applications.

Historically, the maturity method was not classified as a nondestructive test method, but it is now regarded as a useful technique for estimating in-place strength. Its origin can be traced to a

series of papers from England dealing with accelerated curing methods [McIntosh, 1949; Nurse, 1949; Saul, 1951]. There was a need for a procedure to account for the combined effects of time and temperature on strength development for different elevated-temperature curing processes. It was proposed that the product of time and temperature could be used for this purpose. These ideas led to the famous **Nurse-Saul maturity function**:

$$M = \sum_0^t (T - T_0) \Delta t \quad (19.1)$$

where

- M = maturity index, degree Celcius-hours (or degree Celcius-days)
- T = average concrete temperature, degree Celcius, during the time interval Δt
- T_0 = datum temperature (usually taken to be) 10°C
- Δt = time interval

The index computed by Eq. (19.1) was called the **maturity**; however, the current terminology is the **temperature-time factor** [ASTM C 1074]. Saul (1951) presented the following principle, which has become known as the **maturity rule**:

Concrete of the same mix at the same maturity (reckoned in temperature-time) has approximately the same strength whatever combination of temperature and time go to make up that maturity.

Equation (19.1) is based on the assumption that the rate of strength gain is a linear function of temperature; it was soon realized that this approximation may not be valid when curing temperatures vary over a wide range. As a result, a series of alternatives to the Nurse-Saul function were proposed by other researchers [Malhotra, 1971]. However, none of the alternatives received widespread acceptance, and the Nurse-Saul function was used worldwide until an improved function was proposed in the 1970s.

In 1977, a new function was proposed to compute a maturity index from the recorded temperature history of the concrete [Freiesleben Hansen and Pedersen, 1977]. This function was based on the Arrhenius equation [Brown and LeMay, 1988] that is used to describe the effect of temperature on the rate of a chemical reaction. The new function allowed the computation of the equivalent age of concrete as follows:

$$t_e = \sum_0^t e^{-\frac{E}{R}(\frac{1}{T} - \frac{1}{T_r})} \Delta t \quad (19.2)$$

where

- t_e = the equivalent age at the reference temperature
- E = apparent activation energy, J/mol
- R = universal gas constant, 8.314 J/mol-K
- T = average absolute temperature of the concrete during interval Δt , degrees Kelvin
- T_r = absolute reference temperature, degrees Kelvin

By using Eq. (19.2), the actual age of the concrete is converted to its equivalent age, in terms of strength gain, at the reference temperature. In European practice, the reference temperature is usually taken to be 20°C , whereas in North American practice it is usually assumed to be 23°C . The introduction of this function overcame one of the main limitations of the Nurse-Saul function (Eq. (19.1)) because it allowed for a nonlinear relationship between the rate of strength development and curing temperature. This temperature dependence is described by the value of the apparent

activation energy. Comparative studies in the early 1980s showed that this new maturity function was superior to the Nurse-Saul function [Byfors, 1980; Carino, 1982].

19.2.7.1 Effect of Temperature on Strength Gain

The key parameter in Eq. (19.2) is the “**activation energy**” which describes the effect of temperature on the rate of strength development. In the early 1980s, the author began a series of studies to gain a better understanding of the maturity method [Carino, 1984]. From this work, a procedure was developed to obtain the activation energy of a given cementitious mixture. The procedure is based on determining the effect of curing temperature on the rate constant for strength development. The rate constant is related to the curing time needed to reach a certain fraction of the long-term strength, and it is obtained by fitting an appropriate equation to the strength-versus-age data acquired under constant temperature (isothermal) curing. The procedure to determine the activation energy consists of the following steps:

- Cure mortar specimens at different constant temperatures.
- Determine compressive strengths at regularly spaced ages.
- Determine the value of the rate constant at each temperature by fitting a strength-age relationship to each set of strength-age data.
- Determine the best-fit Arrhenius equation (to be explained) to represent the variation of the rate constant with the temperature.

By using the above procedure, the activation energy was determined for concrete and mortar specimens made with different cementitious materials [Tank and Carino, 1991; Carino and Tank, 1992]. It was found that for concrete with a water-cement ratio (W/C) of 0.45, the activation energy ranged from 30 and 64 kJ/mol; while for a W/C of 0.60 it ranged from 31 to 56 kJ/mol, depending on the type of cement and additives.

The significance of the activation energy is explained further here. In Eq. (19.2), the exponential term within the integral converts increments of actual curing time at the concrete temperature to equivalent increments at the reference temperature. Thus the exponential term can be considered as an **age conversion factor**, γ :

$$\gamma = e^{\frac{-E}{R}(\frac{1}{T} - \frac{1}{T_r})} \quad (19.3)$$

Figure 19.10 shows how the age conversion factor varies with curing temperature for different values of the activation energy. The reference temperature is taken as 23°C. It is seen that for an activation energy of 30 kJ/mol, the age conversion factor is nearly a linear function of temperature. In this case, the Nurse-Saul equation would be a reasonably accurate maturity function to account for the combined effects of time and temperature, because the Nurse-Saul function assumes that the rate constant varies linearly with temperature [Carino, 1984]. For an activation energy of 60 kJ/mol, the age conversion factor is a highly nonlinear function of the curing temperature. In this instance, the Nurse-Saul function would be an inaccurate maturity function. In summary, Figure 19.10 shows the nature of the error in an age conversion factor if the incorrect value of activation energy were used for a particular concrete mixture. The magnitude of the error would increase with increasing difference of the curing temperature from 23°C.

The reader will have noticed that the term activation energy was introduced within quotation marks. This is because the E -value that is determined when the rate constant is plotted as a function of the curing temperature is not truly an activation energy as implied by the Arrhenius equation. The following discussion is provided for those unfamiliar with the concept of activation energy or the origin of the Arrhenius equation.

The idea of activation energy was proposed by Svante Arrhenius in 1888 to explain why chemical reactions do not occur instantaneously when reactants are brought together, even though the

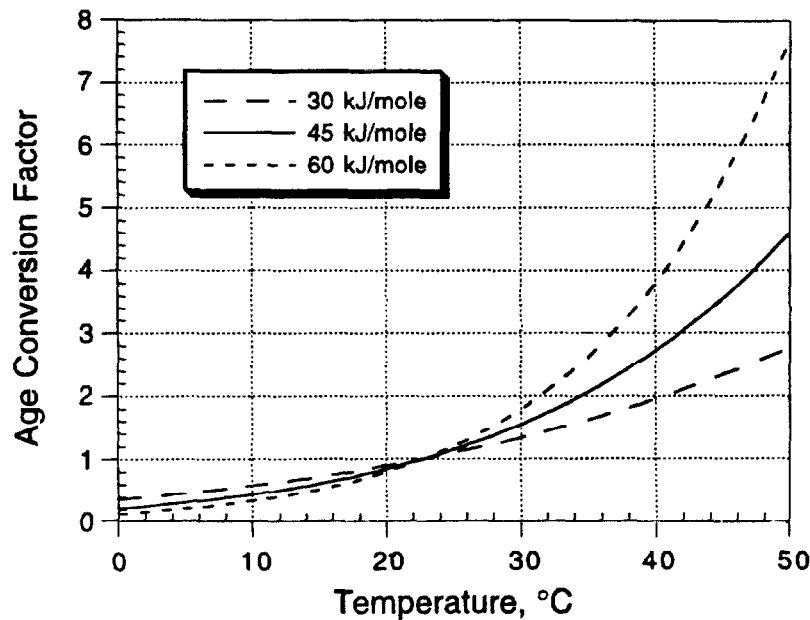


FIGURE 19.10 Effect of activation energy value on the age conversion factor.

reaction products are at a lower energy state [Brown and LeMay, 1988]. Arrhenius proposed that before the lower energy state is achieved, the reactants must have sufficient energy to overcome an energy barrier that separates the unreacted and reacted states. A physical analogy is a brick standing upright. The brick will not instantaneously tip over to its lower, horizontal, energy state. It must be pushed from the higher to the lower energy state. The energy required to push the brick from its upright position to the point of instability, after which the brick falls on its own, is the activation energy for this process.

For molecular systems, the reactant molecules are in constant motion and energy is transferred between them as they collide [Brown and LeMay, 1988]. A certain number of molecules will acquire sufficient energy to surmount the energy barrier and form the lower energy reaction product. As the system is heated, the kinetic energy of the molecules increases and more molecules will surmount the barrier. Thus the rate of reaction increases with increasing temperature. Arrhenius observed that the rate constant, k , of many reactions increased with temperature according to what has since been called the Arrhenius equation, as follows:

$$k = Ae^{-\frac{E}{RT}} \quad (19.4)$$

The term A is called the **frequency factor** and is related to the frequency of collisions and the probability that the molecules will be favorably oriented for reaction [Brown and LeMay, 1988]. It can be seen that the age conversion factor given by Eq. (19.2) is simply the ratio of the rate constants at two different temperatures.

The Arrhenius equation was derived empirically from observations of homogeneous chemical systems undergoing a single reaction. Roy and Idorn (1982) have noted that researchers "... have cautioned that since cement is a multiphase material and also the process of cement hydration is not a simple reaction, homogeneous reaction kinetics cannot be applied." Thus the activation energy obtained from strength-gain data or degree of hydration data is not a true activation energy as originally proposed by Arrhenius.

The author believes that the Arrhenius equation happens to be one of several equations that can be used to describe the variation of the rate constant for strength gain (or degree of hydration) with curing temperature. This has been the motivation for proposing a simpler function than Eq. (19.2) to compute equivalent age [Carino, 1982; Tank and Carino, 1991; Carino and Tank, 1992]. It is suggested that the temperature dependence of the rate constant for strength gain can be represented by the following:

$$k = A_0 e^{BT} \quad (19.5)$$

where

- A_0 = the value of the rate constant at 0°C
- B = temperature sensitivity factor, 1/°C
- T = concrete temperature degrees Celcius.

Using Eq. (19.5), the equation for equivalent age at the reference temperature T_r is as follows:

$$t_e = \sum_0^t e^{B(T-T_r)} \Delta t \quad (19.6)$$

where

- B = temperature sensitivity factor, 1/°C
- T = average concrete temperature during time interval Δt , degrees Celcius
- T_r = reference temperature, degrees Celcius.

It was shown that Eqs. (19.2) and (19.6) would result in similar values of equivalent age [Carino, 1992a]. However, the author believes Eq. (19.6) has the following advantages over Eq. (19.2):

- The temperature sensitivity factor, B , has more physical significance compared with the apparent activation energy: for each temperature increment of $1/B$, the rate constant for strength development increases by a factor of approximately 2.7.
- Temperatures do not have to be converted to the absolute scale.
- Equation (19.6) is a simpler equation.

19.2.7.2 Strength Development Relationships

The key to developing an accurate maturity function for a particular concrete mixture is to determine the variation of the rate constant with curing temperature. Strictly speaking, a rate constant represents the rate at which a chemical reaction occurs at a given temperature. However, in the context of this discussion, the rate constant is related to the rate of strength gain at a constant temperature, and it can be obtained from the equation of strength gain versus age. Thus it is necessary to consider some of the relationships that have been used to represent the strength development of concrete.

The author has successfully used the following hyperbolic equation for strength gain up to equivalent ages at 23°C of about 28 d:

$$S = S_u \frac{k(t - t_0)}{1 + k(t - t_0)} \quad (19.7)$$

where

- S = strength at age t , d
- S_u = "limiting" strength
- k = rate constant, 1/d
- t_0 = age at start of strength development, d

The basis of this equation has been explained elsewhere [Carino, 1984; Knudsen, 1980]. This model assumes that strength development begins instantaneously at age t_0 . Thus the gradual strength development during the setting period is not considered. The parameters S_u , k , and t_0 are obtained by least-squares curve fitting to strength versus age data. The limiting strength, S_u , is the asymptotic value of the strength for the hyperbolic function that fits the data. As will be discussed below, the best-fit value for S_u does not necessarily represent the actual long-term strength of the concrete, and that is why the quotation marks were used in the definition following Eq. (19.7). For the hyperbolic model, the rate constant has the following property: when the age beyond t_0 is equal to $1/k$, the strength equals 50% of the limiting strength, S_u .

An equation similar to Eq. (19.7) was also used by Knudsen (1980) and Geiker (1983) to represent the degree of hydration and development of chemical shrinkage as a function of age. However, Geiker (1983) noted that Eq. (19.7) gave a poor fit for certain cementitious systems. It was found that the following version of the hyperbolic equation gave a better fit to that data than Eq. (19.7) [Knudsen, 1984]:

$$S = S_u \frac{\sqrt{k(t - t_0)}}{1 + \sqrt{k(t - t_0)}} \quad (19.8)$$

Knudsen explained the differences between Eq. (19.7) and (19.8) in terms of the hydration kinetics of individual cement particles. Equation (19.7) is based on **linear kinetics**, which means that the degree of hydration of an individual cement particle is a linear function of the product of time and the rate constant. Equation (19.8) is based on **parabolic kinetics** which means that the degree of hydration is a function of the **square root** of the product of time and the rate constant. Thus Eqs. (19.7) and (19.8) are called the **linear hyperbolic** and **parabolic hyperbolic** models.

Friesleben Hansen and Pedersen (1985) proposed the following exponential equation to represent the strength development of concrete:

$$S = S_u e^{-(\frac{t}{\tau})^\alpha} \quad (19.9)$$

where

- τ = a time constant
- α = a shape parameter

This equation can model the gradual strength development occurring during the setting period, and it is also asymptotic to a limiting strength. The time constant τ represents the age at which the strength has reached $0.37S_u$. Thus the value of $1/\tau$ is the rate constant for this equation. The shape parameter α affects the slope of the curve during the acceleratory period (following the induction period⁷), and it affects the rate at which the strength approaches the limiting strength.

Figure 19.11 illustrates the performance of these models in representing actual strength development data. Figure 19.11a shows strength data for mortar cubes cured at room temperature and tested at ages from 0.4 to 56 d. Figure 19.11b shows data for standard-cured concrete cylinders tested at ages from 7 d to 3.5 y [Carette and Malhotra, 1991]. The curves are the best-fit curves for Eqs. (19.7), (19.8), and (19.9). For the mortar data, the linear hyperbolic function and the exponential function fit the data well, and these curves in Figure 19.11a are nearly indistinguishable. For the concrete data, the parabolic hyperbolic function and the exponential function fit the data well and these curves cannot be distinguished in Figure 19.11b.

⁷After cement and water are mixed together, there is a time delay before strength development begins. This period, is called the *induction period*. After the induction period, there is rapid strength development, and this is the *acceleratory period*.

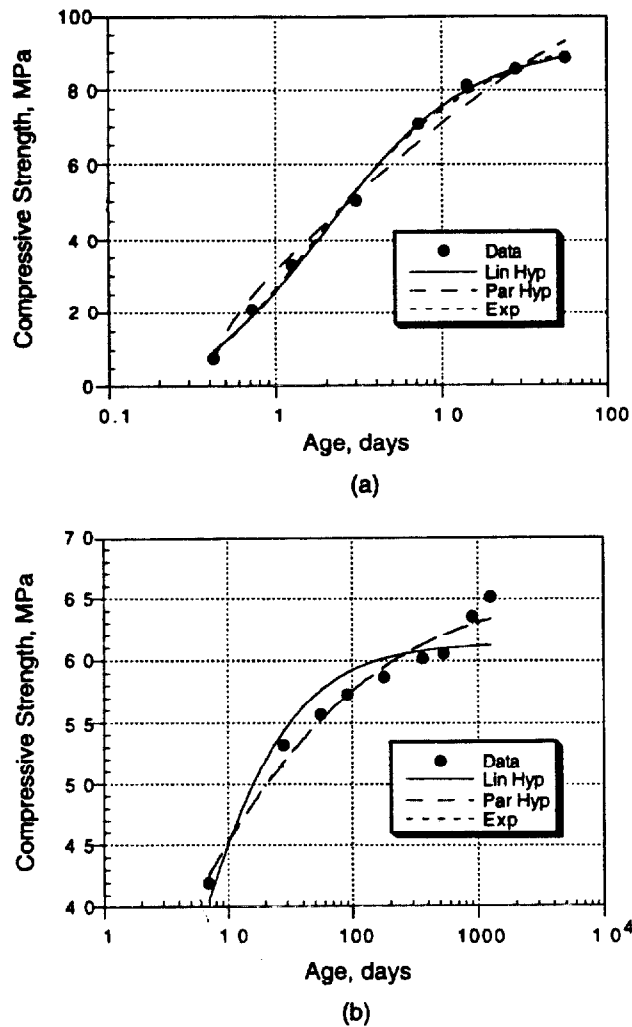


FIGURE 19.11 Fit of strength-age models to data: (a) mortar cubes and (b) concrete cylinders.

The results shown in Figure 19.11 highlight the capabilities of the various strength-age functions. The linear hyperbolic function appears to be a good model for strength development up to about 28 d (equivalent age) but not for later-ages. The parabolic hyperbolic model appears to be better suited for modeling later-age strength gain. The exponential model appears to be capable of modeling strength gain over the full spectrum of ages.

The inherent limitation of the linear hyperbolic function can be understood by considering the ratio of the limiting strength to the 28-day strength. If the t_0 term in Eq. (19.7) is neglected, the following equation is obtained for this ratio:

$$\frac{S_u}{S_{28}} = \beta = 1 + \frac{1}{28k} \quad (19.10)$$

Thus the value of β is directly related to the rate constant. A higher-value k results in a lower value of β , which means a smaller difference between the limiting strength and the 28-day strength. The

rate constant is, in turn, controlled primarily by the initial rate of strength development. The fact is that the ratio of the actual long-term strength of concrete to the 28-day strength does not obey Eq. (19.10). This means that values of S_u obtained by fitting the linear hyperbolic model to strength-age data will be lower than the actual long-term strength of concrete if it is allowed to cure for a long time.

On the basis of the above discussion, one might conclude that the exponential model given by Eq. (19.9) is the best model to use for determining the rate constant at a particular curing temperature. This would be correct if the shape parameter, α , were independent of the curing temperature. Recent test results show that this is not always the case [Carino et al., 1992]. Thus a maturity function based solely upon the variation of the rate constant ($1/\tau$) with temperature would not be able to account accurately for the combined effects of time and temperature on strength development.

Which strength-gain model should be used? The maturity method is typically used to monitor strength development during construction. Therefore it is not necessary to accurately model the strength gain at later ages. Thus the author believes that the linear hyperbolic model can be used to analyze strength data, up to 28-day equivalent age, to determine the variation of the rate constant with curing temperature. Knudsen⁸ suggests that the linear hyperbolic model is suitable up to a degree of hydration of 85%. The suitability of the linear hyperbolic model was also demonstrated in a recent study on the applicability of the maturity method to mortar mixtures with low ratios of water to cementitious materials, typical of those in high-performance concrete [Carino et al., 1992].

19.2.7.3 Estimating Strength

The final discussion deals with estimating strength by the maturity method. The maturity method is generally used to estimate the in-place strength of concrete by using the in-place maturity index and a previously established relationship between maturity index and strength. This assumes that a given concrete possesses a unique relationship between strength and the maturity index. This assumption would be acceptable if the long-term strength of concrete were independent of the curing temperature, but this is not the case. It is known that the long-term strength is affected by the initial temperature of the concrete. Thus if the same concrete mixture were used for a cold-weather placement and a hot-weather placement, the strength would not be the same for a given maturity index. It is proposed that the correct application of the maturity method is to estimate relative strength. Tank and Carino (1991) proposed the following rate constant model of relative strength development in terms of equivalent age:

$$\frac{S}{S_u} = \frac{k_r(t_e - t_{0r})}{1 + k_r(t_e - t_{0r})} \quad (19.11)$$

where

k_r = value of the rate constant at the reference temperature

t_{0r} = age at start of strength development at the reference temperature

However, the previous discussion has shown that, for the linear hyperbolic model, the ratio S/S_u may not indicate the true fraction of the long-term strength because the calculated value of S_u may not be the actual long-term strength. This deficiency can be overcome by expressing relative strength as a fraction of the strength at an equivalent age of 28 d. By using the definition of β in Eq. (19.10), the relative strength gain equation would be as follows:

$$\frac{S}{S_{28}} = \beta \frac{k_r(t_e - t_{0r})}{1 + k_r(t_e - t_{0r})} \quad (19.12)$$

The value of β would be obtained by fitting Eq. (19.7) to data of strength versus equivalent age.

⁸T. Knudsen, the Technical University of Denmark, April 1985, personal communication.

Then the value of S_u is divided by the estimated strength, from the best-fit curve, at an equivalent age of 28 d.

To summarize, the following points represent the author's ideas about the maturity method:

- There is no single maturity function that is applicable to all concrete mixtures. The applicable maturity function for a given concrete can be obtained by determining the variation of the rate constant with the curing temperature.
- The linear hyperbolic function can be used to analyze strength-age data to obtain the rate constants at different curing temperatures.
- Equation (19.5) can be used to represent the variation of the rate constant with curing temperature. The temperature-sensitivity factor governs the rate at which the rate constant increases with temperature and is analogous to the activation energy in the Arrhenius equation.
- The equivalent age can be calculated from the temperature history using Eq. (19.6).
- The maturity method is more reliable for estimating relative strength development than for estimating absolute strength.

19.2.8 Statistical Methods

In 1983, the ACI Code recognized in-place test methods as alternatives to testing field-cured cylinders for assessing concrete strength during construction. The following sentence was added to Section 6.2.1.1, dealing with form removal, of the 1983 Code⁹:

“Concrete strength data may be based on tests of field-cured cylinders or, when approved by the Building Official, on other procedures to evaluate concrete strength.”

The Commentary to the Code listed acceptable alternative procedures and further stated that these alternative methods “require sufficient data using job materials to demonstrate correlation of measurements on the structure with compressive-strength of molded cylinders or drilled cores.” Thus, to use the alternative methods, an empirical relationship has to be developed to convert in-place test results to equivalent compressive-strength values. In addition, a procedure is needed to analyze in-place test results so that compressive strength can be estimated with a high degree of confidence. The latter issue is not mentioned in the Code.

The report of ACI Committee 228 [ACI 228.1R, 1995] provides information on developing the **strength relationship**¹⁰ and how it is used to estimate the in-place strength. Basically, the procedure is to perform in-place tests (X values) and standard compressive strength tests (Y values) on companion specimens at different levels of strength and use regression analysis to determine a best-fit curve ($Y = f(X)$) to the data. The relationship and the results of in-place tests on the structure are used to estimate the concrete strength in the structure. In order to obtain a reliable estimate of the in-place strength, statistical methods are needed to account for the various sources of uncertainty. The procedures that can be used for this purpose are reviewed in this section after a brief review of recent developments related to statistical analysis.

19.2.8.1 Background

During the 1960s and 1970s, the traditional method of ordinary least squares (OLS) analysis was used to analyze correlation data and establish the best-fit equation for the strength relationship

⁹*Building Code Requirements for Reinforced Concrete*, ACI 318-83. American Concrete Institute, Farmington Hills, MI.

¹⁰The term “strength relationship” refers to the empirical equation, obtained from a correlation testing program, that relates the compressive strength (or other measure of strength) of concrete to the quantity measured by the in-place test.

and its confidence limits [Natrella, 1963]. In the 1980s, simple procedures were used to estimate lower confidence limits of estimated in-place strength [Bickley, 1982b; Hindo and Bergstrom, 1985]. However, it was recognized that the existing methods were not statistically rigorous and the stated confidence levels were not accurate [Stone et al., 1986]. One of the major deficiencies in using OLS to establish the strength relationship is that OLS assumes the X variable (the in-place test result) has no measurement error. In fact, the within-test coefficient of variation of in-place tests can be two to three times those of compression tests of cores or cylinders. To overcome these deficiencies, a study was undertaken at the National Institute of Standards and Technology (NIST) to develop a rigorous method for obtaining the strength relationship and for estimating the lower confidence limit of the in-place strength [Stone and Reeve, 1986]. The procedure that was developed used a method for least-squares fitting that accounted for error in the X variable [Mandel, 1984]. The rigorous method was discussed in the original report of ACI Committee 228 [ACI 228.1R, 1989], but it has found little use owing to its complexity. Subsequently, a simplification of the rigorous method was proposed, which could be implemented by using a computerized spreadsheet [Carino, 1993]. This simplified method was incorporated into a revision of the ACI 228 report [ACI 228.1R, 1995], and the step-by-step procedure for its implementation is included in the appendices to the report.

During the late 1980s and early 1990s, A. Leshchinsky published a series of papers on statistical methods for in-place tests, which were based largely on work at the Institute for Research of Building Structures in Kiev. These papers compared practices in different countries with those in the former Soviet Union, which had a long history in using in-place methods for quality control in precast plants.

In a review of various national standards, Leshchinsky (1990) concluded that (1) greater numbers of in-place tests are required compared with tests of standard specimens, which makes in-place testing economically unattractive; (2) the number of test specimens necessary to establish the strength relationship and the number of in-place tests on the structure have been established arbitrarily, based on the experiences of those writing the standards; and (3) the number of replicate tests to establish the strength relationship differ from the replications at a test location in a structure. Procedures were presented for selecting in-place tests based on consideration of cost and reliability of the estimated strength, and recommendations were made to reduce the cost of in-place testing.

In another paper, procedures for developing correlations were discussed and criteria were suggested for verifying the correlation at periodic intervals [Leshchinsky and Leshchinsky, 1991]. The notion of a **stable** correlation was introduced. This refers to a strength relationship that is little affected by changes in concrete composition and the construction process. It was noted that methods that have a close connection between concrete strength and the quantity measured by the in-place test tend to have more stable correlations, but they also tend to be more costly than the methods that don't have this close connection. Pullout, break-off, and pull-off tests were identified as possessing stable correlations. It was also shown that the correlations may be affected by the location on the test specimens (top, middle, bottom) where the in-place test is performed [Leshchinsky, 1991a].

Leshchinsky also discussed factors to consider when deciding whether combined methods are justified [Leshchinsky, 1991b]. In addition, the following situations were identified where the combined use of a reliable, expensive method could be combined with a less expensive but less reliable method to achieve an overall cost savings in testing:

- The reliable method is used to **calibrate** the strength correlation of the less reliable method; a *correction factor* is determined and applied to the strength estimated by the less reliable method.
- The less reliable method is used to identify areas of lower quality concrete where reliable tests should be performed.
- For new construction, a less reliable method is used to determine when tests by the more reliable method should be performed.

There have been few instances in North America where in-place testing has been used for acceptance testing. The major barrier is the lack of a consensus-based, statistical procedure for this

application. Leshchinsky (1992) discussed some of the considerations in using in-place testing for acceptance testing. Because the strength of the actual concrete in the structure is measured, the acceptable in-place strength could be less than the design strength. Leshchinsky also reviewed provisions in existing national standards that allow acceptance based on in-place tests. In some of these standards, the required in-place strength depends on the number of tests and the variability of the in-place results. For high variability, the required in-place strength might exceed the design strength. The 1995 revision of the ACI Committee 228 report [ACI 228.1R, 1995] provided the following proposal for acceptance of concrete based on in-place testing:

The concrete in a structure is acceptable if the estimated average, in-place, compressive strength based on a reliable in-place test procedure equals at least 85 percent of f'_c and no test result estimates the compressive strength to be less than 75 percent of f'_c .

The report states that in order to implement such criteria there needs to be a standard practice for statistical analysis of in-place test results.

19.2.8.2 Correlation Testing

The following is a summary of the guidelines provided in the ACI 228 report for establishing the strength relationship for a specific job [ACI 228.1R, 1995]. The procedure differs depending on whether in-place testing will be used to estimate strength during construction or in an existing structure.

For new construction, the strength relationship is established from a laboratory testing program performed before using the in-place test method in the field. Test specimens are made using the same concreting materials to be used in construction. At regular intervals, measurements are made using the in-place test techniques and the corresponding compressive strengths of standard specimens are also measured. The number of strength levels has a significant effect on the confidence limits of the strength relationship. It is recommended that at least six strength levels be used to establish the strength relationship. More than about nine strength levels may not be economically justified. The range of strengths in the correlation testing must include the range of strengths that are to be estimated in the structure.

For some techniques, such as rebound number and pulse velocity, it is possible to perform the in-place test on standard specimens without damaging them and the specimens can be subsequently tested for compressive strength. For other methods that result in local damage, in-place tests are carried out on separate specimens. It is important that the in-place tests and standard tests are performed on specimens having similar compaction and the same maturity. Curing companion test specimens in the same water bath is a convenient way to assure similar temperature histories. Alternatively, internal temperatures can be recorded and test ages can be adjusted so that the in-place and standard tests are performed at the same maturity index.

For existing construction, the strength relationship is established by performing the in-place tests on the structure and determining the compressive strength from cores taken from adjacent locations. To obtain a wide range of strength, a rebound hammer or pulse velocity survey may be performed first to identify locations with apparently different quality. At each test location, a minimum of two cores should be taken to evaluate the compressive strength. Thus the proper application of in-place testing for existing construction requires taking at least 12 cores to establish the strength relationship. As a result, the procedure may be economical when large volumes of concrete are to be evaluated.

More detailed information on the number of replicate in-place tests and the companion test specimens to use for different test methods may be found in the ACI report [ACI 228.1 R, 1995]. After paired values of in-place test results and concrete compressive strengths are obtained, regression analysis is used to establish the equation of the strength relationship. The ACI 228 report recommends that the natural logarithms of the test results be used so that the following equation is

fitted:

$$\ln C = a + b \ln I \quad (19.13)$$

where

$\ln C$ = average of natural logarithms of compressive strengths

$\ln I$ = average of natural logarithms of in-place test results

a = intercept of line

b = slope of line

The report also recommends that the regression analysis to determine the values of a and b be performed using a procedure that accounts for the error on the X variable (in-place test results). This procedure is explained in detail in the appendix of the ACI report. Basically, the ratio of the variances of the in-place test results and compressive strength results are used to define a parameter λ , which is applied to the equations of OLS to obtain the slope and intercept. This approach results in a more reliable estimate of the uncertainty of the strength relationship.

19.2.8.3 In-Place Strength Estimate

In making estimates of the in-place strength, there are several important points to consider:

- Where should the in-place tests be performed?
- How many in-place tests should be performed?
- How should the data be analyzed to obtain a reliable estimate of in-place strength?

These points are also covered in the ACI 228 report. In the case of new construction, a preconstruction meeting should be held to establish where and how many in-place tests should be performed. The ACI report provides guidelines that can be used as a starting point in arriving at these decisions. For existing construction, a pretesting meeting should be held among all parties who share an interest in the test results. Agreement should be reached on the procedures for obtaining, analyzing, and interpreting the test results.

After the in-place test results have been obtained, statistical analysis is used to arrive at a reliable estimate of the in-place concrete strength. The term "reliable estimate" means that there should be a high likelihood that the actual in-place strength exceeds the estimated strength. The statistical procedure that is used should account for the following sources of uncertainty or variability:

- the uncertainty of the strength relationship,
- the variability of the in-place test results, and
- the variability of the in-place concrete strength.

The ACI 228 report includes several approaches that may be used for this purpose. One of these is based on a simplification by Carino (1993) of a rigorous procedure developed earlier by NIST researchers [Stone and Reeve, 1986]. The underlying steps of this procedure are illustrated in Figure 19.12. The average of the in-place test results are used to estimate the average concrete strength using a strength relationship. Next, the lower confidence limit of the average concrete strength is obtained by taking into account the uncertainty of the estimate from the strength relationship. This uncertainty includes a component based on the correlation testing and a component based on the variability of the in-place test results. Finally, the variability of the in-place concrete strength is used to obtain the tenth percentile strength, that is, the strength expected to be exceeded by 90% of the concrete in the structure. This variability is estimated using the assumption that the ratio of the standard deviation of compressive strength tests to the standard deviation of in-place test results has the same value in the field as was obtained during the correlation testing [Stone and Reeve, 1986]. The details for applying this procedure are given in the ACI 228 report [ACI 228.1 R, 1995] and additional background information may be found in Carino (1993). This procedure has been implemented in a Windows-based computer program that may be obtained by contacting the author of this chapter.

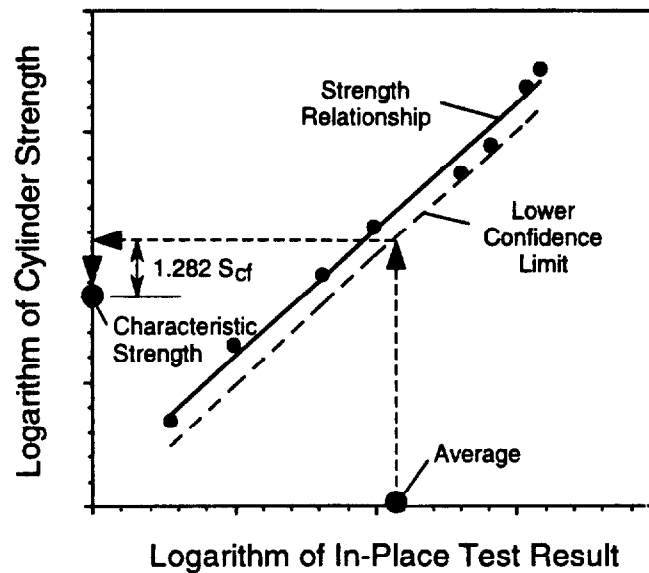


FIGURE 19.12 Statistical procedure to estimate the in-place compressive strength [Carino, 1993].

19.3 Methods for Flaw Detection and Condition Assessment¹¹

19.3.1 Introduction

Other types of NDT methods are those used for flaw detection and condition assessment. In this context the term **flaw** can include voids, honeycombing, delaminations, cracks, lack of subbase support, etc. Recent research and development efforts for these methods have far exceeded those for methods to estimate strength. The research impetus has come primarily from the transportation industry, since much of the highway infrastructure is in need of repair as a result of natural aging or the damage resulting from corrosion of reinforcing steel or deterioration of concrete.

The techniques for flaw detection are generally based on the following simple principle: the presence of an internal anomaly interferes with the propagation of certain types of waves. By monitoring the response of the test object when it is subjected to these waves, the presence of the anomaly can be inferred. The interpretation of the results of these types of NDT methods usually requires an individual who is knowledgeable both in concrete technology and in the physics governing the wave propagation.

This section of the chapter reviews the following techniques:

- Visual inspection
- Stress-wave propagation methods
- Infrared thermography
- Ground-penetrating radar
- Electrical/magnetic methods
- Nuclear methods

¹¹Some of text in this section is based on a draft prepared by the author for a report on NDT methods under preparation by ACI Committee 228.

Emphasis is placed on explaining the underlying principles of the methods, and the reader may find additional information in Malhotra and Carino (1991) and in Bungey (1989).

19.3.2 Visual Inspection

Visual inspection is one of the most versatile and powerful of the NDT methods, and it is typically one of the first steps in the evaluation of a concrete structure [Perenchio, 1989]. Visual inspection can provide a wealth of information that may lead to positive identification of the cause of observed distress. However, its effectiveness depends on the knowledge and experience of the investigator. Broad knowledge in structural engineering, concrete materials, and construction methods is needed to extract the most information from visual inspection. Useful guides are available to assist less experienced individuals in recognizing different types of damage and determining the probable cause of the distress [ACI 201.1R, ACI 207.3R, ACI 224.1R, ACI 362R].

Before performing a detailed visual inspection, the investigator should develop and follow a definite plan to maximize the quality of the recorded data. Various ACI documents should be consulted for additional guidance on planning and carrying out the complete investigation [ACI 207.3R, ACI 224.1R, ACI 362R, ACI 437R]. A typical investigation might involve the following activities:

- perform a walk-through visual inspection to become familiar with the structure;
- gather background documents and information on the design, construction, maintenance, and operation of the structure;
- plan the complete investigation;
- perform a detailed visual inspection; and
- perform any necessary sampling or in-place tests.

19.3.2.1 Supplemental Tools

Visual inspection has the obvious limitation that only visible surfaces can be inspected. Internal defects go unnoticed and no quantitative information is obtained about the properties of the concrete. For these reasons, a visual inspection is usually supplemented by one or more of the other NDT methods discussed in this chapter. The inspector should consider other useful tools that can enhance the power of a visual inspection.

Optical magnification allows a more detailed view of local areas of distress. Available instruments range from simple magnifying glasses to more expensive hand-held microscopes. Some fundamental principles of optical magnification can help in selecting the correct tool. The focal length decreases with increasing magnifying power, which means that the primary lens must be placed closer to the surface being inspected. The field of view also decreases with increasing magnification, making it tedious to inspect a large area at high magnification. The depth of field is the maximum difference in elevation of points on rough textured surface that are simultaneously in focus; this also decreases with increasing magnification of the instrument. To assure that the "hills" and "valleys" are in focus simultaneously, the depth of field has to be greater than the elevation differences in the texture of the surface that is being viewed. Finally, the illumination required to see clearly increases with magnification level, and artificial lighting may be needed at high magnification.

A very useful tool for crack inspection is a small hand-held magnifier with a built-in measuring scale on the lens closest to the surface being viewed [ACI 224.1R]. With such a crack comparator, the width of surface opening cracks can be measured accurately.

A stereo microscope includes two viewing lenses that allow a three-dimensional view of the surface. By calibrating the focus-adjustment screw, the investigator can estimate the elevation differences in surface features.

Fiberscopes and borescopes allow inspection of regions that are otherwise inaccessible to the naked eye. A fiberscope is composed of a flexible bundle of optical fibers and a lens system, and it allows cavities within a structure to be viewed by means of small access holes. The fiberscope

is designed so that some fibers transmit light to illuminate the cavity. In some systems, the operator can rotate the viewing head to allow a wide viewing angle from a single access hole. A borescope is composed of a rigid tube with mirrors and lenses and is designed to view straight ahead or at right angles to the tube. The image is clearer using a borescope, while the fiberscope offers more flexibility in the field of view. Use of these scopes requires drilling small holes if other access channels are absent, and the holes must intercept the cavity to be inspected. Some methods discussed in the remainder of the chapter may be used to locate these cavities. Hence the fiberscope or borescope may be used to verify the results of other NDT methods without removing cores.

A recent development that expands the flexibility of visual inspection is the small digital video camera. These are used in a manner similar to borescopes, but they offer the advantage of a video output that can be displayed on a monitor or stored on appropriate recording media. These charge coupled device (CCD) cameras come in a variety of sizes, resolutions, and focal lengths. Miniature versions as small as 12 mm in diameter, with a resolution of 460 scan lines, are available. They can be inserted into holes drilled into the structure for views of internal cavities, or they can be mounted on robotic devices for inspections in pipes or areas with biological hazards.

In summary, visual inspection is a very powerful NDT method. Its efficiency, however, is to a large extent governed by the experience and knowledge of the investigator. A broad knowledge of structural behavior, materials, and construction methods is desirable. Visual inspection is typically one aspect of the total evaluation plan, which will often be supplemented by a series of other NDT methods or invasive procedures.

19.3.3 Stress-Wave Propagation Methods

Tapping an object with a hammer or steel rod (sounding) is one of the oldest forms of nondestructive testing based on stress-wave propagation. Depending on whether the result is a high-pitched **ringing** sound or a low frequency **rattling** sound, the integrity of the member can be assessed. The method is subjective, as it depends on the experience of the operator, and it is limited to detecting near-surface defects. Despite these inherent limitations, **sounding** is a useful method for detecting near-surface delaminations, and it has been standardized by ASTM (D4580).

In NDT of metals, the **ultrasonic pulse-echo** (UP-E) method has proven to be a reliable method for locating small cracks and other defects. The principle of UP-E is similar to sonar. An electro-mechanical transducer is used to generate a short pulse of ultrasonic stress waves that propagates into the object being inspected. Reflection of the stress pulse occurs at boundaries separating materials with different densities and elastic properties (these determine the acoustic impedance of a material). The reflected pulse travels back to the transducer, which also acts as a receiver. The received signal is displayed on an oscilloscope, and the round-trip travel time of the pulse is measured electronically. By knowing the speed of the stress waves, the distance to the reflecting interface can be determined. If there is no internal defect, the opposite face of the test object is detected.

Attempts to use UP-E equipment designed for metal inspection to test concrete have been unsuccessful because of the heterogeneous nature of concrete. The presence of paste-aggregate interfaces, air voids, and reinforcing steel result in a multitude of echoes that obscure those of real defects. However, in the last 10 to 15 years there has been considerable progress in the development of usable techniques based on the propagation of impact-generated stress waves. This section reviews the basic concepts of stress-wave propagation and reviews the principles of some of the more promising methods. A more comprehensive review is provided by Sansalone and Carino (1991).

19.3.3.1 Basic Relationships

When a disturbance (stress or displacement) is applied suddenly at a point on the surface of a solid, such as by impact, the disturbance propagates through the solid as three different waves: a *P*-wave,

an S-wave, and an R-wave. The P-wave and S-wave propagate into the solid along spherical wavefronts. The P-wave is associated with the propagation of normal stress and the S-wave is associated with shear stress. In addition, there is an R-wave that travels away from the disturbance along the surface. In an infinite isotropic, elastic solid, the P-wave speed, C_p , is related to the Young's modulus of elasticity, E , Poisson's ratio, ν , and the density, ρ , as follows [Krautkrämer and Krautkrämer, 1990]:

$$C_p = \sqrt{\frac{E(1-\nu)}{\rho(1+\nu)(1-2\nu)}} \quad (19.14)$$

The S-wave propagates at a slower speed, C_s , given by

$$C_s = \sqrt{\frac{G}{\rho}} = \sqrt{\frac{E}{\rho 2(1+\nu)}} \quad (19.15)$$

where G is the shear modulus of elasticity.

The ratio of S-wave speed to P-wave speed depends on Poisson's ratio, as, follows:

$$\frac{C_s}{C_p} = \sqrt{\frac{1-2\nu}{2(1-\nu)}} \quad (19.16)$$

For a Poisson's ratio of 0.2, which is typical of concrete, this ratio equals 0.61. The ratio of the R-wave speed, C_r , to the S-wave speed is given by the following approximate formula:

$$\frac{C_r}{C_s} = \frac{0.87 + 1.12\nu}{1 + \nu} \quad (19.17)$$

For Poisson's ratio equal to 0.2, the R-wave travels at 92% of the S-wave speed.

In the case of bounded solids, the wave speed is also affected by the geometry of the solid. For rod like solids, the P-wave speed is independent of Poisson's ratio and is given by the following:

$$C_p = \sqrt{\frac{E}{\rho}} \quad (19.18)$$

Thus, for $\nu = 0.2$, the wave speed in a slender rod is about 5% slower than in a large solid.

When a stress wave traveling through **material 1** is incident on the interface between a dissimilar **material 2**, a portion of the incident wave is reflected. The amplitude of the reflection is a function of the angle of incidence and is a maximum when this angle is 90° (normal incidence). For normal incidence, the reflection coefficient, R , is given by the following:

$$R = \frac{Z_2 - Z_1}{Z_2 + Z_1} \quad (19.19)$$

where

Z_2 = specific acoustic impedance of material 2

Z_1 = specific acoustic impedance of material 1

The specific acoustic impedance is the product of the wave speed and density of the material. The following are approximate Z values for some materials [Sansalone and Carino, 1991]:

Material	Specific Acoustic Impedance, $\text{kg}/(\text{m}^2\text{s})$
Air	0.4
Water	1.5×10^6
Soil	$0.3 \text{ to } 4 \times 10^6$
Concrete	$7 \text{ to } 10 \times 10^6$
Steel	47×10^6

Thus it can be shown that when a stress wave traveling through concrete encounters an interface with air, there is almost total reflection at the interface. This is why NDT methods based on stress-wave propagation have proven to be successful for locating defects within concrete.

19.3.3.2 Impact Methods

The greatest success in the practical application of stress-wave methods for testing concrete has been to use mechanical impact to generate the stress pulse. Impact causes a high-energy pulse that results in high penetration of the stress waves. Several techniques have been developed that are similar in principle but that differ in the specific instrumentation and signal-processing methods that are used [Davis and Dunn, 1974; Steinbach and Vey, 1975; Higgs, 1979; Stain, 1982; Sansalone and Carino, 1986; Nazarian and Stokoe, 1986a; Davis and Hertlein, 1991].

Figure 19.13 is a schematic of an impact test. The principle is analogous to other echo methods that have been discussed. Impact on the surface produces a disturbance that travels into the object along spherical wavefronts as P - and S -waves. In addition, a surface wave (R -wave) travels away from the impact point. The P - and S -waves are reflected by internal defects (difference in elastic constants and density) or external boundaries. When the reflected waves, or echoes, return to the surface, they produce displacements that are measured by a receiving transducer. If the transducer is placed close to the impact point, the response is dominated by P -wave echoes [Sansalone and

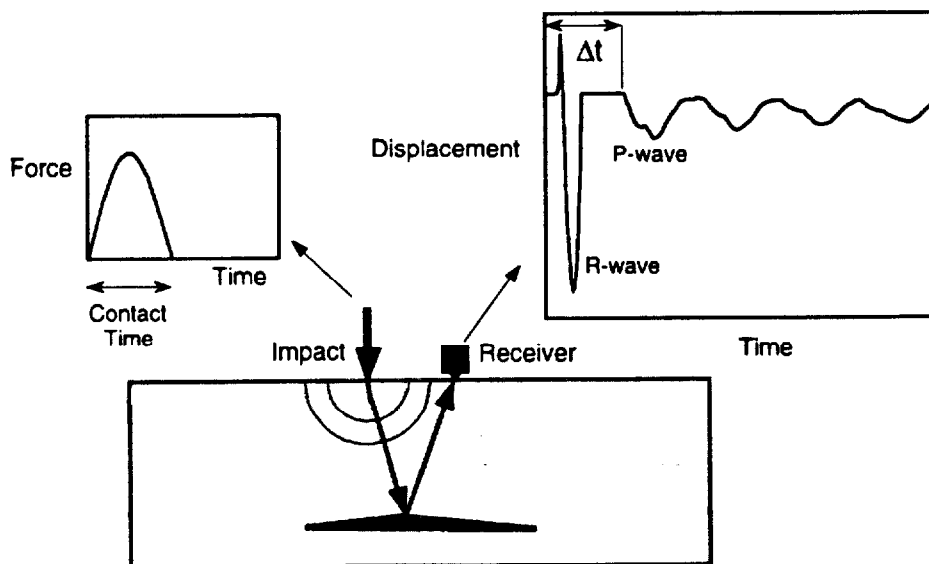


FIGURE 19.13 Schematic of test using impact to generate stress waves.

Carino, 1986]. Using **time-domain** analysis, the time from the start of the impact to the arrival of the *P*-wave echo is measured, and the depth of the reflecting interface can be determined if the *P*-wave speed is known.

The first successful applications of impact methods were used in geotechnical engineering to evaluate the integrity of concrete piles and caissons [Davis and Dunn, 1974; Steinbach and Vey, 1975]. The technique became known as the **sonic-echo** or **seismic-echo** method. The long length of the foundation structures allowed sufficient time separation between the generation of the impact and the echo arrival, and determination of round-trip travel times was relatively simple [Lin et al., 1991b; Olson and Church, 1986]. The impact response of thin concrete members, such as slabs and walls, is more complicated than that of long slender members. Work by Sansalone and Carino (1986) has led to the development of a successful technique for flaw detection in relatively thin concrete structures. The technique is known as the **impact-echo method**.

A key development leading to the success of the impact-echo method was the use of **frequency analysis** instead of time-domain analysis of the recorded wave forms [Carino et al., 1986]. The principle of frequency analysis is as follows: The *P*-wave produced by the impact undergoes multiple reflections between the test surface and the reflecting interface. Each time the *P*-wave arrives at the test surface, it causes a characteristic displacement. Thus the wave form has a periodic pattern that is dependent on the frequency, *f*, of the *P*-wave arrival, which is given by

$$f = \frac{C_p}{2D} \quad (19.20)$$

where C_p is the *P*-wave speed¹² and *D* is the depth of the reflecting interface. This frequency is termed the **thickness frequency**.

To apply frequency analysis, the recorded wave form is transformed into the frequency domain by using the fast Fourier transform technique [Bracewell, 1978]. The computed amplitude spectrum shows the dominant frequencies in the wave form. For slablike structures, the thickness frequency will usually be the *dominant peak in the spectrum*. The value of the peak frequency in the amplitude spectrum can be used to determine the depth of the reflecting interface by expressing Eq. (19.20) as follows:

$$D = \frac{C_p}{2f} \quad (19.21)$$

Figure 19.14 illustrates the use of frequency analysis of impact-echo tests. Figure 19.14a shows the amplitude spectrum from a test over a solid portion of a 0.5-m thick concrete slab. There is a frequency peak at 3.42 kHz, which corresponds to multiple *P*-wave reflections between the bottom and top surfaces of the slab. Using Eq. (19.20) or (19.21) and solving for C_p , the *P*-wave speed is calculated to be 3420 m/s. Figure 19.14b shows the amplitude spectrum from a test over a portion of the slab containing a disk-shaped void [Carino and Sansalone, 1989b]. The peak at 7.32 kHz results from multiple reflections between the top of the slab and the void. Using Eq. (19.21), the calculated depth of the void is $3420/(2 \times 7320) = 0.23$ m, which compares favorably with the known distance of 0.25 m.

In the initial work leading to the impact-echo method [Sansalone and Carino, 1986], it was noted that the duration of the impact was critical to determining the success of the method. As shown in Figure 19.13, the force-time relationship for the impact may be approximated as a half-cycle sine curve, and the duration of the impact is the **contact time**. The contact time determines the frequency content of the stress pulse generated by the impact [Carino et al., 1986]. As an approximation, the highest frequency component of significant amplitude equals the inverse of the contact time. In

¹²Recent studies by Sansalone and co-workers at Cornell University have shown that the *P*-wave speed in impact-echo testing is approximately 96% of the *P*-wave speed in an infinite solid.

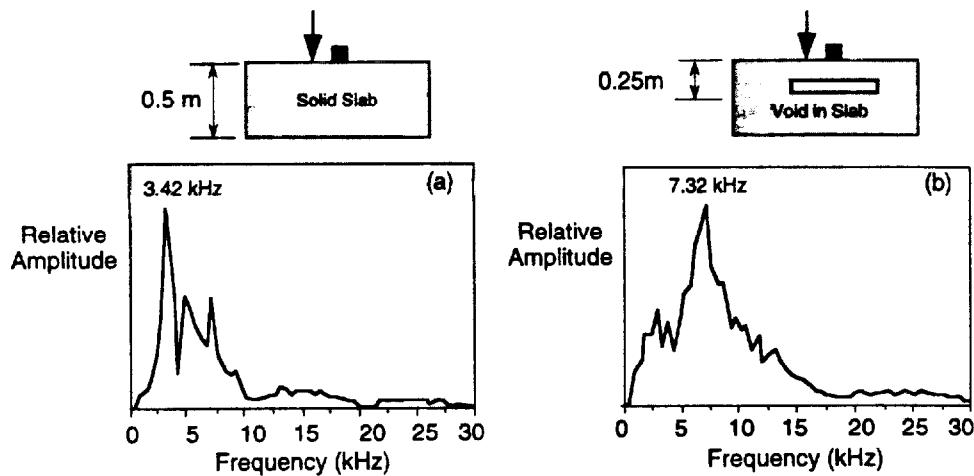


FIGURE 19.14 Examples of amplitude spectra from impact-echo test of concrete slab: (a) solid slab; (b) slab with void.

order to accurately locate shallow defects, the stress pulse must have frequency components greater than the frequency corresponding to the flaw depth (Eq. (19.20)). For example, for a P -wave speed of 4000 m/s, a pulse with a contact time shorter than 100 μ s is needed to determine the depth of defects shallower than about 0.2 m. Various impact sources have been used for impact testing. In evaluation of piles, hammers can be used to produce energetic impacts with long contact times (on the order of 1 ms). Such impacts are acceptable for testing long, slender structures but not for slabs or walls. For testing slabs from 0.15 to 0.5 m thick, steel spheres and spring-loaded spherically tipped impactors have been used successfully. Steel spheres are convenient impact sources because the contact time is proportional to the diameter of the sphere [Goldsmith, 1965].

The impact-echo method has been successful in detecting a variety of defects, such as voids and honeycombed concrete in members, delaminations in bare and overlaid slabs, and voids in tendon ducts [Jaeger et al., 1996; Sansalone and Carino, 1986, 1988, 1989a,b; Carino and Sansalone, 1992]. Experimental studies have been supplemented with analytical studies to gain a better understanding of the propagation of transient waves in bounded solids with and without flaws [Cheng and Sansalone 1993a,b, 1995a,b; Sansalone and Carino, 1987; Lin et al., 1991a,b]. Application of the impact-echo method has been extended to prismatic members, such as columns and beams [Lin and Sansalone, 1992a,b,c]. It has been found that reflections from the perimeter of these members cause complex modes of vibration. As a result, the amplitude spectra have many peaks, and the depth of the member is not related to the dominant frequency in the spectrum according to Eq. (19.21). Nevertheless, it has been shown that defects can still be detected within beams and columns, and a successful field application has been reported [Sansalone and Poston, 1992]. The method has also been applied to evaluate the quality of the bond between an overlay and base concrete [Lin and Sansalone 1996a,b].

As with most methods for flaw detection in concrete, experience is required to interpret stress-wave test results. An advance in the interpretation of impact-echo results from tests of slablike structures has been the application of an artificial intelligence technique known as a neural network [Sansalone et al., 1991]. In this technique, a computer program is trained to recognize amplitude spectra associated with flawed and unflawed structures. After this training, the program can be used to classify the results of tests on a structure under investigation. This technique was incorporated into the first commercial impact-echo test system [Pratt and Sansalone, 1992].

Another variant of the impact method is known as impulse-response, transient dynamic response, or impedance testing [Davis and Dunn, 1974; Higgs, 1979; Stain, 1982; Olson and Wright, 1990; Davis and Hertlein, 1991]. In this approach, the force history of the impact and the response

of the structure are measured. Through a signal-processing technique, the measured response and force history are used to compute the characteristic impulse response spectrum of the structure see [Sansalone and Carino, 1991]. The impulse-response spectrum of a structure depends on its geometry, the support conditions, and the existence of flaws or cracks.

Depending on the measured quantity of the structural response (displacement, velocity, or acceleration), the impulse response spectrum has different meanings. Typically, velocity is measured and the resulting impulse-response spectrum has units of velocity/force which are referred to as **mobility**, and the spectrum is called a **mobility plot**. At frequency values corresponding to resonant frequencies of the structure, mobility values are maximum. In the testing of piles, the mobility plot has a series of peaks that correspond to the fundamental and higher longitudinal modes of vibration. The difference between any two adjacent peaks, Δf , is equal to the fundamental longitudinal frequency [Higgs, 1979]. The length of the pile can be calculated by using Δf in place of f in Eq. (19.21).

To illustrate how the method works, impulse-response spectra obtained from two test piles having the same dimensions are shown in Figure 19.15 [Olson and Church, 1986]. Figure 19.15a is the response spectrum obtained from a sound pile. The P -wave speed in this pile was 4140 m/s. The fundamental longitudinal frequency of 138 kHz was calculated by determining the average frequency difference between four successive peaks. The pile length was calculated to be 15.0 m, while the known length was 15.2 m. For comparison, Figure 19.15b shows the response spectrum from a pile that contained a full-width defect at a depth of 9.8 m. The P -wave speed in this pile

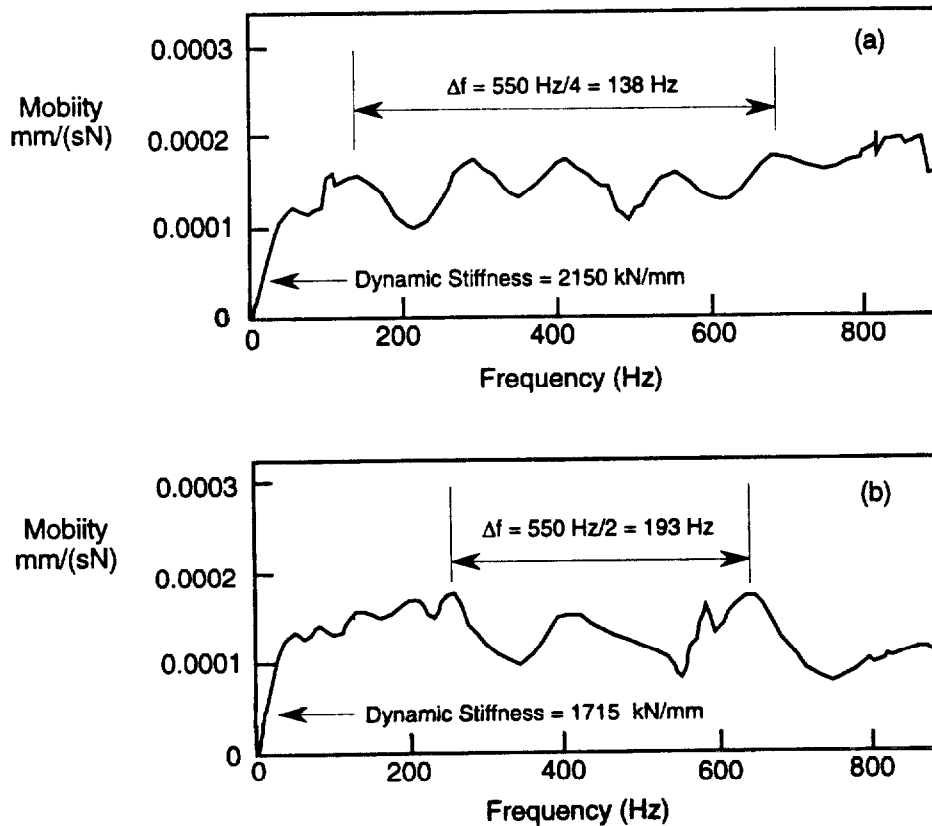


FIGURE 19.15 Examples of mobility plots from impulse-response tests of (a) solid pile and (b) pile with full section defect [adapted from Olson and Church, 1986].

was 4200 m/s. The fundamental frequency of 193 Hz was estimated by averaging the difference between the three successive frequency peaks shown in Figure 19.15b. The depth to the reflecting interface was calculated to be about 11 m. In addition to providing information on the length of a pile, the impulse response function can also indicate the dynamic stiffness of the pile-soil structure. The initial slopes of the spectra in Figure 19.15 are inversely related to the dynamic stiffnesses. Thus the presence of the void is indicated by a reduced pile length and an increased dynamic stiffness.

19.3.3.3 Spectral Analysis of Surface Waves

In the late 1950s and early 1960s, Jones (1955, 1962) reported on the use of **surface waves** to determine the thickness and elastic stiffness of pavement slabs and the underlying layers. The method involved determining the relationship between the wavelength and velocity of surface vibrations as the vibration frequency was varied. Apart from the studies by Jones there seems to have been little use of this technique for testing concrete pavements. In the early 1980s, however, researchers at The University of Texas at Austin began studies of a surface-wave technique that involved an impactor instead of a steady-state vibrator. Digital signal processing was used to develop the relationship between wavelength and velocity. The technique was called **spectral analysis of surface waves (SASW)** [Heisey et al., 1982; Nazarian et al., 1983].

Figure 19.16 shows the configuration for SASW testing [Nazarian and Stokoe, 1986a]. Two receivers are used to monitor the movement of the surface due to the *R*-wave produced by the impact. The received signals are processed, and a complex calculation scheme is used to infer the stiffnesses of the underlying layers.

Just as the impact is composed of a range of frequency components, the *R*-wave also contains a range of components of different frequencies or wavelengths. (Note: the product of frequency and wavelength equals wave speed.) This range depends on the contact time of the impact; a shorter contact time results in a broader range. The longer-wavelength (lower-frequency) components penetrate more deeply, and this is the key to using the *R*-wave to gain information about the properties of the underlying layers [Rix and Stokoe, 1989]. In a layered system, the propagation speed of these different components is affected by the wave speed in the layers through which the components propagate. A layered system is a **dispersive medium** for *R*-waves, which means that different frequency components in the *R*-wave propagate with different speeds, which are called **phase velocities** [Krstulovic-Opara et al., 1996].

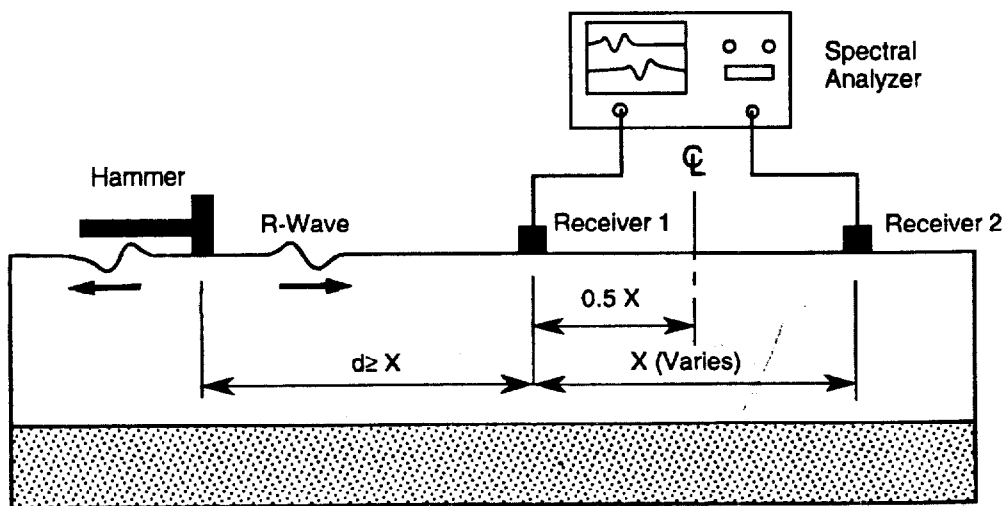


FIGURE 19.16 Schematic of testing configuration for SASW test.

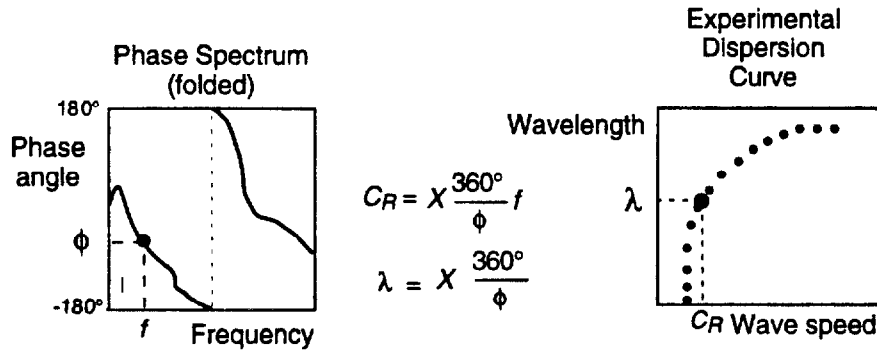


FIGURE 19.17 Schematic of phase spectrum obtained from cross-power spectrum of the receiver waveforms in SASW testing and the dispersion curve relating wavelength and wave speed.

Phase velocities are calculated by determining the time it takes for each frequency (or wavelength) component to travel between the two receivers. These travel times are determined from the phase difference of the frequency components arriving at the receivers [Nazarian and Stokoe, 1986b; Sansalone and Carino, 1991]. The phase differences are obtained by computing the **cross-power spectrum** of the signals recorded by the two receivers. The phase portion of the cross-power spectrum gives phase differences (in degrees) as a function of frequency. A schematic of such a phase spectrum is shown in Figure 19.17.¹³ The phase velocities are determined as follows:

$$C_{R(f)} = X \frac{360}{\phi_f} f \tag{19.22}$$

where

- $C_{R(f)}$ = surface wave speed of component with frequency f
- X = distance between receivers (see Figure 19.16)
- ϕ_f = phase angle of component with frequency f

The wavelength, λ_f , corresponding to a component frequency is calculated using the following equation:

$$\lambda_f = X \frac{360}{\phi_f} \tag{19.23}$$

By repeating the calculations in Eqs. (19.22) and (19.23) for each component frequency, a plot of wavelength versus phase velocity is obtained. Such a plot is called a **dispersion curve**, and is shown on the right side of Figure 19.17.

After the experimental dispersion curve is obtained, a process called **inversion** is used to obtain the stiffness profile at the test site; [Krstulovic-Opara et al., 1996; Nazarian and Desai, 1993; Yuan and Nazarian, 1993; Nazarian and Stokoe, 1986b]. The site is modeled as layers of varying thickness. Each layer is assigned density and elastic constants. Using these assumed properties, the surface motion at the location of the receivers is calculated using surface-wave propagation theory. The calculated responses are subjected to the same signal-processing technique as used for the test data, and a theoretical dispersion curve is obtained. The theoretical and experimental dispersion curves are compared. If the curves match, the problem is solved and the assumed stiffness profile

¹³A phase spectrum is usually plotted so that the phase angle axis ranges from -180° to 180° . Hence the spectrum “folds” over when the phase angle reaches -180° , giving the phase spectrum a “sawtooth” pattern.

is correct. If there are significant discrepancies, the properties of the assumed layered system are changed, and a new theoretical dispersion curve is calculated. This process continues until there is agreement between the theoretical and experimental curves. The user should be experienced in selecting plausible starting values of the elastic constants and have the ability to recognize whether the final values are reasonable. Convergence cannot be assumed to indicate that the correct values have been determined, because it is possible for different combinations of layer thicknesses and elastic moduli to result in similar dispersion curves.

The general configuration for SASW testing was shown in Figure 19.16. For reliable results, tests are repeated with different receiver spacings [Nazarian and Stokoe, 1986a]. The receivers are first located close together, and the spacing is increased by a factor of two for subsequent tests. As a check on the measured phase information for each receiver spacing, a second series of tests is carried out by reversing the position of the source. Typically, five receiver spacings are used at each test site. For tests of concrete pavements, the closest spacing is usually about 150 mm.

The SASW method has been used to determine the stiffness profiles of soil sites and of flexible and rigid pavement systems [Nazarian and Stokoe, 1986b; Rix and Stokoe, 1989]. The method has been extended to the measurement of changes in the elastic properties of concrete slabs during curing [Rix et al., 1990].

19.3.3.4 Summary

The impact techniques discussed above offer great potential as reliable methods for flaw detection. While they appear similar in terms of the physical test procedure, different information about the test object can be obtained by using the correct instrumentation and signal-processing methods. Each method is best suited for particular applications. Persons interested in using NDT methods based on stress-wave propagation should develop the ability to use all the methods, so that the most appropriate one can be used for a particular situation.

19.3.4 Infrared Thermography

Infrared thermography is a technique for locating near-surface defects by measuring surface temperature. It is based on two principles. The first principle is that a surface emits electromagnetic radiation with an intensity that depends on its temperature. At about room temperature, the radiation is in the infrared region of the electromagnetic spectrum. The second principle is that the presence of an anomaly having a lower thermal conductivity than the surrounding material will interfere with the flow of heat and alter the surface-temperature distribution. As a result, the surface temperature will not be uniform. Thus, by measuring the surface temperature, the presence of the defect can be inferred. In practice, the surface temperature is measured with an infrared scanner that works in a manner similar to a video camera [Manning and Holt, 1980]. The output of the scanner is a **thermographic image** of temperature differences.

The following are values of thermal-conductivity coefficients for different materials [Halliday and Resnik, 1978]:

Material	Thermal Conductivity, $\text{J/s} \cdot \text{m} \cdot ^\circ\text{C}$
Steel	46
Ice	1.7
Concrete	0.8
Air	0.024

It can be seen that air has a much lower thermal conductivity than concrete, and this explains why the presence of air voids within concrete can affect the surface temperature distribution when there is heat flow through the concrete.

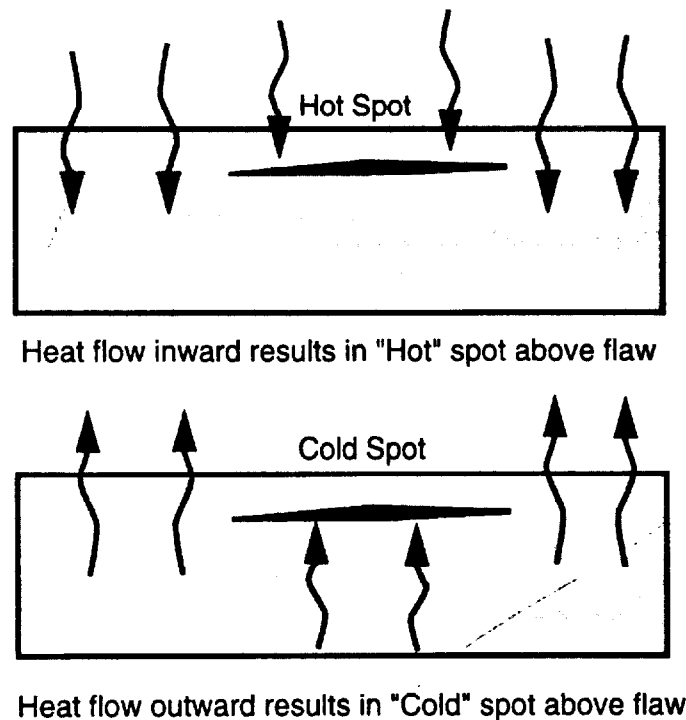


FIGURE 19.18 Effect of a void on the heat flow through a concrete slab.

In civil engineering applications, the method is used primarily to detect corrosion-induced delaminations in reinforced concrete bridge decks. In North America, early research on this application was performed independently in the late 1970s by the Virginia Highway and Transportation Research Council [Clemeña and McKeel, 1978] and by the Ontario Ministry of Transportation and Communication [Manning and Holt, 1983]. Initial studies involved hand-held scanners and photographic cameras to record the thermographic images. This was followed by scanning from a boom attached to a truck and by airborne scanning using a helicopter. Although infrared thermography allowed more rapid surveys than the chain-drag technique [ASTM D 4580], it was not as accurate as chain dragging for determining the extent of the delaminations [Manning and Holt, 1983]. In 1988, ASTM published a standard test method [ASTM D 4788] on the use of the infrared thermography to locate delaminations in exposed and overlaid concrete bridge decks. Additional information on considerations for performing an infrared survey and representative case histories are provided by Weil (1991).

The principle of infrared thermography is illustrated in Figure 19.18. The presence of a void in the concrete slab has a local insulating effect that disrupts the heat flow through the slab and affects the surface temperature. When heat flows into the slab, the area above the void is warmer than the surrounding area; and when heat flows out of the slab, the area above the void is cooler. By measuring the surface temperature distribution, one can infer the presence of the void. Hence, to apply infrared thermography, there must be a heat-flow condition through the test object and a means for measuring small differences in surface temperature.

The required heat-flow condition can be created artificially by using heating lamps, or it can occur naturally through solar heating (heat flow into structure) and nighttime cooling (heat flow out of structure). The latter method is obviously the economical approach. The best time for doing infrared surveys is two to three hours after sunrise or after sunset [Weil, 1991]. Heat flow

becomes very low and the surface temperatures become uniform as time elapses following sunrise or sunset.

Even with the proper heat-flow conditions, not all delaminations are detectable. Maser and Roddis (1990) performed analytical studies to gain an understanding of the factors affecting the differences in the surface temperature of a solid concrete slab and a slab with a delamination. It was found that the maximum differential temperature decreased as the depth of the delamination increased and as the width decreased. Also, a water-filled delamination resulted in nearly identical surface temperatures as a solid slab.

In infrared thermography, differences in surface temperature are measured by using an imaging infrared scanner, a device similar to a video camera, which measures the amount of infrared radiation emitted by a surface. As mentioned, the underlying principle of this measurement method is that an object at a temperature above absolute zero emits electromagnetic radiation, whose wavelength depends on the temperature. As the temperature increases, wavelengths become shorter, and, at sufficiently high temperature, the radiation is in the visible spectrum. This is the operating principle of incandescent light bulbs. At room temperature range, the wavelength of the radiation emitted by surfaces is on the order of $10\ \mu\text{m}$, which is in the infrared region of the spectrum. This radiation cannot be detected by the naked eye. The infrared scanner has a detector that sees the infrared radiation. The detector output is related to the amount of incident radiant energy.

The energy emitted by a surface is related to its temperature according to the Stefan-Boltzman law [Halliday and Resnik, 1978]:

$$R = e\sigma T^4 \quad (19.24)$$

where

- R = rate of energy radiation per unit area of surface, W/m^2
- e = the emissivity of the surface
- σ = the Stefan-Boltzman constant, $5.67 \times 10^{-8}\ \text{W}/(\text{m}^2 \cdot \text{K}^4)$
- T = absolute temperature of the surface, Kelvin

By proper calibration, the output from the infrared sensor can be converted to a temperature. The emissivity is characteristic of the material and surface texture and has a value ranging from 0 to 1. Since the rate of energy radiation depends on temperature and emissivity, care must be exercised in interpreting thermographic images to assure that apparent temperature differences are not caused by differences in emissivity. The emissivity of bridge deck surfaces can be affected by the type of texturing, oil spots, tire marks, paint, and loose debris.

Equipment for performing a thermographic survey includes an infrared scanner with associated hardware capable of producing a video image of the temperature distribution of the scanned surface; a conventional video camera to provide a visual record for comparison with the infrared record; video recorders to record infrared and conventional video images; analog-to-digital converters to transform the video images into digital data; a computer system and software for data storage and signal enhancement; and a distance-referencing system to correlate the infrared scan with position on the bridge deck [Weil, 1991; Kunz and Eales, 1985]. The equipment is typically contained in a mobile van that travels along the roadway while data are recorded. The resolution of the infrared scanner is improved by lowering its temperature; therefore, a liquid nitrogen cooling system is used to cool the sensor. Available equipment allows resolution of differences in surface temperature as low as 0.1°C .

The following is a summary of the procedure given in ASTM D 4788 for performing an infrared thermographic survey to detect delaminations in bridge decks:

- Remove debris from the surface.
- Allow the surface to dry for at least 24 h before testing.

- There must be at least 0.5°C difference between the surface temperatures in areas above delaminations and in sound concrete. A minimum of 3 h of direct sunlight are generally sufficient to establish this temperature difference. A contact thermometer with a minimum resolution of 0.1°C is used to determine whether the minimum temperature difference has been established.
- Do not test when the wind speed exceeds 50 km/h because the surface temperature will be affected.
- Do not test when the ambient air temperature is less than 0°C because ice in delaminations will give false indications of sound concrete. As a guide, an ambient temperature rise of 10°C, 4 h of sunshine, and a wind speed below 25 km/h should result in accurate data on bare concrete surfaces during winter. For asphalt-covered concrete, at least 6 h of sunshine are necessary during winter.
- Collect data with the van moving at speeds not greater than 15 km/h.

The results of the inspection are usually reported in terms of delaminated area and percentage of delaminated area. After the delaminated areas are identified in the infrared images, the visible video images should be compared to assure that apparent temperature differences were not due to emissivity changes [Kunz and Eales, 1985]. The ASTM standard states that 80 to 90% of the delaminations in a bare bridge deck can be located with this method. It has also been found that the inspection of the same deck by four different operators resulted in a variation of $\pm 5\%$ of the known delaminated area.

In summary, instrumentation and computer software have been developed so that inspection of bridge decks is a fairly routine procedure [Kunz and Eales, 1985]. Trained individuals are required to assure that meaningful data are collected and that the data are correctly interpreted. Infrared thermography is a global inspection method. This permits large surface areas to be scanned in a short period of time, which is an advantage over other methods that have been discussed.

19.3.5 Ground-Penetrating Radar (GPR)

Radar is analogous to the ultrasonic pulse-echo technique previously discussed, except that pulses of electromagnetic waves (short radio waves or microwaves) are used instead of stress waves. While the early uses of the technique were for military applications, radar techniques are now used in a variety of fields, such as weather, aerial mapping, and civil-engineering applications. The earliest civil-engineering applications for radar were probing into soil to detect buried pipelines and tanks. This was followed by studies to detect cavities below airfield pavements and more recently for determining concrete thickness, locating voids and reinforcing bars, and identifying deterioration [Bungey and Millard, 1993; Cantor, 1984; Carter et al., 1986; Clemeña, 1983; Kunz and Eales, 1985; Maser, 1986; Maser and Roddis, 1990; Alongi et al., 1982; Cantor and Kneeter, 1982; Steinway et al., 1981; Ulriksen, 1983]. Clemeña (1991) provides a comprehensive review of GPR.

In civil-engineering applications, relatively short distances are involved compared with other uses of radar. As a result, devices for these applications emit very short pulses of electromagnetic waves (microwaves). For this reason, the technique is often called **short-pulse radar** or **impulse radar**. Others call it **ground-penetrating radar** (GPR). In this chapter it will be called GPR. This section discusses the principles of GPR, the instrumentation that is used, and some of the inherent difficulties in using the method.

Propagation of electromagnetic waves is complex. The following presentation is simplified based on assumptions suitable for civil-engineering applications. More detailed treatments are available [Daniels et al., 1988; Halabe et al., 1993, 1995]. The operating principle of GPR is illustrated in Figure 19.19. An antenna above the test object sends out a short-duration pulse (on the order of nanoseconds) of electromagnetic waves. The pulse travels through the test object and when it

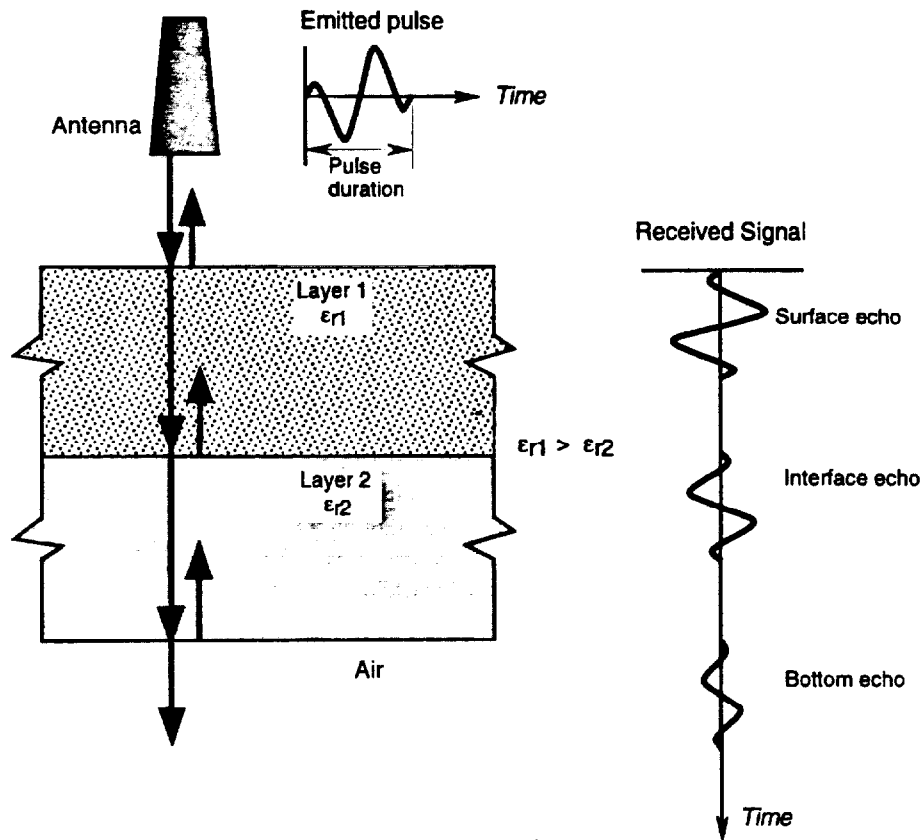


FIGURE 19.19 Reflection of radar pulse at interfaces between materials with different relative dielectric constants and antenna signal caused by arrival of echoes.

encounters an interface between dissimilar materials, some of the energy is reflected back toward the antenna as an **echo**. The antenna receives the echo and generates an output signal, as shown to the right of Figure 19.19. By measuring the time from the start of the pulse until the reception of the echo, one can determine the depth of the interface if the propagation speed through the material is known.

The amplitude of reflection at an interface depends on the difference between the relative dielectric constants¹⁴ of the two materials and is given by the following equation [Clemeña, 1991; Bungey and Millard, 1993]:

$$\rho_{1,2} = \frac{\sqrt{\epsilon_{r1}} - \sqrt{\epsilon_{r2}}}{\sqrt{\epsilon_{r1}} + \sqrt{\epsilon_{r2}}} \quad (19.25)$$

where

- $\rho_{1,2}$ = reflection coefficient
- ϵ_{r1} = relative dielectric constant of material 1
- ϵ_{r2} = relative dielectric constant of material 2

¹⁴The relative dielectric constant is related to the alignment of charges that occurs in an insulating material when placed in an electric field.

By definition, the relative dielectric constant of air equals 1, and typical values for other materials are as follows [ASTM D 4748]:

Material	Range of Relative Dielectric Constant
Portland cement concrete	6 to 11
Asphalt-cement concrete	3 to 5
Gravel	5 to 9
Sand	2 to 6
Rock	6 to 12
Water	8

The relative dielectric constants for materials such as concrete and soil depend on the moisture content and ionic concentrations [Morey, 1974]. Note that the dielectric constant of water is much higher than the other listed materials. This makes water the most significant dielectric contributor to construction materials and explains why radar is highly sensitive to moisture. As the moisture content increases, the dielectric constant of the material, such as concrete, also increases. Eq. (19.25) shows that when the value of ϵ_r of material 2 is greater than that of material 1, the reflection coefficient is negative. This signifies that there is a phase reversal in the reflected wave, which means that the positive part of the wave is reflected as a negative part. At a metal interface, such as between concrete and steel reinforcement, there is complete reflection, and the reflected wave has reversed polarity. This makes GPR very effective for locating metallic embedments. On the other hand, strong reflections from embedded metals can obscure weaker reflections from other reflecting interfaces that may be present, and reflections from reinforcing bars may mask signals from greater depths.

An important difference between GPR and stress-wave methods, such as the impact-echo method, is the amplitude of the reflections at a concrete-air interface. For stress waves, the reflection is almost 100% because the acoustic impedance of air is negligible compared with concrete. On the other hand, the mismatch in dielectric constants at a concrete-air interface is not as drastic, and only about 50% of the incident energy is reflected at a concrete-air interface. This results in two significant differences between GPR and stress-wave methods. GPR is not as sensitive to the detection of concrete-air interfaces as are stress-wave methods. However, because not all the energy is reflected at a concrete-air interface, GPR is able to penetrate beyond such an interface and "see" features below the interface.

The depth of the reflecting interface is obtained from the measured round trip travel time and the speed of the electromagnetic wave, C , which is dependent upon the relative dielectric constant:

$$C = \frac{C_0}{\sqrt{\epsilon_r}} \quad (19.26)$$

where

C_0 = speed of light in air (3×10^8 m/s)

ϵ_r = relative dielectric constant

If the round trip travel time is Δt , the depth, D , would be

$$D = \frac{C \Delta t}{2} \quad (19.27)$$

Equations (19.25) through (19.27) form the basis for using GPR to inspect concrete structures.

Typical instrumentation for GPR includes the following main components: an antenna unit, a control unit, a display device, and a storage device. The antenna emits the electromagnetic pulse and receives the echoes. The length of the pulse is largely controlled by the antenna design. Longer pulses are associated with longer wavelengths (or lower frequency) and have more penetrating ability, but poorer resolution (poorer ability to detect small objects), than shorter pulses. Typically, an antenna with a predominant frequency of about 1 GHz is used to inspect pavements and bridge decks, and the pulse length is about 1 ns. In air, such a pulse is about 0.3 m long and in concrete the length would depend on the value of ϵ_r . For $\epsilon_r = 6$, the pulse length would be about 120 mm. To be able to measure depths accurately, the echo must arrive after the initial pulse has ceased. Therefore the round trip travel path must exceed the pulse length. For $\epsilon_r = 6$, the minimum depth that can be measured accurately is about 60 mm. As ϵ_r increases, the minimum measurable depth decreases. The pulse is attenuated as it travels through the test object, and there is a limit to the thickness that can be inspected. For concrete, the depth of penetration would depend on the characteristics of the GPR system, the moisture content, and the amount of reinforcement. With increasing moisture content and amount of reinforcement, the penetration decreases. For dry unreinforced concrete, the maximum penetration of the pulse produced by a 1-GHz antenna is about 0.6 m [Clemeña, 1991]. In Figure 19.19, the antenna is in contact with the test objects. It is also possible to use a noncontact horn antenna. In this case, the received signal includes an echo from the concrete surface.

The control unit is the heart of a GPR system. It controls the repetition frequency of the pulse, provides the power to emit the pulse, acquires and amplifies the received signal, and provides output to a display device. Data are usually stored in an analog recorder and played back for later analysis and interpretation.

Display devices include oscillographs, which plot the recorded wave forms as a **waterfall plot**, or graphic-facsimile recorders. As an example, Figure 19.20 shows a waterfall plot obtained by plotting the received wave forms next to each other. The plot takes on a topographic appearance, and changes in the pattern of the received signals are relatively easy to identify [Cantor, 1984]. Computer software is also available that permits sophisticated signal processing of the data to aid in interpretation. The operation of the graphic recorder is discussed further here because it is commonly used in the field. Figure 19.21a shows an antenna emitting a radar pulse into a test object

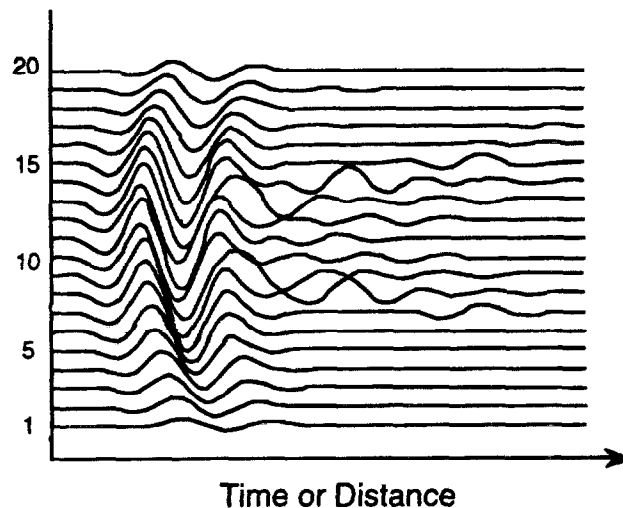


FIGURE 19.20 Waterfall plot of radar wave forms as an antenna is scanned across the surface of the test object [adapted from Cantor, 1984].

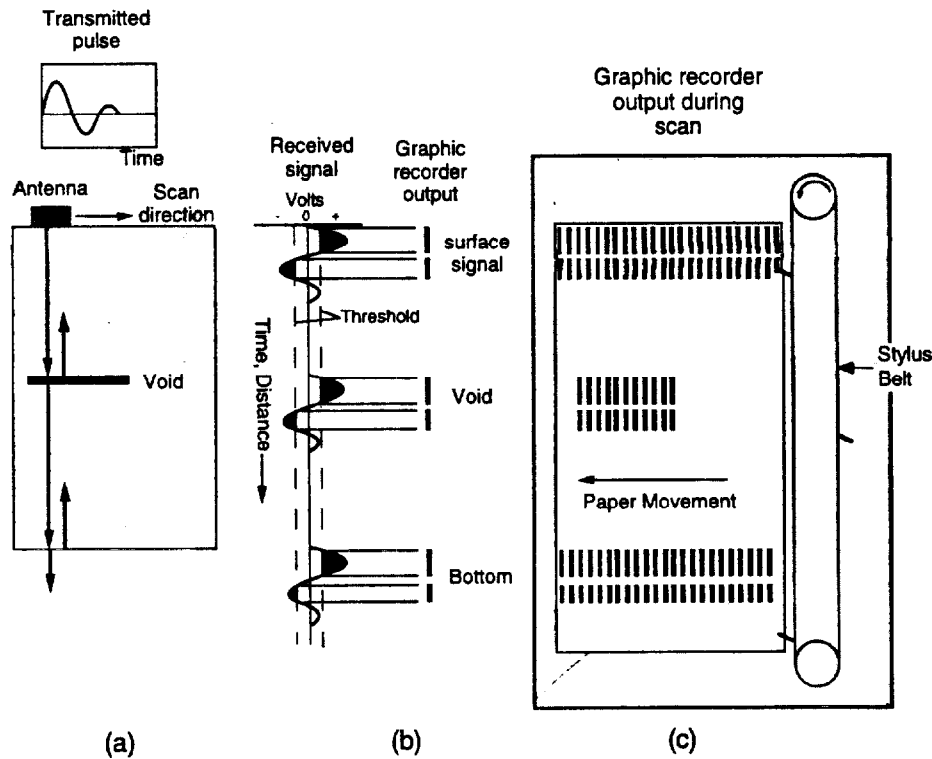


FIGURE 19.21 Schematic to illustrate peak-plotting technique used with graphic recorder: (a) reflections of electromagnetic pulse in test object; (b) received wave form threshold limits; (c) graphic recorder output during surface scan of test object.

containing a void. The shape of the emitted pulse is sketched above the antenna. Figure 19.21b shows the wave form from the receiving side of the antenna. The vertical axis represents time, or it can be transformed to depth by knowing ϵ_r and using Eq. (19.27). The received signal at the start of the waveform represents the transmitted pulse, which is picked up directly by the receiving side of the antenna. The second received signal is the echo from the void, and the third is the echo from the bottom boundary of the test object.

The output of the graphic recorder is obtained by a technique known as **peak plotting**, which is illustrated in Figure 19.21b. First, the operator selects a threshold voltage range. When the amplitude of the received signal goes beyond the threshold range, the pen of the graphic recorder plots a solid line on recording paper. The line is plotted in varying shades of gray, depending on the actual amplitude of the signal. Thus the antenna output is represented on the graphic recorder as a series of dashes as shown in Figure 19.21b. Note that each echo is associated with two dashes. The actual number of dashes depends on the number of cycles in the emitted pulse and the threshold level. This is an important point to understand for proper interpretation of GPR results. As the antenna is moved along the surface, the output is displayed on the graphic recorder. The paper on the recorder moves at a constant speed that is independent of the speed of the antenna motion. The resulting picture on the graphic recorder represents a cross-sectional view of the test object, as illustrated in Figure 19.21c. The test equipment provides a means for correlating the position of the antenna during the scan with the location on the paper record. Thus it is possible to determine the depth and approximate size of the reflecting interface.

As was already mentioned, metals are strong reflectors of electromagnetic waves. This makes GPR very effective for locating buried metal objects such as reinforcing bars and conduit. Reinforcing

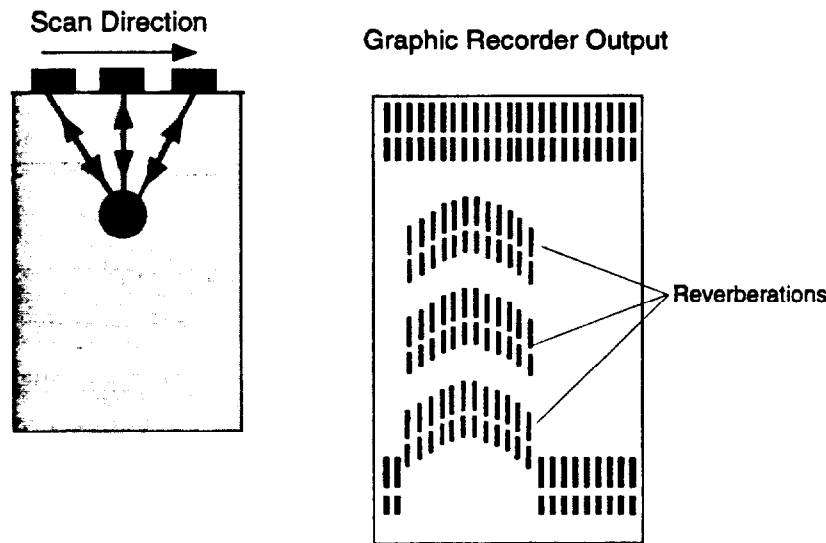


FIGURE 19.22 Schematic to illustrate characteristic graphic recorder output during scan over a reinforcing bar.

bars result in characteristic patterns in the graphic-recorder output, which make them relatively easy to locate. There are two main factors leading to these patterns, which are discussed here with the aid of Figure 19.22. First of all, an antenna behaves like a flashlight in that the beam of radiation has a conical shape. Thus a reinforcing bar produces echoes before the antenna passes directly over the bar; however, the apparent depth of the bar will be larger than the actual cover because of the inclined travel path. Secondly, the pulse undergoes multiple reflections, or reverberations, between the reinforcing bar and the surface, and the output will show multiple echoes from the same bar. The resulting characteristic pattern is shown on the right side of Figure 19.22. The top of the bar is associated with the uppermost part of the arched bands.

When multiple reinforcing bars are present, there will be multiple arch patterns. As the bars become closer together, the arch patterns overlap. Below a certain spacing, the individual bars can no longer be discerned, and the echo pattern is similar to the case of a solid embedded steel plate. The ability to discern individual bars depends on bar size, bar spacing, cover depth, and the configuration of the antenna [Bungey et al., 1994]. Closely spaced bars will also prevent detection of features below the layer of reinforcement. This **masking** effect depends on the wavelength of the electromagnetic waves, the bar size, and cover depth. It has been found that for the 1-GHz, hand-held antenna, 32-mm bars at cover depths of 25 to 50 mm will prevent detection of underlying features when bar spacings are less than 200 mm [Bungey et al., 1994].

Simple methods do not exist to determine bar size from graphic-recorder output. Researchers have attempted to better understand the interactions of GPR with cracks, voids, and reinforcing bars [Mast et al., 1990]. The objective of these studies is to develop procedures to use the recorded data to construct an image of the interior of the concrete. Some advances in this direction have occurred in France, where a prototype system has been developed that uses tomographic techniques to reconstruct the two-dimensional layout of reinforcement in concrete [Pichot and Trouillet, 1990]. In the United States, successful three-dimensional reconstruction of artificial defects and reinforcement embedded in a concrete slab have been demonstrated [Mast and Johansson, 1994]. These imaging methods rely on an antenna array to make multiple measurements and require extensive computational time to reconstruct the internal image.

The detection of delaminations in reinforced bridge decks using GPR is not straightforward. In studies by Maser and Roddis (1990), it was found that a 3-mm air gap in concrete produced little

noticeable effect in the received wave form. However, the addition of moisture to the simulated crack resulted in stronger reflections that were noticeable in the wave form. It was also found that the presence of chlorides in moist concrete resulted in high attenuation, because of the increased relative dielectric constant. Thus the ability to detect delaminations will depend on the *in situ* conditions at the time of testing. In addition, the reflections from reinforcing bars are much stronger than from a delamination, and it is difficult to “see” the delamination.

Owing to difficulties in using GPR in reinforced concrete, standardized test procedures for flaw detection do not exist. However, an ASTM standard has been developed (Test Method D 4748) to measure the thickness of the upper layer of a multilayer pavement system. Basically, the technique involves measuring the transit time of the pulse through the pavement layer, and using relationships similar to Eqs. (19.26) and (19.27) to calculate the layer thickness. The procedure is based on using a noncontact horn antenna, and some modifications are required for measurements with a contact antenna. The calculated depth depends on the value of the relative dielectric constant. Errors in the assumed value of the relative dielectric constant can lead to substantial inaccuracies in depth estimations [Bungey et al., 1994]. For data obtained with a horn antenna, the relative dielectric constant of the concrete can be computed directly from the radar signals. For data obtained using a contact antenna, it is necessary to take occasional cores to determine the appropriate value for the pavement materials. The user is cautioned against using the method on saturated concrete because of the high attenuation and limited penetration of the pulse. In ASTM D 4748, it is stated that interoperator testing of the same materials resulted in thickness measurements within ± 5 mm of the actual thickness. Finally, it is noted that reliable interpretation of received signals can only be performed by an experienced data analyst.

While the majority of the applications of GPR have dealt with locating reinforcing bars in structures, locating delaminations in bridge decks, and measuring the thickness of pavement layers, there are other potential uses. Since the dielectric properties of a material like concrete are strongly dependent on the moisture content, microwave measurements can be used to monitor the progress of hydration [Otto et al., 1990; Clemeña, 1991]. This is made possible because the relative dielectric constant of free water is much higher than that of chemically bound water. Clemeña (1991) has also reported on potential applications of microwave measurements to determine water content of fresh concrete.

19.3.6 Electrical and Magnetic Methods for Reinforcement

Information about the quantity, location, and condition of reinforcement is needed to evaluate the strength of reinforced concrete members. This section discusses some of the magnetic and electrical methods that are used to gain information about embedded-steel reinforcement. Additional information may be found in the following references: Malhotra (1976), Bungey (1989), and Lauer (1991).

19.3.6.1 Covermeters

Devices to locate reinforcing bars and estimate the diameter and depth of cover are known as **covermeters**. These devices are based on interactions between the bars and low-frequency electromagnetic fields. The physical principle that is employed is that of **electromagnetic induction**, whereby an alternating magnetic field induces an electrical potential in an electrical circuit intersected by the field. Commercial covermeters can be divided into two classes: those based on the principle of **magnetic reluctance** and those based on **eddy currents**. These differences are summarized below [Carino, 1992b].

19.3.6.2 Magnetic-Reluctance Meters

When current flows through an electrical coil, a magnetic field is created and there is a flow of magnetic flux lines between the magnetic poles. This leads to a magnetic circuit, in which the flow of magnetic flux between poles is analogous to the flow of current in an electrical circuit [Fitzgerald

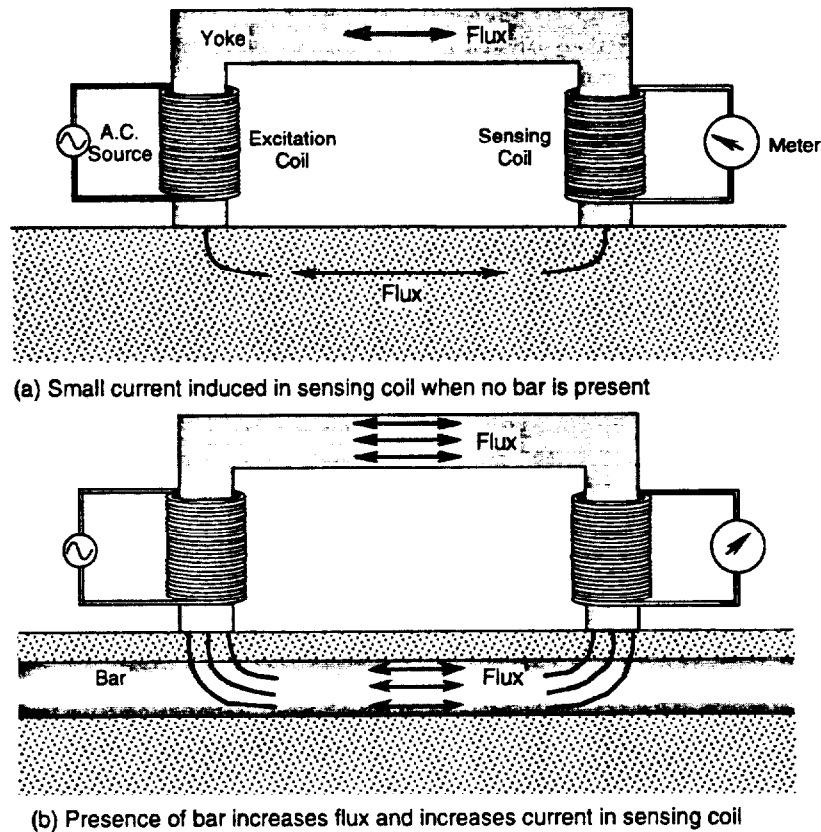
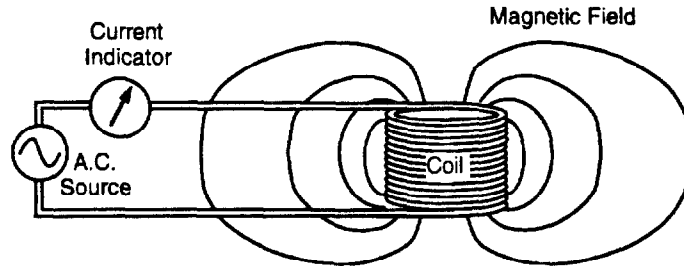


FIGURE 19.23 Covermeter based on the principle of magnetic reluctance [adapted from Carino, 1992b].

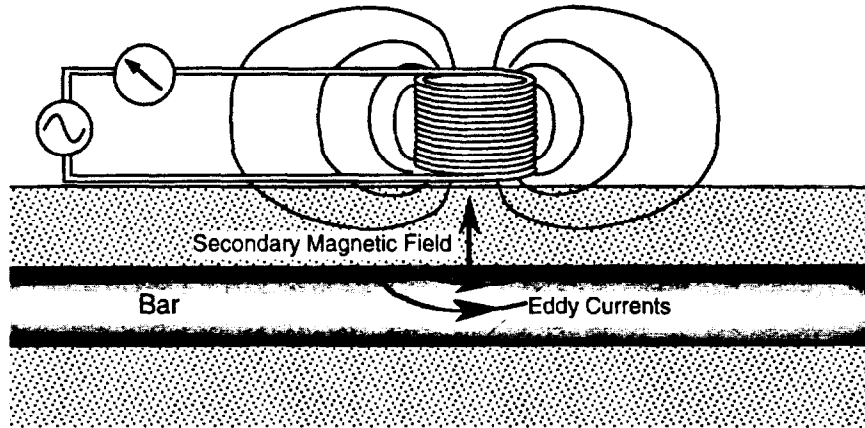
et al., 1967]. The resistance to flow of magnetic flux is called **reluctance**, which is analogous to the resistance to flow of current in an electrical circuit. Figure 19.23 is a schematic of a covermeter that is based on changes in the reluctance of a magnetic circuit caused by the presence or absence of a bar within the vicinity of the search head. The search head is composed of a ferromagnetic U-shaped core (yoke), an excitation coil, and a sensing coil. When alternating current (less than 100 Hz) is applied to the excitation coil, an alternating magnetic field is created and magnetic flux flows between the poles of the yoke. In the absence of a bar (Figure 19.23a), the magnetic circuit, composed of the yoke and the concrete between the ends of the yoke, has a high reluctance and the alternating magnetic flux flowing between the poles will be small. The alternating flux induces a small, secondary current in the sensing coil. If a ferromagnetic bar is present (Figure 19.23b), the reluctance decreases, the magnetic flux amplitude increases, and the sensing-coil current increases. Thus the presence of the bar is indicated by a change in the output from the sensing coil. For a given reinforcing bar, the reluctance of the magnetic circuit depends strongly on the distance between the bar and the poles of the yoke. An increase in concrete cover increases the reluctance and reduces the current in the sensing coil. If the meter output were plotted as a function of the cover, a calibration relationship would be established that could be used to measure the cover. Since the size of the bar affects the reluctance of the magnetic circuit, there would be a separate relationship for each bar size.

19.3.6.3 Eddy-Current Meters

If a coil carrying an alternating current is brought near an electrical conductor, the changing magnetic field induces circulating currents in the conductor. These are known as **eddy currents**.



(a) Coil in air results in a characteristic current amplitude



(b) Interaction with reinforcing bar causes changes in coil impedance and current amplitude

FIGURE 19.24 Covermeter based on eddy-current principle [adapted from Carino, 1992b].

Because any current flow gives rise to a magnetic field, eddy currents produce a secondary magnetic field that interacts with the field of the coil. The second class of covermeters is based on monitoring the effects of the eddy currents induced in a reinforcing bar. Figure 19.24 is a schematic of a continuous eddy-current covermeter. In the absence of a reinforcing bar, the magnitude of the alternating current (usually at about 1 kHz) in the coil depends on the coil impedance.¹⁵ If the coil is brought near a reinforcing bar, alternating eddy currents are established within the surface of the bar. The eddy currents give rise to an alternating secondary magnetic field that induces a secondary current in the coil. In accordance with Lenz's law [Serway, 1983], the secondary current opposes the primary current. As a result, the net current flowing through the coil is reduced, and the apparent impedance of the coil increases [Hagemaier, 1990]. Thus the presence of the bar is inferred by monitoring the change in current flowing through the coil.

19.3.6.4 Characteristics

A reinforcing bar is detected by a covermeter when the bar lies within the zone of influence of the search head (yoke or coil). The response is maximum when the search head lies directly above the reinforcing bar. An important characteristic of a covermeter is the relationship between meter amplitude and the horizontal distance from the center of the bar to the center of the search head. The variation has approximately the same shape as the bell-shaped curve of a normal probability

¹⁵When direct current is applied to a circuit, the amount of current equals the voltage divided by the electrical resistance of the circuit. When alternating current is applied to the coil, the amount of current is governed by the value of the applied voltage, the resistance, and another quantity called **inductance**. The vector sum of resistance and inductance defines the **impedance** of the coil.

distribution. The width of the curve defines the **zone of influence** of the search head. A search head with a smaller zone of influence is better able to discern individual bars when they are closely spaced than is a search head with a wider zone of influence. However, focused search heads generally have less penetrating ability. The influence zone of the search head also affects the accuracy when trying to detect the end of a reinforcing bar [Carino, 1992b].

An important distinction between covermeters is the directionality characteristics of the search heads. Owing to the shape of the yoke, a magnetic reluctance meter is directional compared with a continuous eddy-current meter with a symmetrical coil. Maximum response occurs when the yoke is aligned with the axis of the bar. This directionality can be used to advantage when testing a structure with an orthogonal grid of reinforcing bars [Tam et al., 1977].

For a given covermeter, there are unique relationships between meter amplitude and depth of cover. Figures 19.25a and 19.25b show these relationships for a magnetic reluctance and for an eddy-current meter, respectively. These relationships illustrate a basic limitation of covermeters. Since the amplitude is a function of bar diameter and depth of cover, one cannot determine both parameters from a single measurement. As a result, dual measurements are needed to be able to estimate both depth of cover and diameter [BS 1881; Das Gupta and Tam, 1983]. This is done by first

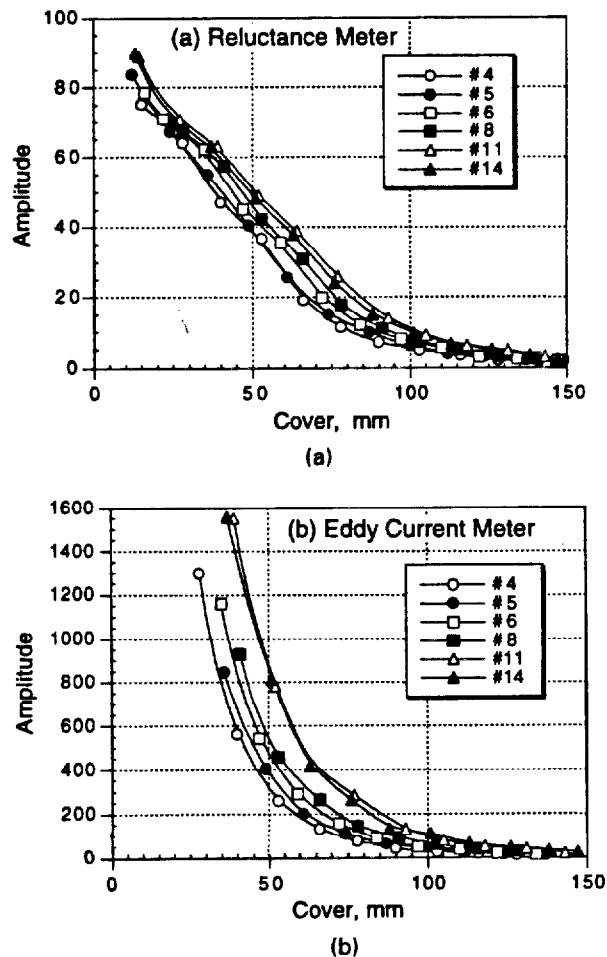


FIGURE 19.25 Amplitude versus cover: (a) results for magnetic reluctance meter, and (b) results for eddy-current meter [adapted from Carino, 1992b].

recording the meter amplitude with the search head in contact with the concrete and then when the search head is located a known distance above the concrete. The difference in amplitudes and the amplitude-cover relationships are used to estimate the cover and bar diameter. The accuracy of this spacer technique depends on how distinct the amplitude-cover relationships are for the different bar sizes. Because these relationships are generally similar for adjacent bar sizes, it is generally only possible to estimate bar diameter within two sizes [Bungey, 1989].

The single-bar, amplitude-cover relationships are only valid when the bars are sufficiently far apart that there is little interference by adjacent bars. For multiple, closely spaced bars, the amplitude may exceed the amplitude for a single bar at the same cover depth. If they are closer than a critical amount, the individual bars cannot be discerned. The critical spacing depends on the type of covermeter and the cover depth. In general, as cover increases, the critical spacing also increases [Carino, 1992b]. Since the response of a covermeter to the presence of multiple, closely spaced bars depends on its design, the user should follow the manufacturer's recommendations regarding minimum bar spacings.

The presence of two layers of reinforcement within the zone of influence cannot generally be identified with ordinary covermeters [Bungey, 1989; Carino, 1992b]. The upper layer produces a much stronger signal than the deeper second layer so that the presence of the second layer cannot be discerned. However, it has been shown that it may be possible to determine lap length when bars are in contact [Carino, 1992b].

In summary, covermeters are effective for locating individual bars, provided that the spacing exceeds a critical value that is dependent on the meter design and the cover depth. By using multiple measurement methods, bar diameter can generally be estimated to within two adjacent bar sizes if the spacing exceeds certain limits that are also dependent on the particular meter. Meters are available that can estimate bar diameter without using spacers to make multiple measurements. Again, the accuracy of these estimates decreases as bar spacing decreases. To obtain reliable measurements, it is advisable to prepare mock-ups of the expected reinforcement configuration to establish whether the desired accuracy is feasible. These mock-ups can be made without using concrete [Carino, 1992b; BS 1881], provided the in-place concrete does not contain significant amounts of iron-bearing aggregates.

19.3.6.5 Corrosion Activity

Electrical methods are used to evaluate corrosion activity of steel reinforcement. As is the case with other NDT methods, an understanding of the underlying principles of these electrical methods is needed to obtain meaningful results. In addition, an understanding of the factors involved in the corrosion mechanism is essential for reliable interpretation of data. The subsequent sections provide basic information about these methods. However, because of the complex interaction of factors, a corrosion specialist should be consulted in planning an investigation.

Corrosion is an electrochemical process involving the flow of charges (electrons and ions). At active sites on the bar, called **anodes**, iron atoms lose electrons and move into the surrounding concrete as ferrous ions. This process is called a **half-cell oxidation reaction**, or the anodic reaction, and is represented as follows:



The electrons remain in the bar and flow to sites, called **cathodes**, where they combine with water and oxygen that are present in the concrete. The reaction at the cathode is called a **half-cell reduction reaction** and is represented as follows:



To maintain electrical neutrality, the ferrous ions migrate through the concrete to these cathodic sites where they combine with water and oxygen to form hydrated iron oxide, or rust. Thus, when the bar is corroding, there is a flow of electrons through the bar and a flow of ions through the concrete. When the bar is not corroding, there is no flow of electrons and ions.

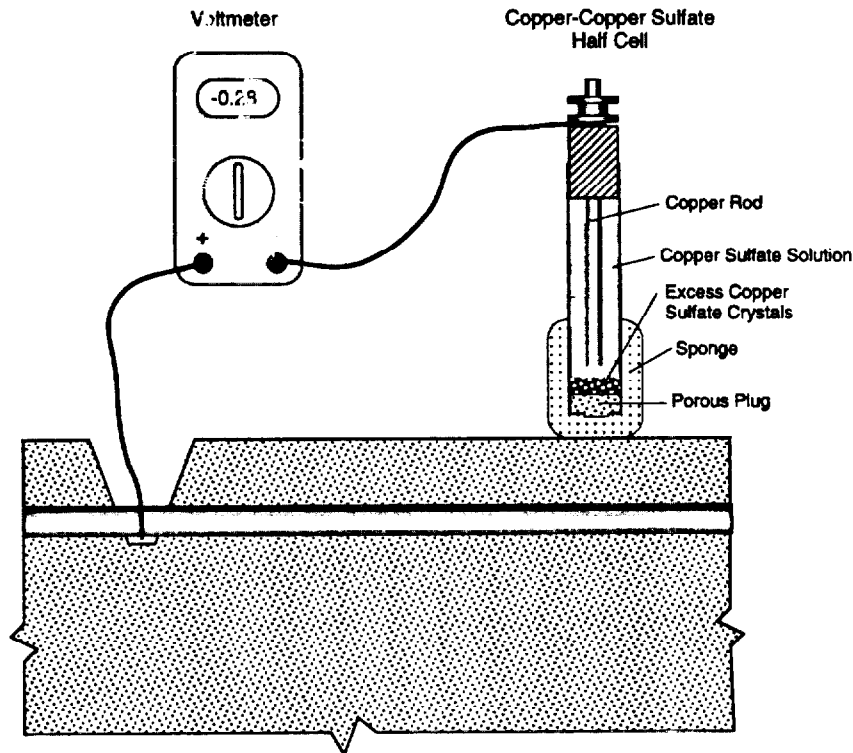


FIGURE 19.26 Apparatus for half-cell potential method described in ASTM C 876.

As the ferrous ions move into the surrounding concrete, the electrons that are left behind in the bar give the bar a negative charge. The **half-cell potential method** is used to detect this negative charge and thereby provide an indication of corrosion activity.

19.3.6.6 Half-Cell Potential Method

Figure 19.26 is a schematic of the apparatus given in ASTM C 876. The apparatus includes a copper-copper sulfate half cell¹⁶, connecting wires, and a high-impedance voltmeter. The positive terminal of the voltmeter is attached to the reinforcement and the negative terminal is attached to the copper-copper sulfate half cell. A high-impedance voltmeter is used so that very little current flows through the circuit. The half-cell makes electrical contact with the concrete by means of a porous plug and a sponge that is moistened with a wetting solution (such as liquid detergent).

If the bar is corroding, electrons would tend to flow from the bar to the half-cell. At the half-cell, the electrons are consumed in a reduction reaction that transforms copper ions in the copper sulfate solution into copper atoms deposited on the rod. Because of the way the terminals of the voltmeter are connected, the voltmeter would indicate a negative value. The more negative the voltage reading, the higher the likelihood that the bar is corroding. The half-cell potential is also called the **corrosion potential** and it is an open-circuit potential because it is measured under the condition of no current in the measuring circuit [ASTM G 15].

¹⁶This half-cell is composed of a copper bar immersed in a saturated copper sulfate solution. It is one of many half-cells that can be used as a reference to measure the electrical potential of embedded bars. The measured voltage depends on the type of half-cell, and conversion factors are available to convert readings obtained with other reference cells to the copper-copper sulfate half-cell.

The half-cell potential readings are indicative of the probability of corrosion activity of reinforcement located beneath the reference cell. However, this is true only if all the reinforcement is electrically connected. To assure that this condition exists, electrical resistance measurements between widely separated reinforcing bars should be carried out [ASTM C 876]. This means that access to the reinforcement has to be provided. The method cannot be applied to concrete with epoxy-coated reinforcement.

A key aspect of the test is assuring that the concrete is sufficiently moist. If the measured potential at a test point does not change by more than ± 20 mV within a 5-min period [ASTM C 876], the concrete is sufficiently moist. If this condition is not satisfied, the concrete surface must be wetted; two methods are given in ASTM C 876.

According to ASTM C 876, two techniques can be used to evaluate the results: (1) the **numeric** technique or (2) the **potential-difference** technique. In the numeric technique, the value of the potential is used as an indicator of the likelihood of corrosion activity. If the potential is more positive than -200 mV, there is a high likelihood that no corrosion is occurring at the time of the measurement. If the potential is more negative than -350 mV, there is a high likelihood that there is active corrosion. Corrosion activity is uncertain when the voltage is in the range of -200 to -350 mV. ASTM C 876 also states that, unless there is positive evidence to suggest their applicability, these numeric criteria should **not** be used under the following conditions:

- carbonation extends to the level of the reinforcement,
- to evaluate indoor concrete that has not been subjected to frequent wetting,
- to compare corrosion activity in outdoor concrete with highly variable moisture or oxygen content, and
- to formulate conclusions about changes in corrosion activity due to repairs that changed the moisture or oxygen content at the level of the steel.

In the potential-difference technique, the areas of active corrosion are identified on the basis of half-cell potential gradients. An equipotential contour map is created by locating the test locations on a scaled plan view of the test area. The half-cell voltage readings at each test point are marked on the plan, and contours of equal voltage values are sketched. Regions of corrosion activity are indicated by closely spaced contours.

As has been stated, valid potential readings are possible only if the concrete is sufficiently moist, and the user must understand how to recognize when there is insufficient moisture. Because of the factors involved in corrosion testing, a corrosion specialist is recommended to properly interpret half-cell potential surveys under the following conditions [ASTM C 876]:

- the concrete is saturated with water,
- the concrete is carbonated to the depth of the reinforcement, or
- the steel is coated (galvanized).

In addition, potential surveys should be supplemented with tests for carbonation and water-soluble chloride content. A major limitation of the half-cell potential method is that it does **not** measure the **rate of corrosion**. It only provides an indication of the **likelihood** of corrosion activity at the time the measurement is made. The corrosion rate of the reinforcement depends on the availability of oxygen that is needed for the cathodic reaction. It also depends on the electrical resistance of the concrete that controls the ease with which ions can move through the concrete. The electrical resistance depends on the microstructure of the paste and the moisture content of the concrete.

19.3.6.7 Linear Polarization

The major drawback of the half-cell potential method has led to the development of several techniques to measure the rate of corrosion [Rodriguez et al., 1994]. The **linear polarization method** is the approach used most frequently in the field [Flis et al., 1992], and efforts were begun for standardization [Cady and Gannon, 1992]. This section provides an overview of the method.

In the field of corrosion science, the term **polarization** refers to the change in the open-circuit potential as a result of the passage of current [ASTM G 15]. In the polarization resistance test, the current necessary to cause a small change in the value of the half-cell potential of the corroding bar is measured. For a small perturbation about the open-circuit potential, there is a linear relationship between the change in voltage, ΔE , and the change in **current per unit area** of bar surface, Δi . This ratio is called the **polarization resistance**, R_p :

$$R_p = \frac{\Delta E}{\Delta i} \quad (19.30)$$

Because the current is expressed per unit surface area of bar that is polarized, the units of R_p are ohms times area. It has been pointed out that R_p is not a resistance in the usual sense of the term [Stern and Roth, 1957], but the term is widely used [ASTM G 15]. The underlying relationships between the corrosion rate of the bar and the polarization resistance were established by Stern and Geary (1957). No attempt is made to explain these relationships, but in simple terms, the corrosion rate is inversely related to the polarization resistance. The corrosion rate is usually expressed as the a corrosion current per unit area of bar, and it is determined as follows:

$$i_{\text{corr}} = \frac{B}{R_p} \quad (19.31)$$

where

- i_{corr} = corrosion rate in ampere per square centimeter
- B = a constant in volts
- R_p = polarization resistance in ohms square centimeter

The constant B is a characteristic of the corrosion system and a value of 0.026 V is commonly used for corrosion of steel in concrete [Feliu et al., 1989]. It is possible to convert the corrosion rate into the mass of steel that corrodes per unit of time, and if the bar size is known, it can be converted to a loss in diameter of the bar [Clear, 1989].

Figure 19.27 is a schematic of basic apparatus for measuring the polarization resistance [Escalante, 1989; Clear, 1989]. It is composed of three electrodes. One electrode is composed of a reference half-cell, and the reinforcement is a second electrode called the **working electrode**. The third electrode is called the **counter electrode**, and it supplies the polarization current to the bar. Supplementary instrumentation measures the voltages and currents during different stages of the test. Such a device can be operated in the **potentiostatic mode**, in which the current is varied to maintain constant potential of the working electrode; or it can be operated in the **galvanostatic mode**, in which the potential is varied to maintain constant current from the counter electrode to the working electrode.

The procedure for using such a three-electrode device to obtain the polarization resistance was provided by Cady and Gannon (1992). The basic steps are as follows:

- Locate the reinforcing-steel grid with a covermeter and mark it on the concrete surface.
- Make an electrical connection to the reinforcement (the working electrode).
- Locate the bar whose corrosion rate is to be measured, wet the surface, and locate the device over the center of the bar.
- Measure the half-cell potential of the reinforcement relative to the reference electrode (Figure 19.27b).
- Measure the current from the counter electrode to the working electrode that is necessary to produce a -4 mV change in the potential of the working electrode (Figure 19.27b).
- Repeat the previous step for values of potential of -8 and -12 mV beyond the corrosion potential.

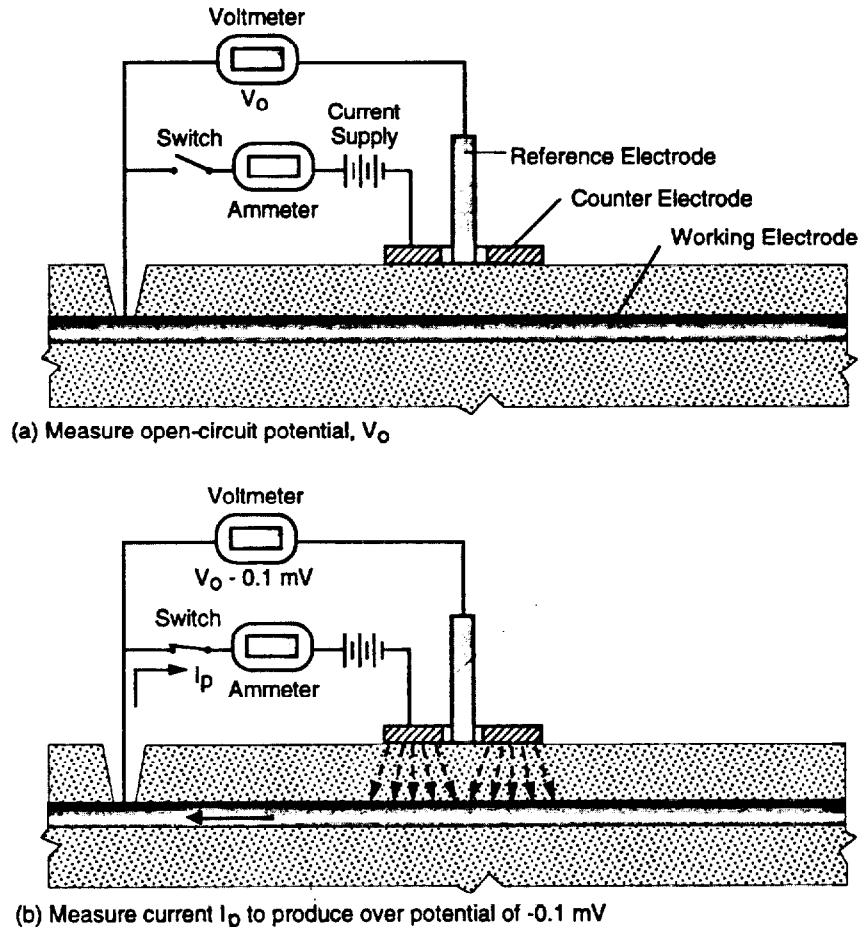


FIGURE 19.27 Three-electrode, linear polarization method to measure corrosion current.

- Determine the surface area of bar that is affected by the measurement (perimeter of bar multiplied by the length below the counter electrode).
- Plot the potential versus the current per unit surface area of the bar, and determine the slope of the best-fit straight line. This is the polarization resistance.

A major uncertainty in obtaining the polarization resistance is the area of the steel bar that is affected by the current flowing from the counter electrode. In the application of the three-electrode device, it is assumed that current flows in straight lines perpendicular to the bar (working electrode) and the counter electrode. Thus the bar area affected during the tests is the bar circumference multiplied by the length of the bar below the counter electrode. However, numerical simulations show that the above assumption is incorrect and that the current lines are not confined to the region directly below the counter electrode [Feliu et al., 1989; Flis et al., 1992]. In an effort to better control the current path from the counter electrode to the bar, a device has been developed that includes a fourth electrode, called a **guard** or **auxiliary electrode**, that surrounds the counter electrode [Feliu et al., 1990a,b]. The guard electrode is maintained at the same potential as the counter electrode and, as a result the current flowing to the working electrode, is confined to the region below the counter electrode.

The corrosion rate based on measuring the polarization resistance represents the corrosion rate at the time of the test. The corrosion rate at a particular point in a structure is expected to depend

on several factors, such as the moisture content of the concrete, the availability of oxygen, and the temperature. Thus the corrosion rate at any point in an exposed structure would be expected to have seasonal variations. Such variations were observed during multiple measurements that extended over a period of more than one year [Clemeña et al., 1992]. To project the amount of corrosion that would occur after an extended period, it is necessary to repeat the corrosion-rate measurements at different times of the year.

At this time, there are no standard procedures for interpreting corrosion-rate measurements obtained with different devices, and a qualified corrosion specialist should be consulted. For example, based on years of experience from laboratory and field testing, Clear (1989) developed guidelines for interpreting measurements obtained with a corrosion-rate device.

There are other limitations that should be considered when planning corrosion rate testing. Some of these have been outlined by Cady and Gannon (1992):

- The concrete surface has to be smooth (not cracked, scarred, or uneven).
- The concrete surface has to be free of water-impermeable coatings or overlays.
- The cover depth has to be less than 100 mm.
- The reinforcing steel can not be epoxy coated or galvanized.
- The steel to be monitored has to be in direct contact with the concrete.
- The reinforcement can not be cathodically protected.
- The reinforced concrete must not be near areas of stray electric currents or strong magnetic fields.
- The ambient temperature must be between 5 and 40°C.
- The concrete surface at the test location must be free of visible moisture.
- Test locations must not be closer than 300 mm to discontinuities, such as edges and joints.

19.3.7 Nuclear (Radioactive) Methods

Nuclear (or radioactive) methods for nondestructive evaluation of concrete involve the use of high-energy electromagnetic radiation to gain information about the internal structure of the test object. These involve a source of penetrating electromagnetic radiation and a sensor to measure the intensity of the radiation after it has traveled through the object. If the sensor is in the form of special photographic film, the technique is called **radiography**. If the sensor is an electronic device that converts the incident radiation into electrical pulses, the technique is called **radiometry**. A review of the early developments in the use of nuclear methods was presented by Malhotra (1976), and more recent developments were reviewed by Mitchell (1991).

Initial work in the late 1940s focused on the use of X rays to produce radiographs that revealed the internal structure of concrete elements, but in the 1950s attention turned to the use of gamma rays. The fundamental differences between these two forms of penetrating radiation are the sources used to generate them and their penetrating ability. X rays are produced by high-voltage electronic devices, and gamma rays are produced by the byproducts of the disintegration of radioactive isotopes. The penetrating ability of gamma rays depends on the radioactive isotope and its age, while the penetration of X rays depends on the voltage of the generating instrument.

Some of the earliest reported work using gamma rays was at Ontario Hydro [de Hass, 1954]. Slabs were constructed with artificial flaws, a pipe containing a radioactive isotope of cobalt was placed beneath the slab, and a Geiger-Müller tube was placed on the top surface of the slab to measure the intensity of radiation. Other early efforts at using gamma ray methods took place in Great Britain during the 1950s, where they were used to locate reinforcing bars, measure density, and locate voids in grouted posttensioning ducts [Forrester, 1970]. Eastern Europe and the Soviet

Union also conducted early studies that eventually led to the development of portable density meters for concrete and soil.

19.3.7.1 Radiometric Methods

There are two basic radiometric methods that use X-rays and gamma rays in nondestructive testing of concrete. In the **transmission** method, the amplitude of the radiation passing through a member is measured. As the radiation passes through a member, the attenuation is dependent on the density of the material and the path length from the source to the sensor. Direct transmission techniques can be used to detect reinforcement. However, the main use of the technique is to measure the in-place density, both in fresh and hardened concrete. Structures of heavyweight and roller-compacted concretes are cases where this method is of particular value. For such applications, the radioactive source is contained in a tube that is pushed into the fresh concrete and the detector is set on the surface of the concrete. The density meter developed at the Technical University of Brno (Czechoslovakia) is an example of such a device. The source can be lowered up to a depth of 200 mm into a hollow steel needle that is pushed into the fresh concrete. A spherical lead shield suppresses the radiation when the source is in its retracted position. Detectors are located beneath the treads used to push the needle into the concrete. It is claimed that the instrument has a resolution of 10 kg/m^3 [Hönig, 1984]. ASTM C 1040 provides procedures for using nuclear methods to measure the in-place density of fresh or hardened concrete. The key element of the procedure is development of the calibration curve for the instrument. This is accomplished by making test specimens of different densities and determining the gauge output for each specimen. The gauge output is plotted as a function of the density, and a best-fit curve is determined.

In the **backscatter method**, a radioactive source is used to supply gamma rays, and a detector close to the source is used to measure the backscattered rays. The scattered rays are lower in energy than the transmitted ones and are produced when a photon collides with an electron in an atom. Part of the photon energy is imparted to the electron, and a new photon emerges, traveling in a new direction with lower energy. This process is known as Compton scattering [Mitchell, 1991]. Backscatter techniques are particularly suitable for applications where a large number of *in situ* measurements are required. Since backscatter measurements are affected by the top 40 to 100 mm, the method is best suited for measurement of the surface zone of a concrete element. A good example of the use of this method is the monitoring of the density of bridge deck overlays. Noncontacting equipment has been developed that is used for continuous monitoring of concrete pavement density during slip-form operations [Mitchell et al., 1979].

Procedures for using backscatter methods to measure concrete density are given in ASTM C 1040. As is the case with direct transmission measurements, it is necessary to establish a calibration curve prior to using a nuclear backscatter gauge to measure in-place density. The inherent precision of backscatter density gauges is less than that of direct transmission devices. ASTM C 1040 requires that a suitable backscatter gauge for density measurement result in a standard deviation of less than 16 kg/m^3 , while the standard deviation should be less than 8 kg/m^3 for a direct transmission gauge. According to ASTM C 1040, backscatter gauges are typically influenced by the top 75 to 125 mm of material. The top 25 mm determines 50 to 70% of the count rate, and the top 50 mm determines 80 to 95% of the count rate.

19.3.7.2 Radiographic Methods

Radiography provides a radiation-based photograph of the interior of concrete. From this photograph, the location of reinforcement, voids in concrete, or voids in grouting of posttensioning ducts can be identified. A radiation source is placed on one side of the test object and a beam of radiation is emitted. As the radiation passes through the member, it is attenuated by different amounts, depending on the density and thickness of the material that is traversed. The radiation that emerges from the opposite side of the object strikes a special photographic film that is exposed in proportion

to the intensity of the incident radiation. When the film is developed, a two-dimensional visualization (a photograph) of the interior structure of the object is obtained. The presence of high-density material, such as reinforcement, is shown on the developed film as a light area, and a region of low density, such as a void, is shown as a dark area.

The British Standards Institute has adopted a standard for radiographic testing of concrete, BS 1881: Part 205 (Recommendations for radiography of concrete). The standard provides recommendations for investigators considering radiographic examinations of concrete [Mitchell, 1991].

In X-radiography, the radiation is produced by an X-ray tube [Mitchell, 1991]. The penetrating ability of the X rays is dependent on the operating voltage of the X-ray tube. In gamma radiography, a radioactive isotope is used as the radiation source. The selection of a source depends on the density and thickness of the test object and on the exposure time that can be tolerated. The most intense source is cobalt-60, which can be used to penetrate up to 500 mm of concrete. For members with thickness of 150 mm or less, iridium-192 or cesium-137 can be used [Mitchell, 1991]. The film type will depend on the thickness and density of the member being tested.

Most field applications have used radioactive sources because of their greater penetrating ability (higher energy radiation) compared with X rays. However, a system, known as Scorpion II, was developed in France that uses a linear accelerator to produce very high energy X rays than can penetrate up to 1 m of concrete. This system was developed for the inspection of prestressed members to establish the condition and location of prestressing strands and to determine the quality of grouting in tendon ducts [Mitchell, 1991].

19.3.7.3 Summary

While nuclear methods have the ability to “see” into concrete, they are cumbersome and require trained and licensed personnel [Mitchell, 1991]. Testing across the full thickness of a concrete element is particularly hazardous and requires extensive precautions, skilled personnel, and highly specialized equipment. Radiographic procedures are costly and require evacuation of the structure by persons not involved in the actual testing. The use of X-ray equipment poses an additional danger owing to the high voltages that are used. There are limits on the thicknesses of the members that can be tested by radiographic methods. For gamma-ray radiography the maximum thickness is about 500 mm, because thick members require unacceptably long exposure times. Radiography is not very useful for locating crack planes perpendicular to the radiation beam. Because of these major drawbacks, radiographic methods are not used routinely for flaw detection. However, there may be situations where the ability to see the internal structure of the member surpasses these drawbacks.

19.4 Concluding Remarks

This chapter has summarized the available nondestructive techniques for assessing the properties or condition of concrete in structures. The techniques have been divided into two groups:

- those used for estimating the in-place strength, and
- those used for flaw detection and condition assessment.

Emphasis has been placed on describing their underlying principles and highlighting some of their inherent limitations. The user is referred to applicable publications of the American Concrete Institute and relevant ASTM standards for additional information on using these methods.

The key feature of the methods for estimating in-place strength is the strength relationship that correlates the concrete strength to the results of the in-place tests. The strength relationship should be developed experimentally before using the test method to estimate in-place strength. For new construction, test specimens should be made of concrete similar to what will be used in the structure. Care must be exercised to ensure that the companion in-place tests and standard strength tests are carried out on specimens of the same maturity at each strength level. For existing construction, it

is necessary to perform in-place tests and obtain cores at different locations so that a wide range of concrete strengths can be used to develop the strength relationship. After the strength relationship has been established, in-place tests are done on the structure, and statistical methods are used to convert the average of in-place test results to a reliable estimate of in-place strength. Generally, in-place test methods that result in local failure of the concrete are more reliable than those that are totally nondestructive.

A variety of methods are available for flaw detection and condition assessment. Most of these methods are based on monitoring the response of the structure when it is subjected to some type of disturbance. Two broad classes of nondestructive methods are those based on stress-wave propagation and those based on electromagnetic-wave propagation. Except for visual inspection, these methods generally require sophisticated instrumentation. All nondestructive test methods have inherent strengths and weaknesses. It is often advantageous to use more than one method to make the assessment. Methods based on stress-wave propagation are suited for identifying the presence of internal concrete-air interfaces, such as those due to cracking or voids. An understanding of the basics of stress-wave propagation is essential for proper interpretation of test results. Electrical methods are well suited for gaining information about embedded reinforcement, such as location, approximate size, and whether active corrosion exists. Radar is appropriate for finding deep metallic embedments and is also sensitive to the presence of moisture. Radar has the added advantage that large portions of a structure can be scanned in a short time.

The importance of having qualified operators cannot be overemphasized. Nondestructive tests are indirect methods by which the property or characteristic of primary interest is inferred by measuring other properties or characteristics. A lack of understanding of the underlying principles and the interferences associated with the method can lead to incorrect assessments of the concrete. When used by properly trained operators, nondestructive test methods offer technical and economic advantages compared with other destructive sampling techniques.

References

ACI Reports, available from American Concrete Institute, Farmington Hills, MI:

201.1R: Guide for Making a Condition Survey of Concrete in Service

207.3R: Practices for Evaluation of Concrete in Existing Massive Structures for Service Conditions

224.1R: Causes, Evaluation and Repair of Cracks in Concrete Structures

228.1R(1989): In-Place Methods for Determination of Strength of Concrete

228.1R(1995): In-Place Methods to Estimate Concrete Strength

362R: State-of-the-Art Report on Parking Structures

437R: Strength Evaluation of Existing Concrete Buildings

ASTM Standards, available from ASTM, West Conshohocken, PA

1995 Annual Book of ASTM Standards, Vol. 04.02

C 597: Standard Test Method for Pulse Velocity Through Concrete

C 803: Standard Test Method for Penetration Resistance of Hardened Concrete

C 805: Standard Test Method for Rebound Number of Hardened Concrete

C 876: Test Method for Half-Cell Potential of Uncoated Reinforcing Steel in Concrete

C 900: Standard Test Method for Pullout Strength of Hardened Concrete

C 1040: Test Methods for Density of Unhardened and Hardened Concrete in Place by Nuclear Methods

C 1074: Standard Practice for Estimating Concrete Strength by the Maturity Method

C 1150: Standard Test Method for the Break-Off Number of Concrete

1995 Annual Book of ASTM Standards, Vol. 04.03

D 4580: Standard Practice for Measuring Delaminations in Concrete Bridge Decks by Sounding

- D 4788: Standard Test Method for Detecting Delaminations in Bridge Decks Using Infrared Thermography
- D 4748: Standard Test Method for Determining the Thickness of Bound Pavement Layers Using Short-Pulse Radar
1995 Annual Book of ASTM Standards, Vol. 03.02
- G 15: Terminology Relating to Corrosion and Corrosion Testing
British Standard: Available from British Standards Institution, London. BS 1881: Part 204. Recommendations on the Use of Electromagnetic Covermeters.
- Alongi, A.V., Cantor, T.R., Kneeter, C.P., and Alongi, A., Jr. 1982. Concrete evaluation by radar theoretical analysis. *Transportation Research Record No. 853*, pp. 31–37. Transportation Research Board, Washington, DC.
- Arni, H.T. 1972. Impact and Penetration Tests of Portland Cement Concrete. *Highway Research Record 378*, pp. 55–67. Highway Research Board, Washington, DC.
- Ballarini, R., Shah, S.P., and Keer, L.M. 1986. Failure characteristics of short anchor bolts embedded in a brittle material. *Proc. Royal Soc. London A404*:35–54.
- Barker, M.G. and Ramirez, J.A. 1988. Determination of concrete strengths using the break-off tester. *ACI Mater. J.* 82(6):221–228.
- Bickley, J.A. 1982a. Concrete optimization. *Concrete Int.* 4(6):38–41.
- Bickley, J.A. 1982b. Variability of pullout tests and in-place concrete strength. *Concrete Int.* 4(4):44–51.
- Bracewell, R. 1978. *The Fourier Transform and its Applications*, 2nd ed., 444 pp. McGraw-Hill Co., New York.
- Brown, T.L. and LeMay, H.E. 1988. Chemistry: *The Central Science*, 4th ed., pp. 494–498. Prentice Hall, Upper Saddle River, NJ.
- Bungey, J.H. 1981. Concrete strength determination by pull-out tests on wedge anchor bolts. *Proc. Inst. Civ. Eng. Part 2* 71:379–394.
- Bungey, J.H. 1989. *Testing of Concrete in Structures*, 2nd ed., 228 pp. Chapman and Hall, NY.
- Bungey, J.H. and Millard, S.G. 1993. Radar inspection of structures. *Proc. Inst. Civ. Eng. Struct. Buildings J.* 99:173–186.
- Bungey, J.H., Millard, S.G., and Shaw, M.R. 1994. The influence of reinforcing steel on radar surveys of structural concrete. *Constr. Building Mater.* 8(2):119–126.
- Byfors, J. 1980. Plain Concrete at Early Ages. Swedish Cement and Concrete Research Institute Report 3:80, 464 pp. Stockholm, Sweden.
- Cady, P.D. and Gannon, E.J. 1992. Condition Evaluation of Concrete Bridges Relative to Reinforcement Corrosion, Volume 8: Procedure Manual. *SHRP-S/FR-92-110*, 124 pp. Strategic Highway Research Program, National Research Council, Washington, DC.
- Cantor, T.R. 1984. Review of penetrating radar as applied to nondestructive evaluation of concrete. In *In Situ/Nondestructive Testing of Concrete*, V.M. Malhotra, ed. ACI SP-82, pp. 581–601. American Concrete Institute, Farmington Hills, MI.
- Cantor, T. and Kneeter, C. 1982. Radar as applied to evaluation of bridge decks. *Transportation Research Record No. 853*, pp. 37–42. Transportation Research Board, Washington, DC.
- Carette, G.G. and Malhotra, V.M. 1991. Long-Term Strength Development of Silica Fume Concrete. Paper presented at CANMET/ACI International Workshop on the Use of Silica Fume. April 7–9, 1991. Washington, DC.
- Carino, N. J. 1982. Maturity functions for concrete. In *Proc. RILEM Int. Conf. Concr. Early Ages (Paris)*, Vol. I, pp. 123–128. Ecole Nationale des Ponts et Chaussées. Paris.
- Carino, N.J. 1984. The maturity method: Theory and application. *J. Cement, Concr. Aggregates* 6(2):61–73.
- Carino, N.J. 1991a. The maturity method. In *Handbook on Nondestructive Testing of Concrete*, V.M. Malhotra and N.J. Carino, eds., pp. 101–146. CRC Press, Boca Raton, FL.

- Carino, N.J. 1991b. Pullout test. In *Handbook on Nondestructive Testing of Concrete*, V.M. Malhotra and N.J. Carino, eds., pp. 39–82. CRC Press, Boca Raton, FL.
- Carino, N.J. 1992a. Recent developments in nondestructive of concrete. In *Advances in Concrete Technology*, V.M. Malhotra, ed. MSL 92-6(R), pp. 281–328. Energy, Mines and Resources, Ottawa.
- Carino, N.J. 1992b. Performance of electromagnetic covermeters for nondestructive assessment of steel reinforcement, *NISTIR 4988*, 130 pp. National Institute of Standards and Technology. Gaithersburg, MD.
- Carino, N.J. 1993. Statistical methods to evaluate in-place test results. In *New Concrete Technology: Robert E. Philleo Symposium*, ACI SP-141, pp. 39–64. American Concrete Institute, Farmington Hills, MI.
- Carino, N.J. 1994. Nondestructive testing of concrete: History and challenges. In *Concrete Technology Past, Present, and Future*. Proceedings of V. Mohan Malhotra Symposium, ACI SP-144, pp. 623–678. American Concrete Institute, Farmington Hills, MI.
- Carino, N.J. and Sansalone, M. 1992. Detecting voids in metal tendon ducts using the impact-echo method. *ACI Mater. J.* 89(3):296–303.
- Carino, N.J. and Tank, R.C. 1992. Maturity functions for concrete made with various cements and admixtures. *ACI Mater. J.* 89(2):188–196.
- Carino, N.J., Sansalone, M., and Hsu, N.N. 1986. Flaw detection in concrete by frequency spectrum analysis of impact-echo waveforms. In *International Advances in Nondestructive Testing*, W.J. McGonnagle, ed., pp. 117–146. Gordon & Breach Science Publishers, New York.
- Carino, N.J., Knab, L.I., and Clifton, J.R. 1992. Applicability to the maturity method to high-performance concrete, *NISTIR-4819*, 64 pp. National Institute of Standards and Technology. Available from NTIS, Springfield, VA, 22161. PB93-157451/AS.
- Carter, C.R., Chung T., Holt, F.B., and Manning D. 1986. An automated signal processing system for the signature analysis of radar waveforms from bridge decks. *Can. Electr. Eng. J.* 11(3):128–137.
- Chabowski, A.J. and Bryden-Smith, D.W. 1980. Assessing the strength of concrete of in-situ Portland cement concrete by internal fracture tests. *Mag. Concr. Res.* 32(112):164–172.
- Cheng, C. and Sansalone, M. 1993a. The impact-echo response of concrete plates containing delaminations: Numerical, experimental, and field studies. *Mater. Struct.* 26(159):274–285.
- Cheng, C. and Sansalone, M. 1993b. Effects on impact-echo signals caused by steel reinforcing bars and voids around bars. *ACI Mater. J.* 90(5):421–434.
- Cheng, C. and Sansalone, M. 1995a. Determining the minimum crack width that can be detected using the impact-echo method, Part 1: Experimental study. *Mater. Struct.* 28(176):74–82.
- Cheng, C. and Sansalone, M. 1995b. Determining the minimum crack width that can be detected using the impact-echo method, Part 2: Numerical fracture analyses. *Mater. Struct.* 28(177):125–132.
- Clear, K.C. 1989. Measuring rate of corrosion of steel in field concrete structures. *Transportation Research Record 1211*, pp. 28–37. Transportation Research Board, Washington, DC.
- Clemeña, G.G. 1983. Nondestructive inspection of overlaid bridge decks with ground-penetrating radar, *Transportation Research Record No. 899*, pp. 21–32. Transportation Research Board, Washington, DC.
- Clemeña, G.G. 1991. Short-pulse radar methods. In *Handbook on Nondestructive Testing of Concrete*. V.M. Malhotra and N.J. Carino, eds., pp. 253–274. CRC Press, Boca Raton, FL.
- Clemeña, G.G. and McKeel, W.T., Jr. 1978. Detection of delamination in bridge decks with infrared thermography, *Transportation Research Record No. 664*, pp. 180–182. Transportation Research Board, Washington, DC.
- Clemeña, G.G., Jackson, D.R., and Crawford, G.C. 1992. Inclusion of rebar corrosion rate measurements in condition surveys of concrete bridge decks, *Transportation Research Record 1347*, pp. 37–45. Transportation Research Board, Washington, DC.

- Daniels, D.J., Gunton, D.J., and Scott, H.F. 1988. Introduction to subsurface radar. *Proc. Inst. Electr. Eng.* 135, Part F(4):278–320.
- Das Gupta, N.C. and Tam, C.T. 1983. Non-destructive technique for simultaneous detection of size and cover of embedded reinforcement. *Br. J. Non-Destructive Test.* 25(6):301–304.
- Davis, A. and Dunn, C. 1974. From theory to field experience with the nondestructive vibration testing of piles. *Proc. Inst. Civ. Eng.* 57, Part 2:571–593.
- Davis, A.G. and Hertlein, B.H. 1991. Developments of nondestructive small-strain methods for testing deep foundations: A review. *Transportation Research Record No. 1331*, pp. 15–20. Transportation Research Board, Washington, DC.
- de Hass, E. 1954. Letter to editor. *J. Am. Concrete Inst.* 25(10):890–891.
- Domone, P.L. and Castro, P.F. 1986. An expandable sleeve test for in-situ concrete strength evaluation. *Concrete* 20(3):24–25.
- Escalante, E. 1989. Elimination of IR error in measurements of corrosion in concrete. In *The Measurement and Correction of Electrolyte Resistance in Electrochemical Tests*. ASTM STP 1056, L.L. Scribner and S.R. Taylor, eds., pp. 180–190. American Society for Testing and Materials, Philadelphia, PA.
- Făcăoaru, I. 1969. Chairman's Report, Meeting of RILEM TC on Non-Destructive Testing of Concrete, Varna, September, 1968. *Mater. Struct.* 2(10):253–267.
- Feliu, S., González, J.A., Andrade, C., and Feliu, V. 1989. Polarization resistance measurements in large concrete specimens: Mathematical solution for unidirectional current distribution. *Mater. Struct. Res. Test.* 22(129):199–205.
- Feliu, S., González, J.A., Feliu, S., Jr., and Andrade, M.C. 1990a. Confinement of the electrical signal for in-situ measurement of polarization resistance in reinforced concrete. *ACI Mater. J.* 87(5):457–460.
- Feliu, S., González, J.A., Escudero, M.L., Feliu, S. Jr., and Andrade, M.C. 1990b. Possibilities of the guard ring for electrical signal confinement in the polarization measurements of reinforcements. *J. Sci. Eng. Corrosion* 46(12):1015–1020.
- Fitzgerald, A.E., Higginbotham, D.E., and Gabel, A. 1967. *Basic Electrical Engineering*. McGraw-Hill Book Co., New York.
- Flis, J., Sehgal, A., Li, D., Kho, Y.T., Sabol, S., Pickering, H., Osseo-Asare, K., and Cady, P.P. 1992. Condition evaluation of concrete bridges relative to reinforcement corrosion, Volume 2: Method for measuring the corrosion rate of reinforcing steel. *SHRP-S/FR-92-104*, 105 pp. Strategic Highway Research Program, National Research Council, Washington, DC.
- Freiesleben Hansen, P. and Pedersen J. 1977. Maturity computer for controlled curing and hardening of concrete. *Nordisk Betong* 1:19–34.
- Freiesleben Hansen, P. and Pedersen, J. 1985. Curing of concrete structures. *CEB Inf. Bull.* 166, 42 pp. Comite Euro. International du Beton, Lausanne, Switzerland.
- Forrester, J.A. 1970. Gamma radiography of concrete. *Proc. Symp. Non-Destructive Test. Concr. Timber*, pp. 13–17. Institution of Civil Engineers, London.
- Gaynor, R. D. 1969. In-place strength of concrete—A comparison of two test systems. *NRMCA Technical Information Letter No. 272*. National Ready Mixed Concrete Assn., Silver Spring, MD.
- Geiker, M. 1983. Studies of Portland cement hydration by measurements of chemical shrinkage and systematic evaluation of hydration curves by means of the dispersion model, Ph.D. Dissertation, 259 pp. Technical University of Denmark, Lyngby, Denmark.
- Goldsmith, W. 1965. *Impact: The Theory and Physical Behavior of Colliding Solids*, pp. 24–50. Edward Arnold Press, Ltd., London.
- Greene, G.W. 1954. Test hammer provides new method of evaluating hardened concrete. *J. Am. Concr. Inst.* 26(3):249–256.
- Hagemaiier, D.J. 1990. *Fundamentals of Eddy Current Testing*. American Society for Nondestructive Testing, Inc., Columbus, OH.

- Halabe, U.B., Sotoodehnia, A., Maser, K.R., and Kausel, E.A. 1993. Modeling the electromagnetic properties of concrete. *ACI Mater. J.* 90(6):552–563.
- Halabe, U.B., Maser, K.R., and Kausel, E.A. 1995. Condition assessment of reinforced concrete structures using electromagnetic waves. *ACI Mater. J.* 92(5):511–523.
- Halliday, D. and Resnick, R. 1978. *Physics*, 3rd ed., John Wiley & Sons, New York.
- Heisey, J.S., Stokoe, K.H., II, and Meyer, A.H. 1982. Moduli of pavement systems from spectral analysis of surface waves. *Transportation Research Record No. 853*, pp. 22–31. Transportation Research Board, Washington, DC.
- Hellier, A.K., Sansalone, M., Carino, N.J., Stone, W.C., and Ingraffea, A.R. 1987. Finite-element analysis of the pullout test using a nonlinear discrete cracking approach. *J. Cement, Concr. Aggregates* 9(1):20–29.
- Higgs, J. 1979. Integrity testing of piles by the shock method. *Concrete* 13(10):31–33.
- Hindo, K.R. and Bergstrom, W.R. 1985. Statistical evaluation of the in-place strength of concrete. *Concr. Int.* 7(2):44–48.
- Holt, F.B. and Eales, J.W. 1987. Nondestructive evaluation of pavements. *Concr. Int.* 9(6): 41–45.
- Hönig, A. 1984. Radiometric determination of the density of fresh shielding concrete in situ. In *In Situ/Nondestructive Testing of Concrete*, V.M. Malhotra, ed. ACI SP-82, pp. 603–618. American Concrete Institute, Farmington Hills, MI.
- Jaeger, B.J., Sansalone, M.J., and Poston, R.W. 1996. Detecting voids in grouted tendon ducts of post-tensioned concrete structures using the impact-echo method. *ACI Struct. J.* 93(4):462–472.
- Jensen, B.C. and Braestrup, M.W. 1976. Lok-tests determine the compressive strength of concrete. *Nordisk Betong* 2:9–11.
- Johansen, R. 1977. A new method for the determination of in-place concrete strength at form removal. *Proc. RILEM Int. Symp. Testing In Situ Concr. Struct.*, Part II. Budapest, September 12–15, pp. 276–288, Institut des Sciences de la Construction, Budapest.
- Johansen, R. 1979. In situ strength evaluation of concrete—The break-off method. *Concr. Int.* 1(9):45–51.
- Jones, R. 1949a. Measurement of the thickness of concrete pavements by dynamic methods: A survey of the difficulties. *Mag. Concr. Res.* 1:31–34.
- Jones, R. 1949b. The non-destructive testing of concrete. *Mag. Concr. Res.* 2:67–78.
- Jones, R. 1953. Testing of concrete by ultrasonic-pulse technique. *Proc. Highway Res. Board*, No. 32, pp. 259–275. National Research Council, Washington, DC.
- Jones, R. 1955. A vibration method for measuring the thickness of concrete road slabs in situ. *Mag. Concr. Res.* 7(20):97–102.
- Jones, R. 1962. Surface wave technique for measuring the elastic properties and thickness of roads: Theoretical development. *Br. J. Appl. Phys.* 13:21–29.
- Jones, R. and Făcăoaru, I. 1969. Recommendations for testing concrete by the ultrasonic pulse method. *Mater. Struct.* 2(10):275–284.
- Kierkegaard-Hansen, P. 1975. Lok-strength. *Nordisk Betong*. 3:19–28.
- Kolek, J. 1958. An appreciation of the Schmidt rebound hammer. *Mag. Concr. Res.* 10(28):27–36.
- Knudsen, T. 1980. On particle size distribution in cement hydration. *Proc. 7th Int. Congr. Chem. Cement (Paris, 1980)*, Vol. II, I-170–175. Editions Septima, Paris.
- Knudsen, T. 1984. The dispersion model for hydration of Portland cement: I. General concepts. *Cement Concr. Res.* 14:622–630.
- Krautkrämer, J. and Krautkrämer, H. 1990. *Ultrasonic Testing of Materials*, 4th ed., Springer-Verlag, New York.
- Krenchel, H. and Bickley, J.A. 1987. Pullout testing of concrete: Historical background and scientific level today. *Nordisk Betong* 6:155–168.
- Krenchel, H. and Shah, S.P. 1985. Fracture analysis of the pullout test. *Mater. Struct.* 18(108):439–446.

- Krstulovic-Opara, N., Woods, R.D., and Al-Shayea, N. 1996. Nondestructive testing of concrete structures using the Rayleigh wave dispersion method. *ACI Mater. J.* 93(1):75–86.
- Kunz, J.T. and Eales, J.W. 1985. Remote sensing techniques applied to bridge deck evaluation. In *Strength Evaluation of Existing Concrete Bridges*, T.C. Liu, ed., ACI SP-88, pp. 237–258. American Concrete Institute, Farmington Hills, MI.
- Lauer, K.R. 1991. Magnetic/electrical methods. In *Handbook on Nondestructive Testing of Concrete*, V.M. Malhotra and N.J. Carino, eds., pp. 203–225. CRC Press, Boca Raton, FL.
- Leslie, J.R. and Cheesman, W.J. 1949. An ultrasonic method of studying deterioration and cracking in concrete structures. *J. Am. Concr. Inst.* 21(1):17–36.
- Leshchinsky, A.M. 1990. Determination of concrete strength by nondestructive methods. *Cement Concr. Aggregates* 12(2):107–113.
- Leshchinsky, A.M. 1991a. Correlation of concrete strength and non-destructive tests. *Indian Concr. J.* 65(4):184–190.
- Leshchinsky, A.M. 1991b. Combined methods of determining control measures of concrete quality. *Mater. Struct.* 24(141):177–184.
- Leshchinsky, A.M. 1992. Non-destructive testing of concrete strength: Statistical control. *Mater. Struct.* 25(146):70–78.
- Leshchinsky, A.M. and Leshchinsky, M. Yu. 1991. Correlation formulae in nondestructive testing for concrete strength. *J. Struct. Eng.* 18(3):99–113.
- Lin, J.M. and Sansalone, M.J. 1996a. Impact-echo studies of interfacial bond quality in concrete: Part I—Effects of unbonded fraction of area. *ACI Mater. J.* 93(3):223–232.
- Lin, J.M. and Sansalone, M.J. 1996b. Impact-echo studies of interfacial bond quality in concrete: Part II—Effects of bond tensile strength. *ACI Mater. J.* 93(4):318–326.
- Lin, Y. and Sansalone, M. 1992a. Detecting flaws in concrete beams and columns using the impact-echo method. *ACI Mater. J.* 89(4):394–405.
- Lin, Y. and Sansalone, M. 1992b. Transient response of thick circular and square bars subjected to transverse elastic impact. *J. Acoust. Soc. Am.* 91(2):885–893.
- Lin, Y. and Sansalone, M., 1992c. Transient response of thick rectangular bars subjected to transverse elastic impact. *J. Acoust. Soc. Am.* 91(5):2674–2685.
- Lin, Y., Sansalone, M., and Carino, N.J. 1991a. Finite element studies of the impact-echo response of plates containing thin layers and voids. *J. Nondestructive Eval.* 9(1):27–47.
- Lin, Y., Sansalone, M., and Carino, N.J. 1991b. Impact-echo response of concrete shafts. *ASTM Geotechn. J.* 14(2):121–137.
- Long, B.G., Kurtz, H.J., and Sandenaw, T.A. 1945. An instrument and a technic for field determination of elasticity, and flexural strength of concrete (pavements). *J. Am. Concr. Inst.* 16(3):217–231.
- Mailhot, G., Bisailon, G., Carette, G.G., and Malhotra, V.M. 1979. In-place concrete strength: New pullout methods. *ACI J.* 76(12):1267–1282.
- Malhotra, V.M. 1975. Evaluation of the pull-out tests to determine strength of in-situ concrete. *Mater. Struct.* 8(43):19–31.
- Malhotra, V.M. 1976. *Testing Hardened Concrete: Nondestructive Methods*. American Concrete Institute Monograph No. 9, 204 pp. ACI/Iowa State University Press, Ames, IA.
- Malhotra, V.M. 1991. Surface hardness methods. In *Handbook on Nondestructive Testing of Concrete*, V.M. Malhotra and N.J. Carino eds., pp. 1–17. CRC Press, Boca Raton, FL.
- Malhotra, V.M. and Carette, G.G. 1980. Comparison of pullout strength of concrete with compression strength of cylinders and cores, pulse velocity, and rebound number. *ACI J.* 77(3):17–31.
- Malhotra, V.M. and Carette, G.G. 1991. Penetration resistance methods. In *Handbook on Non-destructive Testing of Concrete*, V.M. Malhotra and N.J. Carino, eds., pp. 19–38. CRC Press, Boca Raton, FL.
- Malhotra, V.M. and Carino, N.J., eds. 1991. *Handbook on Nondestructive Testing of Concrete*, 343 pp. CRC Press, Boca Raton, FL.

- Malhotra, V.M. 1974. Evaluation of the Windsor probe test for estimating compressive strength of concrete. *Mater. Struct.* 7(37):3–15.
- Malhotra, V.M. 1971. Maturity concept and the estimation of concrete strength. *Information Circular IC 277*, 43 pp. Department of Energy Mines Resources, Canada.
- Mandel, J. 1984. Fitting straight lines when both variables are subject to error. *J. Qual. Technol.* 16(1):1–14.
- Manning, D.G. and Holt, F.B. 1983. Detecting deterioration in asphalt-covered bridge decks. *Transportation Research Record No. 899*, pp. 10–20. Transportation Research Board, Washington, DC.
- Manning, D.G. and Holt, F.B. 1980. Detecting deterioration in concrete bridge decks. *Concr. Inter.* 2(11):34–41.
- Mast, J.E. and Johansson, E.M. 1994. Three-dimensional ground penetrating radar imaging using multi-frequency diffraction tomography. *Proc. SPIE Int. Soc. Opt. Eng. Adv. Microwave Millimeter-Wave Detectors* 2275:196–204.
- Mast, J.E., Lee, H., Chew, C., and Murtha, J. 1990. Pulse-echo holographic techniques for microwave subsurface NDE. *Proc. Conf. Nondestructive Eval. Civ. Struct. Mater.*, Oct. 15–17, Boulder, Colo., pp. 177–191. National Science Foundation (sponsor).
- Maser, K.R. 1986. Detection of progressive deterioration in bridge decks using ground penetrating radar. In *Experimental Assessment of the Performance of Bridges*. Proceedings of ASCE/EM Division Specialty Conference, pp. 42–57. Boston, MA. Oct.
- Maser, K.R. and Roddis, W.M.K. 1990. Principles of thermography and radar for bridge deck assessment. *J. Transp. Eng.* 116(5):583–601.
- McIntosh, J. D. 1949. Electrical curing of concrete, *Mag. Concr. Res.* 1(1):21–28.
- Mitchell, T.W. 1991. Radioactive/nuclear methods. In *Handbook on Nondestructive Testing of Concrete*, V.M. Malhotra and N.J. Carino, eds., pp. 227–252. CRC Press, Boca Raton, FL.
- Mitchell, T.M., Lee, P.L., and Eggert, G.J. 1979. The CMD: A device for the continuous monitoring of the consolidation of plastic concrete. *Public Roads* 42(148).
- Morey, R.M. 1974. Continuous subsurface profiling by impulse radar. *Proc. Eng. Found. Conf. Subsurface Explor. Underground Excavation Heavy Const.* N.H. Henniker, Aug., pp. 213–232. Engineering Foundation, New York.
- Naik, T.R. 1991. The break-off test method. In *Handbook on Nondestructive Testing of Concrete*, V.M. Malhotra and N.J. Carino, eds., pp. 83–100. CRC Press, Boca Raton, FL.
- Naik, T.R. and Malhotra, V.M. 1991. The ultrasonic pulse velocity method. In *Handbook on Nondestructive Testing of Concrete*, V.M. Malhotra and N.J. Carino, eds., pp. 169–188. CRC Press, Boca Raton, FL.
- Naik, T.R., Salameh, Z., Hassaballah, A. 1987. *Evaluation of In-Place Strength of Concrete by the Break-Off Method*, 101 pp. Dept. of Civil Engineering and Mechanics, University of Wisconsin, Milwaukee.
- Nasser, K.W. and Al-Manseer, A.A. 1987a. A new nondestructive test. *Concr. Int. Design Const.* 9(1):41–44.
- Nasser, K.W. and Al-Manseer, A.A. 1987b. Comparison of nondestructive testers of hardened concrete. *ACI Mater. J.* 84(5):374–380.
- Natrella, M.G. 1963. National Bureau of Standards. *Experimental Statistics*, Chapter 5. Handbook 91. Washington, DC.
- Nazarian, S. and Desai, M.R. 1993. Automated surface wave method: Field testing. *J. Geotech. Eng.* 119(7):1094–1111.
- Nazarian, S. and Stokoe, K.H., II. 1986a. In-situ determination of elastic moduli of pavement systems by spectral-analysis-of-surface-waves method (practical aspects). *Research Report 368-1F*. Center for Transportation Research, The University of Texas at Austin.
- Nazarian, S. and Stokoe, K.H., II. 1986b. In-situ determination of elastic moduli of pavement

- systems by spectral-analysis-of-surface-waves method (theoretical aspects). *Research Report 437-2*. Center for Transportation Research, The University of Texas at Austin.
- Nazarian, S., Stokoe, K.H., II, and Hudson W.R. 1983. Use of spectral analysis of surface waves method for determination of moduli and thickness of pavement systems. *Transportation Research Record. No. 930.*, pp. 38–45. Transportation Research Board, Washington, DC.
- Nurse, R. W. 1949. Steam curing of concrete. *Mag. Concr. Res.* 1(2):79–88.
- Olson, L. and Church, E. 1986. Survey of nondestructive wave propagation testing methods for the construction industry. *Proc. 37th Ann. Highway Geol. Symp.*, Helena, Mont., Aug.
- Olson, L.D. and Wright, C.C. 1990. Seismic, sonic, and vibration methods for quality assurance and forensic investigation of geotechnical, pavement, and structural systems. In *Proceedings of Conference on Nondestructive Testing and Evaluation for Manufacturing and Construction*, H.L.M. dos Reis, ed., pp. 263–277. Hemisphere Publishing, New York.
- Otto, G., Chew, W.C., and Young, J.F. 1990. A large open-ended coaxial probe for dielectric measurements of cements and concretes. *Proc. Conf. Nondestructive Eval. Civ. Struct. Mater.*, pp. 193–209. National Science Foundation, Washington, DC.
- Ottosen, N.S. 1981. Nonlinear finite element analysis of pullout test. *J. Struct. Div. ASCE.* 107(ST4):591–603.
- Parker, W.E. 1953. Pulse velocity testing of concrete. *Proc. Am. Soc. Test. Mater.* 53:1033–1042.
- Perenchio, W.F. 1989. The condition survey. *Concr. Int.* 11(1):59–62.
- Petersen, C.G. 1984. LOK-test and CAPO-test development and their applications. *Proc. Inst. Civ. Eng.* 76 Part I:539–549.
- Pichot, C. and Trouillet, P. 1990. Diagnosis of reinforced structures: An active microwave imaging system. In *Proceedings, NATO Advanced Research Workshop on Bridge Evaluation, Repair and Rehabilitation*, A.S. Nowak, ed., pp. 201–215. Kluwer Academic Publishers, New York.
- Pratt, D. and Sansalone, M. 1992. Impact-echo signal interpretation using artificial intelligence. *ACI Mater. J.* 89(2):178–187.
- Richards, O. 1977. Pullout strength of concrete. *Reproducibility and Accuracy of Mechanical Tests.* ASTM SP 626, pp. 32–40. American Society for Testing and Materials, Philadelphia, PA.
- Rix, G.J., Bay, J.A., and Stokoe, K.H. 1990. Assessing in situ stiffness of curing Portland cement concrete with seismic tests. *Transportation Research Record 1284*, pp. 8–15. Transportation Research Board, Washington, DC.
- Rix, G.J. and Stokoe, K.H. 1989. Stiffness profiling of pavement subgrades. *Transportation Research Record 1235*, pp. 1–9. Transportation Research Board, Washington, DC.
- Rodríguez, P., Ramírez, E., and González, J.A., 1994. Methods for studying corrosion in reinforced concrete. *Maga. Concr. Res.* 46(167):81–90.
- Roy, D.M. and Idorn, G. M. 1982. Hydration, structure, and properties of blast furnace slag cements, mortars and concrete. *J. Am. Concr. Inst.* 79(6):444–457.
- Rutenbeck, T. 1973. New developments in-place testing of concrete. In *Use of Shotcrete for Underground Structural Support*, ACI SP-45, pp. 246–262. American Concrete Institute, Farmington Hills, MI.
- Sansalone, M. and Carino, N.J. 1986. Impact-echo: A method for flaw detection in concrete using transient stress waves. *NBSIR 86-3452*, 222 pp. National Bureau of Standards. Available from NTIS, Springfield, VA, 22161, PB #87-104444/AS.
- Sansalone, M. and Carino, N.J. 1987. Transient impact response of plates containing flaws. *J. Res. Nat. Bur. Stand.* 92(6):369–381.
- Sansalone, M. and Carino, N.J. 1988. Impact-echo method: Detecting honeycombing, the depth of surface-opening cracks, and ungrouted ducts. *Concr. Int.* 10(4):38–46.
- Sansalone, M. and Carino, N.J. 1991. Stress wave propagation methods. In *Handbook on Nondestructive Testing of Concrete*, V.M. Malhotra and N.J. Carino, eds., pp. 275–304. CRC Press, Boca Raton, FL.

- Sansalone, M. and Carino, N.J. 1989a. Laboratory and field study of the impact-echo method for flaw detection in concrete. In *Nondestructive Testing of Concrete*, H.S. Lew, ed., ACI SP-112, pp. 1–20. American Concrete Institute, Farmington Hills, MI.
- Sansalone, M. and Carino, N.J. 1989b. Detecting delaminations in concrete slabs with and without overlays using the impact-echo method. *J. Am. Concr. Inst.* 86(2):175–184.
- Sansalone, M. and Poston, R. 1992. Detecting cracks in the beams and columns of a post-tensioned parking garage structure using the impact-echo method. *Proc. Conf. Nondestructive Eval. Civ. Struct. Mater.*, pp. 129–143. National Science Foundation, Washington, DC.
- Sansalone, M., Lin, Y., Pratt, D., and Cheng, C. 1991. Advancements and new applications in impact-echo testing. In *Proceedings, ACI International Conference on Evaluation and Rehabilitation of Concrete Structures and Innovations in Design, Hong Kong*, V.M. Malhotra, ed., ACI SP-128, pp. 135–150. American Concrete Institute, Farmington Hills, MI.
- Saul, A.G.A. 1951. Principles underlying the steam curing of concrete at atmospheric pressure. *Mag. Concr. Res.* 2(6):127–140.
- Serway, R.A. 1983. *Physics for Scientists and Engineers/with Modern Physics*. Saunders College Publishing Philadelphia.
- Skramtajev, B.G. 1938. Determining concrete strength for control of concrete in structures. *J. Am. Concr. Inst.* 34:285–303.
- Stain, R.T. 1982. Integrity testing. *Civ. Eng.* April:53–59.
- Stehno, G. and Mall, G. 1977. The tear-off method—A new way to determine the quality of concrete in structures on site. *RILEM Int. Symp. Test. In Situ Concr. Struct.* Budapest, Sept. 12–15, pp. 335–347. Institut des Sciences de la Construction, Budapest.
- Steinbach, J. and Vey, E. 1975. Caisson evaluation by stress wave propagation method. *J. Geotech. Eng. Div. ASCE* 101(GT4):361–378.
- Steinway, W.J., Echard, J.D., and Luke, C.M. 1981. Locating voids beneath pavements using pulsed electromagnetic waves. *NCHRP Report 237*, 40 pp. Transportation Research Board, Washington, DC.
- Stern, M. and Geary, A.L. 1957. Electrochemical polarization: I, A theoretical analysis of the shape of polarization curves. *J. Electrochem. Soc.* 104(1):56–63.
- Stern, M. and Roth, R.M. 1957. Anodic behavior of iron in acid solutions. *J. Electrochem. Soc.* 104(6):390–392.
- Stone, W.C. and Carino, N.J. 1983. Deformation and failure in large-scale pullout tests. *ACI J.* 80(6):501–513.
- Stone, W.C. and Reeve, C.P. 1986. A new statistical method for prediction of concrete strength from in-place tests. *ASTM J. Cement, Concr. Aggregates*, 8(1)3–12.
- Stone, W.C., Carino, N.J., and Reeve, C.P. 1986. Statistical methods for in-place strength predictions by the pullout test. *ACI J.* 83(5):745–756.
- Sturup, V.R., Vecchio, F.J., and Caratin, H. 1984. Pulse velocity as a measure of concrete compressive strength. In *In Situ/Nondestructive Testing of Concrete*, V.M. Malhotra, ed., ACI SP-82, pp. 201–227. American Concrete Institute, Farmington Hills, MI.
- Tam, C.T., Lai, L.H., and Lam, P.W. 1977. Orthogonal detection technique for determination of size and cover of embedded reinforcement. *J. Inst. Eng.* 22:6–16.
- Tank, R.C. and Carino, N.J. 1991. Rate constant functions for strength development of concrete. *ACI Mater. J.* 88(1):74–83.
- Te'eni, M. 1970. Discussion of Session B. *Proceedings Symp. Non-Destructive Test. Concr. Timber.* June 11–12, 1969, pp. 33–35. Institution of Civil Engineers.
- Tremper, B. 1944. The measurement of concrete strength by embedded pull-out bars. *Proceedings Am. Soc. Test. Mater.* 44:880–887.
- Ulriksen, C.P.F. 1983. *Application of Impulse Radar to Civil Engineering*. Ph.D. Thesis. Lund University, Dept. of Engineering Geology, Sweden, 1982. Published by Geophysical Survey Systems, Salem, NH.

- Weil, G.J. 1991. Infrared thermographic techniques. In *Handbook on Nondestructive Testing of Concrete*, V.M. Malhotra and N.J. Carino, eds., pp. 305–316. CRC Press, Boca Raton, FL.
- Whitehurst, E.A. 1951. Soniscope tests concrete structures. *J. Am. Concr. Inst. Proc.* 47(6):433–448.
- Whitehurst, E.A. 1967. *Evaluation of Concrete Properties from Sonic Tests*. American Concrete Institute Monograph, No. 2, 94 pp. ACI/Iowa State University Press, Ames, IA.
- Yener, M. 1994. Overview, and progressive finite element analysis of pullout tests. *ACI Struct. J.* 91(1):49–58.
- Yuan, D. and Nazarian, S. 1993. Automated surface wave method: Inversion technique. *J. Geotech. Eng.* 119(7):1112–1126.